Ian Whelan, B.Eng, MSc

Developing Microphysiological Systems of Bone Development, Physiology, and Repair

---

Trinity College Dublin - February 2021

A thesis submitted to the University of Dublin in partial fulfilment of the requirements for the degree of

Doctor in Philosophy

Supervisors: Prof. Daniel J. Kelly, Prof David A. Hoey

Internal Examiner: Prof. Michael G Monaghan

External Examiner: Prof Chelsea S Bahney

Declaration

I declare that this thesis has not been submitted as an exercise for a degree at this or any other university and it is entirely my own work.

I agree to deposit this thesis in the University's open access institutional repository or allow the Library to do so on my behalf, subject to Irish Copyright Legislation and Trinity College Library conditions of use and acknowledgement.

I consent to the examiner retaining a copy of the thesis beyond the examining period, should they so wish (EU GDPR May 2018).

_____

Ian Whelan

Summary

A recent report in The Lancet claimed approximately 1.7 billion people worldwide suffer from a musculoskeletal disease. Bone diseases account for a substantial portion of this burden, with their prevalence only set to increase in line with the aging population. Treatment of these conditions requires an understanding of the underlying physiology, however the complex mechanisms of how bone functions across its life cycle are still poorly understood, and in many cases no curative treatments exist. To advance our understanding of bone physiology and to aid in the development of new therapies, predictive models of human bone are required. However, the evidence suggests that our current models are inadequate and cannot fully predict human response to new therapies as bone is a common adverse target for a number of medications, and bone therapeutics also have off target effects on other organs [1]. Improving current models of bone physiology is essential to advancing understanding and treatment of bone disease. Thus, the overall objective of this thesis is to advance the field by developing advanced models of bone development, physiology and repair.

One of the most prominent platforms for developing advanced models of human tissue and organ function are microphysiological systems (MPS) or organ-on-chip systems. MPSs facilitate development of tissues and organs with superior physiological relevance to traditional *in vitro* culture by incorporating multiple cell types, mechanical stimulation, vascularisation, and multi-organ fluidic coupling, for example. These features make MPS systems an ideal platform upon which to develop advanced models of bone, as these features are so critical in bone physiology. In light of this, the first aim of this thesis was to establish a vascularised MPS platform for engineering bone tissue by integrating physiologically relevant vasculature into an MPS device, where endothelial cells are supported by bone marrow stromal cells (hBMSCs), as

these are the canonical progenitor cell used to engineer bone. The second aim of this thesis was to then apply these vascularisation strategies towards the development a model of endochondral ossification (EO) within a MPS device; specifically modelling the vascular invasion of the cartilage template that is so critical in EO driven bone development and fracture healing. The third and final aim of this thesis was to engineer bone tissue that could recreate physiologically relevant functions of osteoblasts and osteocytes in mature bone, which are essential for modelling bone remodelling and endocrine function. Altogether, achieving these aims establishes MPS platforms that facilitate advanced *in vitro* study of bone repair and regeneration through endochondral ossification, and the cellular functions of mature bone that are so integral in physiological and disease processes.

The first aim of this thesis was to establish methods to vascularise MPS devices with endothelial cells undergoing vasculogenesis with hBMSCs acting as a support cell. Vascularisation is critical is critical to bone development, growth, and regeneration [2, 3], thus is a key consideration for building advanced models of bone. hBMSC and human umbilical vein endothelial cells (HUVECS) were co-cultured in one hydrogel, or in separate hydrogels, to study how hBMSCs can directly or indirectly (via the release of paracrine factors) support vascularisation within MPS devices. hBMSCs could facilitate formation of physiologically relevant perfusable vasculature using both approaches, although this was strongly dependent on the numbers of hBMSCs introduced into the MPS. Thus, two methods, direct and indirect vascularisation, were developed to vascularise MPS devices with HUVECS undergoing vasculogenesis using hBMSCs as a support cell. The direct vascularisation method was applied in the next chapter of the thesis when developing a model of EO during bone development/regeneration.

Vascular invasion of the cartilage template is essential to initiate bone formation in EO-driven bone development and fracture healing. However no *in vitro* models currently exist that model this process, and MPS systems are an ideal candidate platform on which to build such systems. Thus, the second aim of this thesis was to develop a model of EO within a MPS device that was capable of recreating key events during vascular invasion of a cartilage template. Human developing bone organoids, representing different stages of cartilage maturity in developing/regenerating bone, were fabricated from hBMSCs, and then cultured in the presence of engineered vasculature within a MPS device. Mature cartilage organoids expressing anti-angiogenic factors were found to locally suppress vascularisation, while perfusable vascular network developed in the presence of hypertrophic cartilage organoids. The invading vasculature also regulated the phenotype of the developing bone organoids, with an upregulation of pluripotency associated genes observed in the mature cartilage organoids in the presence of vasculature. Thus, the model of EO can recreate key EO events within an MPS device; establishing an advanced *in vitro* platform for the study of bone development and regeneration.

The final aim of the thesis was to develop an *in vitro* model of bone that recapitulates key regulatory functions of mature osteoblast and osteocytes, as these cells specifically are critical to identify novel approaches to treating diseases of bone and other organs for which bone has endocrine effects. Using a statistical experimental approach, a collagen nanohydroxyapatite hydrogel was developed that can drive osteogenesis of hBMSCs to the point of mature osteoblast / osteocyte-like cells, manifesting in the secretion of factors clinically relevant to bone remodelling and endocrine function. Recreating these physiologically relevant bone functions using an

accessible human derived cell source like hBMSCs will be central to the future development of MPSs of mature bone.

Altogether, this thesis describes the development of *in vitro* models that recapitulate key aspects of bone physiology. This thesis has demonstrated that such models recreate critical functions pertinent to bone development/regeneration and mature bone function. MPS applications of such systems hold great potential to accelerate basic discoveries and improve outcomes for patients suffering with bone disease.

Acknowledgements

I left the typical comfortable ‘good’ job a number of years ago to retrain and upskill in research. I wanted the technical challenge, I wanted to work at the cutting edge on technical problems, I wanted to do a PhD. Sitting here 5 years on and reflecting on the whole experience, it has delivered exactly that, and so much more that I never envisaged. It was, however, also challenging and difficult in ways I never envisaged. Nassim Taleb coined the term ‘anti-fragility’, where entities become stronger when you stress them or attempt to break them down. Perhaps similar to most, my PhD has been an exercise in anti-fragility; a series of tough challenges, both technical and personal, but coming out stronger at the end. It was a great experience, made possible by a number of people throughout the last few years that I wish to acknowledge.

To my family, Tom, Joan, Aimee, Lindsay, Tommy and George, and to my future in-laws family Connie and Tony! You were always there over these last few years; for support and celebrations at every step along the way. Everything was made so much easier with such a strong family as a foundation. I love you all and cannot thank you enough.

Then there is the lab. If you could bottle TCBE’s hiring policy, you wouldn’t keep it on the shelves for long. Throughout the years some fantastic engineers and scientists, and most importantly; people, came and went from the 3rd floor labs in TBSI. I couldn’t have asked to meet and work with a better group. There were so many good times; numerous nights out in Doyles / Probus, tag nights out, harlem shakes, learning Italian blasphemies, desktop goose, eating horrible raw fish in the Netherlands, getting stuck in a pothole at 3am in Mexico, pizza tours of Dublin, dry ice bombs, tunes blaring in cell culture, conferences, gigs, super saturdays, jamming with the lime street massive,

trips away to Sligo, and so, so much more. I have made friends in TCBE I will have forever.

And, of course, I could not forget the two wise men: Danny and Dave. It was a pleasure working with you throughout the four years. As you guys know more than most, a PhD is a challenge that extends beyond the technical, it pushes you in so many other aspects of your professional and personal life. At times you have to cut life events short to feed cells the following morning, you constantly deal with rejection when results don't go your way, or you have a long-term study go in the bin for a contamination. All this on top of whatever else might be going on in your life. The collaborative and supportive environments of your labs, and your own support throughout the PhD cycle were and are essential in navigating and enjoying the whole experience.

And finally, to my now fiancée, Kate. This journey has been a long one for the two of us; return to full time training hasn't been easy on some aspects of our life! Your support throughout, however, was unwavering, and I cannot thank you enough for that. Word would run out of pages before I could list everything you did for me over the course of my PhD. It has been a big chapter for us; we've seen some great places and met some great friends. I could not have gotten through this without you by my side, I love you.

Table of Contents

Publications

Ian T. Whelan, E Moeendarbary, David A. Hoey, Daniel J. Kelly, Biofabrication of Microvasculature within Microphysiological Models and their applications to models of Bone (Patho)physiology (In Review)

Conference Abstracts

Ian T. Whelan, David A. Hoey, Daniel J. Kelly. *3D bioprinting of thick vascularised constructs as models of bone and joint disease (Patho)physiology*. 23rd Annual Conference of the Bioengineering Section of the Royal Academy of Medicine in Ireland, January 20th – 21st, 2017. Hilton Belfast Templepatrick Golf & Country Club, Hotel, Co. Antrim, Ireland.

Ian T. Whelan, David A. Hoey, Daniel J. Kelly. *Development Of A Vascularised Bone-On-A-Chip*. 24th Annual Conference of the Bioengineering Section of the Royal Academy of Medicine in Ireland, January 26th – 28th, 2018. Johnstown House Estate, Enfield, Co. Meath, Ireland.

OOC - Ian T. Whelan, David A. Hoey, Daniel J. Kelly. *Development Of A Vascularised Bone-On-A-Chip*. Organ-on-a-Chip, Tissue-on-a-Chip Europe, Jun 5th-6th, 2018. Rotterdam, Netherlands.

OOC - Ian T. Whelan, Emad Moeendarbary, David A. Hoey, Daniel J. Kelly. *Development of a Microphysiolgical Model of Vascularised Bone Tissue*. Organ-on-a-Chip, Tissue-on-a-Chip Europe, Jun 18th-19th, 2019. Rotterdam, Netherlands.

Ian T. Whelan, David A. Hoey, Daniel J. Kelly. *A Microphysiological Model Of Human Bone Tissue*. 26th Annual Conference of the Bioengineering Section of the Royal Academy of Medicine in Ireland, January 17th – 18th, 2020. Mount Wolseley Hotel, Spa & Golf Resort, Co Carlow, Ireland

Ian T. Whelan, Emad Moeendarbary, David A. Hoey, Daniel J. Kelly. *Vascularising Developing Bone Organoids On A Chip To Model Endochondral Ossification And Fracture Healing*. 27th Annual Conference of the Bioengineering Section of the Royal Academy of Medicine in Ireland, January 15th, 2021. Held online

Chapter 1: Introduction

1.1 The Burden of Bone Disease

The most prevalent diseases of bone are typically not fatal but can have a considerable impact on a patients' quality of life. Bone diseases most commonly affect growth and development or dysregulate the remodelling process once the organ has matured. Treatment of these conditions manifests in substantial economic impact; in a 2013 European Union report, fractures as a result of osteoporosis alone cost in the region of €37 billion [4]. In Ireland it is estimated that the cost of fragility fractures alone will amount to €320 million in 2025 [4, 5]. While developmental abnormalities, osteoporosis and associated bone fractures are the most established and overt manifestations of bone disease, bone may also have a more discreet function as endocrine regulator in other tissues; with evidence suggesting bone has a role in conditions such as obesity and diabetes, the economic cost of which were estimated to be $150 billion [6] and $327 billion [7] in 2016 and 2017 respectively in the United States.

1.2 Modelling Bone Physiology and Disease

An improved understanding of bone (patho)physiology will improve both the health and economic burdens associated with bone diseases. However, this requires appropriate analogues of the human condition to recreate physiological or pathophysiological states, which can then be studied to unveil mechanisms and processes that can be targeted therapeutically. Generally, animal models are used to improve our fundamental understanding of musculoskeletal tissues [8-13]. While *in vitro* methods exist to study bone physiology, they generally cannot replicate the

complexity of an entire organism, thus animals have become the gold standard in many fields of bone research [14-18]. However, despite their utility, animal models are expensive and require specialised expertise and facilities. Additionally, though animals may be able to recreate a specific disease phenotype, the underlying mechanisms can be different to that in humans, limiting their translational benefits [19]. There are also ethical concerns related to the use of animals in research. In contrast, *in vitro* models are less resource intensive platforms to study biological processes in the lab. However, *in vitro* models are far removed from the *in vivo* condition, and to date have been unable to replicate much of its inherent complexity. Thus, a combination of *in vitro* and *in vivo* models are typically employed for both basic mechanistic research and in the evaluation of novel therapeutics [20].

In evaluating these novel therapeutics, *in vitro* and subsequent *in vivo* models with physiological processes analogous to humans are used to predict both therapeutic efficacy and potential adverse effects. However, this seemingly sophisticated and logically coherent development process often breaks down in predicting humans responses; with 8 out every 9 compounds identified in this process failing clinically [21], or showing unexpected adverse effects. In the context of bone, a recent example is that of romosozumab, an anti-sclerostin antibody for the treatment of osteoporosis that caused a higher incidence of cardiac issues in clinical trials [1]. Additionally, other osteoporosis [22], diabetes [23], epileptic [24], and acid reflux [25] medications have all shown negative bone health consequences post marketing, and a number of disease modifying osteoarthritis drugs (DMOAs) show uninspiring efficacy once they reach the clinic [26].

It is clear that an alternative, or updated, approach to modelling human bone is needed. One potential avenue for improving bone model predictivity is addressing the

chasm of biological complexity that exists between *in vitro* and *in vivo* systems. *In vitro* systems that possess the necessary complexity of animal models with the practicality and controllability of traditional *in vitro* systems are a promising approach to improving the predictivity of bone models. Such systems can create complex tissue/organ function from human derived cells to augment both basic research and drug discovery.

1.3 Microphysiological Systems

Microphysiological systems (MPSs), or organs-on-chips, are models of human organs that recreate key tissue/organ functions at the microscale by leveraging microfabrication and tissue engineering techniques [27]. MPSs have a number of advantages over traditional 2D and 3D culture, such as control of cellular and tissue architecture, incorporation of complex loading regimes, the control of media flow and perfusion, and incorporation of biomimetic vasculature. In addition, there is potential for these MPSs to be linked [28], thereby better mimicking the *in vivo* condition by having interconnected and intercommunicating organs.

In the last 10 years, MPSs have advanced to a stage where organ systems have been engineered to exhibit organ form and function not possible in traditional *in vitro* culture. For example, the bone marrow niche has been recreated in a MPS platform; exhibiting a heterogeneous hematopoietic cell population and exhibiting myeloerythroid toxicity after clinically relevant exposures to chemotherapeutic drugs and ionizing radiation [29]. In cancer, extravasation of tumour cells into the perivascular niche within physiologically relevant microvasculature can be recreated and tracked in real time [30]. MPSs can even facilitate complex loading regimes; demonstrating hyperphysiological loading of cartilage alters tissue homeostasis towards catabolism, inflammation and hypertrophy, as observed in osteoarthritis [31]. In addition, the

paradigm of linking multiple MPS systems to build complex multi-organ systems is now being realised. MPS models of bone marrow, liver and kidney have been fluidically linked; predicting pharmacokinetic parameters, and matching pharmacodynamic data of patients administered with cisplatin, a chemotherapeutic [32].

This suggests MPS technology is a promising platform to develop advanced *in vitro* bone models, given that MPS systems can integrate a number of physiological functions relative to bone, such as vascularisation, mechanical stimulation, or fluidic coupling to other organs. However, MPS technology has been applied mostly to organ systems involved in drug metabolism, such as liver, lungs, spleen and kidneys [32], and has been scarcely applied in bone applications. One exception is in bone cancer research, where breast cancer cells have been shown to extravasate from endothelium into bone-associated ECM [33]. Thus, MPS technology has potential to develop advanced models of bone development, physiology and repair.

1.4 Thesis Objectives and Specific Aims

The overall goal of this thesis to develop physiologically relevant models of both human bone development and the mature tissue. Given the critical role of the vasculature in bone development and physiology, the first aim of this thesis was to develop methods of integrating perfusable biomimetic vasculature into MPS devices using hBMSCs as mural or support cells to HUVECs (Chapter 3). hBMSCs, as the canonical progenitor cells in bone, can model the stages of bone development and are the progenitors of the parenchymal cells in mature bone. Thus, means to induce vascularisation of endothelial cells with hBMSCs is a pre-requisite to building physiologically relevant bone models. Leveraging such vascularised MPS devices, the second aim of this thesis was to develop a model of endochondral ossification to study

bone development and fracture healing (Chapter 4). Specifically, this chapter aims to model the vascular invasion of a cartilage template that is integral to bone formation during endochondral ossification. The final aim of this thesis (Chapter 5) is to develop a hydrogel system to support the robust osteogenic differentiation of hBMSCs for incorporation into a mature bone MPS device. Specifically, this chapter sought to develop a hydrogel capable of supporting osteogenic differentiation of BMSCs and the generation of bone cells that exhibit osteoblast and osteocyte like function. Success here is defined as the ability to recapitulate the regulatory function of mature bone cells, such as the production of factors that regulate bone remodelling and endocrine function.

The impact of this work is ultimately to advance the state of *in vitro* models for recreating human biological function, with particular focus on human endochondral ossification and the function of human mature bone. Development of such models is critical for de-risking therapeutic development, and expanding our understanding of these basic biological processes, which are, as yet, not fully understood. While the translation of these models to predictive clinical application requires significant time and resource commitment, the work presented in this thesis represents significant early stage conception and development.

Chapter 2: Literature Review

A better understanding of bone development and the processes that mediate its maintenance and homeostasis will be central to the development of new therapies to treat damaged and diseased bone tissue. Bone development occurs through two process; intramembranous ossification (IO) and endochondral ossification (EO) [34], which also serve critical functions during fracture healing and large bone defect repair. Bone development culminates in mature bone; a complex, highly vascularised and mineralised organ that functions to provide a strong load bearing framework for protection and to facilitate locomotion. This load bearing function of bone tissue is reflected in its adaptation to mechanical loading through anabolic and catabolic remodelling [35]. Though these functions are well described, more recent advances have shown bone has much more diverse functions such as regulation of serum ion levels [36], and endocrine function [16, 37]. The cellular and molecular mechanisms of how bone develops, and performs these remodelling and endocrine functions, are reviewed in detail in this chapter.

2.1 Development

2.1.1 Intramembranous Ossification

Intramembranous ossification (IO) is the direct formation of bone from mesenchymal condensations without the formation of an intermediary cartilage template [38]. IO is typical in the formation of the flat bones in the skull and clavicle. Comparatively little is known about the molecular mechanisms that underpin IO compared to EO, as EO is responsible for the development of the vast majority of the skeleton [38]. What is known about IO has mostly been revealed through study of patients with impaired

ossification in bones of the skull formed by IO due to genetic mutations, such as craniosynostosis.

FGF signalling pathway is now known to be one of the most important regulators of IO in development [39], with a number of FGFs being expressed during IO [40]. FGFs at least in part exert their biological function by inducing growth and proliferation of osteoblasts [41]. Mutations in receptors FGFR1, FGFR2 and FGFR3 have been implicated in impaired ossification of the cranial bones, with FGFR1 and FGFR2 implicated in the majority of cases. Mutations in FGFR1 in mice and humans show it has a crucial role to play, as gain of function mutations are characterized by premature fusion of one or several calvarial sutures [42]. In addition, recombinant FGF2 has been shown to accelerate bone healing in human osteotomies [43, 44] and tibial shaft fractures [45]. Twist 1 is a transcription factor that inhibits the actions of Runx2 in osteoblast development [46], and is particularly involved in IO of the cranial sutures. Twist1 null mice show increased bone formation in the cranial sutures [47], and this is mirrored in the human condition [48]. Finally, TGF-β signalling is critical for IO in mice. TGFβR2 null mice die at birth with an open skull due to undeveloped calvaria [49]. In addition, loss of TGF-β signalling induced by TGFβR2 deletion results in disruption of the basal transcription mechanisms that control IO; with impaired differentiation in neural crest derived osteoprogenitor cells [50]. Manipulation of these molecular pathways has demonstrated their function in animal models that mimic the how the disease presents clinically, however the exact underpinning mechanisms are largely unclear.

IO also has a key role to play in fracture healing. Fracture healing can occur through two mechanisms; primary and secondary bone healing. Primary bone healing does not commonly occur in the natural process of fracture healing, as it requires surgical

reduction and stable fixation. When these conditions exist, healing takes place through formation of a cutting cone [51], and remodelling of the interface to re-establish connection of haversian systems occurs in a process analogous to bone remodelling [52]. Secondary bone healing is the most common form of bone healing and requires both endochondral and intramembranous ossification. IO is zone specific in the fracture site. From day 2 to 5 post fracture, IO begins in the layer of resident osteoblasts in the periosteum [53, 54]. These cells establish the hard callus in secondary fracture healing and give rigidity to the callus.

2.1.2 Endochondral Ossification

Endochondral ossification (EO) is the primary method by which long bones form, grow and regenerate in humans. In development, skeletal cells have origins in the ectoderm, mesoderm, and endoderm, and the multiple derivatives they form as the embryo develops [55]. For example, skeletogenic cells from the neural crest give rise to skeletal elements in the face and throat, and skeletal cells that form the axial skeleton originate from the paraxial mesoderm. The appendicular skeleton has origins in the lateral plate mesoderm and the prechordal mesoderm, where these cells condense and pattern into a cartilage model that outlines the shape and size of future bones [56]. These mesenchymal cells then differentiate into chondrocytes that deposit a cartilaginous template that is vascularised, resorbed and mineralised into bone tissue [38]. In addition, postnatal bone growth, which results from continual proliferation, hypertrophy, and mineralisation of chondrocytes in the epiphyseal growth plate, is a result of EO. Furthermore, bone damage and fractures can heal without fibrous scarring through bona fide tissue regeneration that proceeds through EO [52, 57].

In development, EO begins with condensation of mesenchymal cells in cell-cell adhesion process that requires N-cadherin [56, 58]. Bone morphogenetic proteins

(BMPs) and their antagonists NOTCH are known to be critical for formation of these condensations [59]. Core cells in these condensations differentiate into chondrocytes under the control of the SOX9, SOX5 and SOX6 transcription factors and secrete matrix proteins such as collagen type II, IX, XI and aggrecan [60]. Soluble extracellular factors are potent regulators of this process; for example BMP signalling drives chondrogenesis after the condensation stage [61]. In contrast, canonical wnt signalling [62] and NOTCH signalling [63] are inhibitors, and suppress chondrogenesis. In addition, non-canonical wnt signalling molecules, such as Wnt5a and Wnt11 are also highly expressed in developing cartilage. Chondrocytes then proliferate rapidly; driving growth of the condensation into a cartilage template, as a precursor to vascularisation and subsequent ossification. Chondrocytes at the core of the template then exit the cell cycle and undergo hypertrophy, expressing COLX, MMP-13 and initiating a pro-angiogenic program to drive vascular invasion. This vascular invasion is critical as it initiates a transdifferentiation of hypertrophic chondrocytes to osteoblasts [64, 65]; initiating bone formation at the centre of the condensation (Figure 2.1). This then establishes a linear hierarchical order of chondrocyte maturity that forms the growth plate that facilitates bone growth towards mature bone.

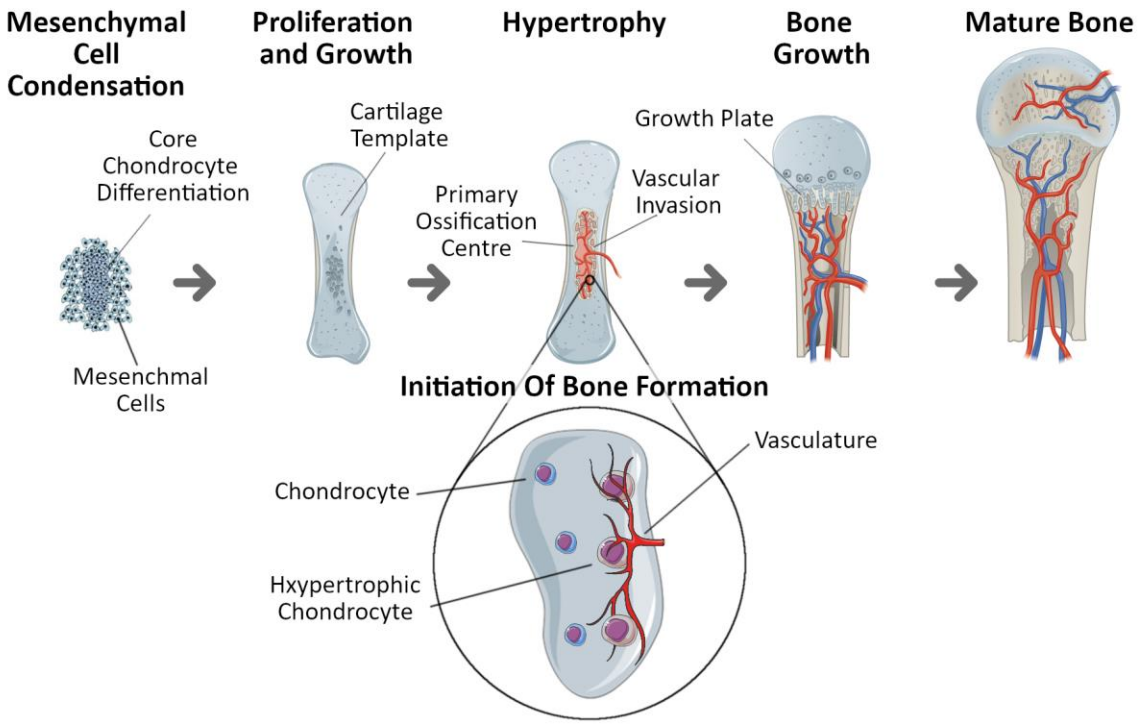

Figure 2.1: Vascular invasion initiates bone formation in endochondral ossification. A condensation of mesenchymal precursors differentiate down a cartilage lineage and secrete a cartilaginous matrix, and proliferate to form a cartilage template of the final bone structure. Chondrocytes at the centre of the template become hypertrophic and secrete angiogenic factors to drive vascular invasion. Vascular invasion initiates ossification at the primary ossification centre and ultimately establishes the growth plate that facilitates long bone growth.

The chondrocyte maturity hierarchy forms a linear organisation of cells in the growth plate that facilitates longitudinal growth This hierarchy consists of osteo-differentiated chondrocytes at the osteochondral junction, followed by hypertrophic chondrocytes, proliferating chondrocytes, and resting chondrocytes (Figure 2.2). The timely maturation of the chondrocytes in this cellular organisation facilitates the longitudinal growth of bones under the control of a number of different molecular players [38]. Most significant of these is the Indian hedgehog (IHH) / parathyroid hormone-related peptide (PTHrP) regulatory axis, which regulates growth and growth plate length through a negative feedback loop [66, 67]. However, a number of other extracellular factors regulate this process, such as thyroxine [65], Bone morphogenetic protein (BMP), GLI, FGF, WNT and NOTCH [60] (Figure 2.2).

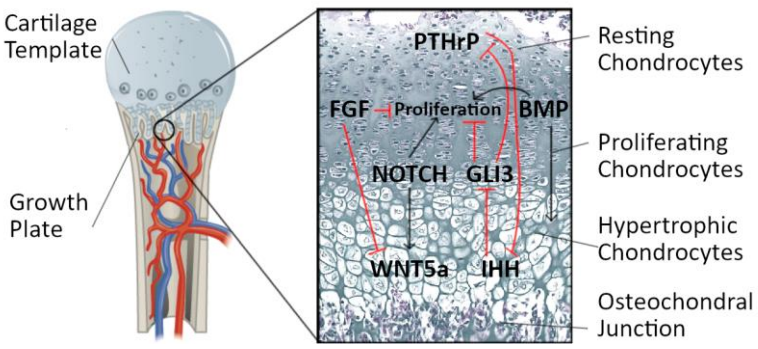

Figure 2.2: Extracellular mechanisms that regulate growth plate development in EO. IHH and PTHrP coordinate chondrocyte proliferation and maturation through a negative-feedback mechanism. IHH is secreted by hypertrophic chondrocytes, which inhibits GLI3; in turn driving chondrocyte proliferation and PTHrP transcription. To complete the feedback loop, PTHrP in turn suppresses IHH expression. This loop regulates growth plate length. FGFs, particularly FGF9/18 from the perichondrium, suppresses chondrocyte proliferation and maturation. BMPs secreted by chondrocytes and perichondrial cells promote proliferation and maturation. NOTCH signalling in chondrocytes promotes both proliferation and maturation. WNT5A expressed by prehypertrophic chondrocytes stimulates hypertrophy in neighbouring chondrocytes.

Post-development, the healing of fractures in bone takes place using a regenerative process analogous to developmental EO (Figure 2.3). Following a fracture, a haematoma is formed, and progenitor cells are recruited to the fracture site from the periosteum [68]. These cells begin to deposit a matrix rich in type II collagen and aggrecan [52]. At this early stage, FGF/FGFR signalling is crucial, and FGF1/2 and FGFR1/2 are upregulated at this stage [39]. Analogous to developmental EO, the next stage of healing is cartilage resorption, chondrocyte hypertrophy and matrix mineralisation. Chondrocytes cease their chondrogenic program with suppression of SOX9, begin a hypertrophic program with expression of the runt domain transcription factors RUNX2 [69, 70] and RUNX3 [71], and MADS box transcription factor Mef3c. This progression into hypertrophy also leads to expression and secretion of angiogenic factors, such as VEGF, MMP-13 and ADAM-TS4, that promote vascular invasion into the cartilaginous callus [14]. This vasculature provides a route for recruitment of cells involved in cartilage resorption, in which osteoclasts are known to play a key role [72-74]. Then Bone formation is initiated by a population of cells whose origin is still under

debate. The dogma postulates that hypertrophic chondrocytes undergo apoptosis [75, 76], and invading vasculature provides a route for skeletal stem cells to enter the fracture site and differentiate into osteoblasts [77]. However, more recent, and arguably more compelling evidence suggests that chondrocytes transdifferentiate into osteoblasts [14, 15, 78]. These studies suggest hypertrophic chondrocytes regain some stem cell functionality through expression of pluripotency genes, which facilitates their transdifferentiation into osteoblasts, and that these cells are responsible for the callus mineralisation.

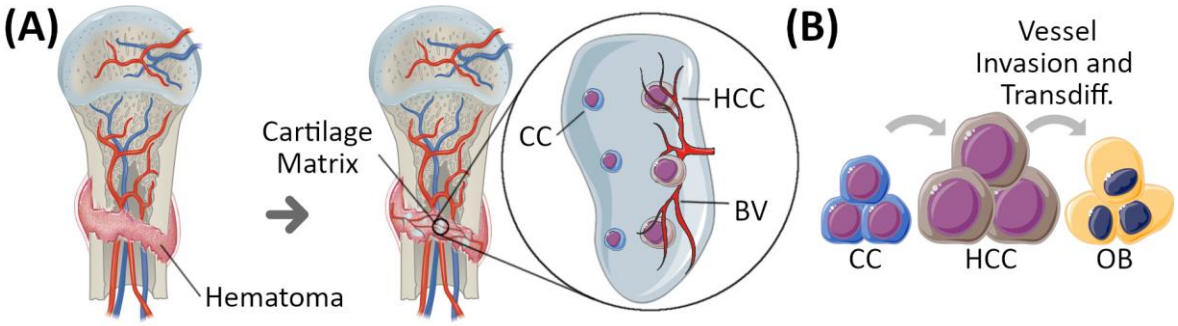

Figure 2.3: EO in fracture healing. (A) After a fracture, a haematoma is formed, where over time progenitor cells are recruited and lay down a cartilage matrix. Chondrocytes (CC) in this matrix become hypertrophic (HCC) and drive vascularisation of the cartilage in the fracture callus. **(B)** Schematic depicting the differentiation process of chondrocytes to osteoblasts mediated by vessel invasion.

This phase of mineralisation results in a hard callus of woven bone imparting rigidity and mechanical integrity to the fracture. The subsequent phase of bone remodelling converts this woven bone into the typical lamellar structure and re-establishes the mechanical stability that existed post fracture, while also re-establishing the medullary cavity. This phase of remodelling is orchestrated biochemically by IL-1, TNF-α, and BMPs, which show increased expression during this phase, as opposed to most other members of the TGF family, which have diminished in expression at this stage [52].

2.1.3 Mature Bone Composition

Mature developed bone tissue derives its strength from its hierarchical structure and highly mineralised extracellular matrix, which can be separated into structural units [79]. At the macroscale, bone is separated into highly porous cancellous bone typically surrounded with denser highly ordered compact bone (Figure 2.4). Compact bone contains osteons, and haversian canals. At the lowest scale, individual molecules of collagen type I are mineralised in between repeating collagen units by plate shaped-bone apatite crystals. The construction of this material at the nanoscale conveys bone its incredible mechanical properties. Attempts to recreate the intricate hierarchy of bone tissue is the aim of many labs, however an analogue of this system has yet to be realised.

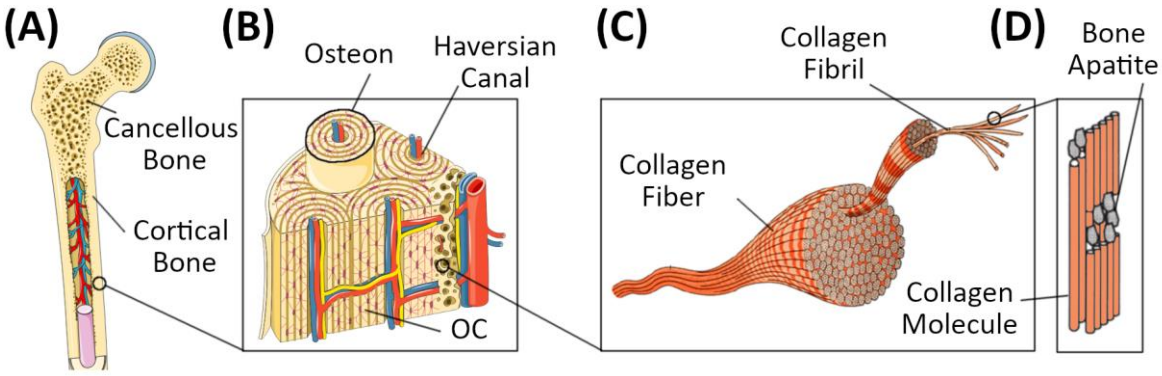

Figure 2.4: Hierarchical structure of bone tissue. **(A)** At the macroscale bone consists of porous cancellous bone and dense cortical bone **(B)** osteocytes (OC) traverse bone tissue in small fluid filled channels, and are the sensors of mechanical strain, and the regulators of bone remodelling. **(C)** Collagen fibres are composed of bundles of collagen fibrils, which in turn are composed of **(D)** collagen molecules mineralised with bone apatite.

Bone apatite accounts for 70-90% of bone tissue, and collagen accounts for around 90% of the remaining organic matrix [80]. Though collagens, and particularly collagen type I, is the most abundant protein in bone, it is also the most abundant structural protein in humans. Thus, collagen type I alone is not responsible for the ability and propensity of bone to mineralise. The intricate mineralisation of collagen I molecules

is initiated and directed by highly acidic non-collagenous bone proteins that are secreted by resident bone cells. Specifically, glycoproteins such as tissue non-specific alkaline phosphatase, osteonectin, and proteins of the small integrin-binding ligand, N-linked glycoprotein (SIBLING) family: osteopontin (OPN), matrix extracellular phosphoglycoprotein (MEPE), bone sialoprotein (BSP), dentin matrix protein 1 (DMP1), and dentin sialophosphoprotein (DSPP) [81] play an integral role in collagen, and hence bone, mineralisation. These proteins have their effects on regulating mineralisation through initiating or inhibiting mineralisation [82]. Additionally, γ-carboxyglutamic acid (GLA) containing proteins such as osteocalcin, which comprises up to 15% of the non-collagenous protein in bone is also critically involved in mineralisation, as bone apatite crystals fail to mature in osteocalcin null mice [83].

The non-collagenous, collagenous and mineral fractions of bone are constantly changing as bone remodels, as it is estimated the entire skeleton turns over every 10 years [84]. Mechanical signals govern this process; external bone loading is transduced down to pressurise microscale fluid filled cavities called canaliculi that traverse bone tissue and stimulate the residing osteocytes [85] (Figure 2.4B). This intricate system allows the cellular component of bone to ‘feel’ the external demands and adjust bone metabolism accordingly to drive bone formation or resorption [86]. This bone metabolism control system is mediated by the actions of osteoblasts and osteoclasts under the orchestration of the mechanically stimulated osteocytes.

2.1.4 Mature Bone Cellular Structure

The mineralised bone matrix is maintained by 3 key cellular players: bone resorbing osteoclasts, bone forming osteoblasts, and osteocytes. Osteoblasts and osteoclasts reside on bone surfaces, building and resorbing bone respectively, during this adaptive process, a small percentage of mature osteoblasts become entrapped in the newly

formed osseous tissue and differentiate further into osteocytes [6], which ultimately populate the bulk bone tissue, and, in adults, comprise over 90% of cells in bone [7] (Figure 2.5). Additionally, mounting evidence suggest bone endothelium is crucial for many aspects of bone development and to the proper function of these 3 canonical bone cells [2, 3].

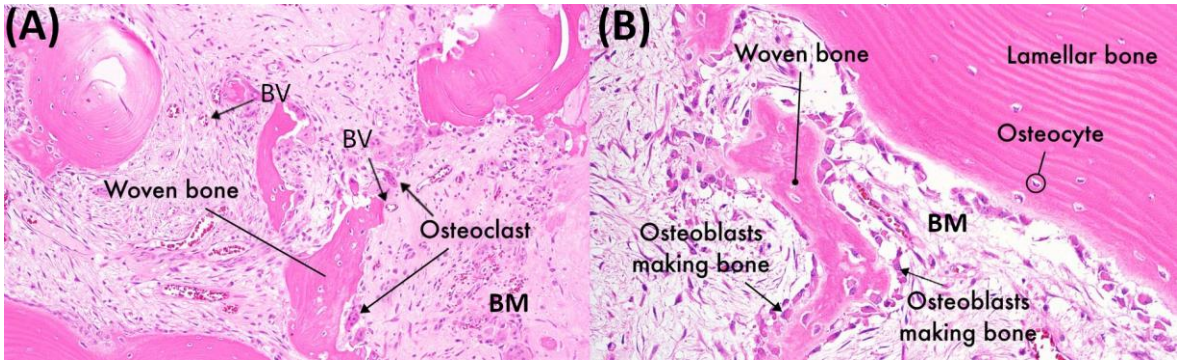

Figure 2.5: Structure of the key cells in bone (A) hematoxylin and eosin (H+E) stain depicting the distinction between bone marrow (BM) and bone tissue, and indicating the location of osteoblasts on the bone surface. Blood vessels (BV) are the conduit for osteoclasts and supply factors essential for remodelling. **(B)** Similar H+E stain indicating the spatial location of osteoblasts on the bone surfaces, with osteocytes embedded in bone tissue.

At the bone surface, osteoclasts are large multinucleated cells that are responsible for bone resorption. Osteoclasts originate from monocytes precursors, which arrive at the site of bone remodelling through the vasculature, anchor to the bone by adhesion to RGD sites on various resident bone proteins [82] through αvβ3 [87], and differentiate into osteoclasts upon stimulation with receptor activator of NF – kappa B ligand (RANKL) and macrophage/monocyte colony stimulating factor (M-CSF) [88]. Osteoclast mediated bone resorption requires breakdown of its two primary components; bone apatite, and collagen type I. The osteoclast has resorptive machinery consistent with bone composition; with a proton pump to locally acidify (pH 4.5) the bone matrix for dissolution of bone apatite, and cathepsin K to degrade the organic matrix [89]. Osteoclastic resorption is tightly integrated with bone formation,

as osteoblasts express a membrane bound RANKL for osteoclast activation, and bone resorption releases osteoblast activating growth factors, such as transforming growth factor β1 (TGF-β1) [90] and insulin-like growth factor (IGF) [91].

Osteoblasts are the effectors of bone formation, and the precursors of osteoblasts depends on the bone development pathway. In intramembranous ossification, bone marrow mesenchymal stem cells (BMSCs) that reside around the blood vessels in the marrow are directly recruited to the bone remodelling site through soluble factors released during bone resorption (TGF-β, PDGFs, LL37) [92]. The key molecular driver of osteoblast differentiation from its precursors is the runt-related transcription factor 2 (RUNX2), which drives the expression of OPN, BSP, OCN, OPG, RANKL, COL1 and a number of other bone related proteins [93]. More critically, upstream of RUNX2 is its key regulating signalling pathway; the canonical WNT/β-catenin pathway. This pathway is the target of many therapeutics to inhibit bone formation.

Once matured, osteoblasts become buried in bone matrix and begin differentiation into osteocytes [94]. It is generally believed that the burying process in osteoblast-osteocyte transition is passive; with osteoblasts not actively involved in becoming buried in the new osteoid matrix. However, there is some evidence that the process is indeed active, and osteoblasts require membrane type matrix metalloproteinases (MT-MMPs) to undergo this process [95]. The transition from osteoblast to osteocyte involves a number of key morphological and molecular changes. Osteoblasts initiate at the bone surface, with a cell body polarised by process extending into the matrix. As osteoblasts differentiate into early osteocytes, they reduce expression of osteoblast related markers, and begin to express osteocyte specific factors DMP-1, MEPE, E11/gp38 and SOST [96]. This molecular transition is accompanied by a concurrent shift to a more stellate morphology, with smaller cell body, many cell processes, and

changes in intracellular organelles. In final stages of osteocyte maturation, as the osteocyte embeds deeper into the bone matrix, expression of DMP-1 and E11/gp38 begin to decrease and cells begin to increase expression of matrix extracellular phosphoglycoprotein (MEPE) and sclerostin, and exhibit an oblong cell shape with many (>50) cell processes Osteocytes are the key parenchymal cell in bone and are directly responsible or indirectly involved in many of its functions, including mechanosensation [86] and calcium release [96]

Finally, one of the most critical tissue compartments in bone tissue is the endothelium [3]. Aside from its canonical role as a conduit for the diffusion of nutrients and metabolites, bone has a dense vascular supply that is involved in the biogenesis of the key aforementioned bone cells, and is responsible for the maintenance of the BMSC stem cell state [97]. Additionally, the vasculature in bone is in fact bone-specific and has different endothelial subtypes; type L vessels that are CD31 and endomucin low and reside primarily in the diaphysis in the marrow, while type H blood are associated with osteoprogenitor cells in the metaphysis involved with bone regeneration [98]. Bone vasculature is critical in bone remodelling, supplying the necessary nutrients and factors to the bone remodelling unit during turnover. Additionally, vascular impairment is believed to be a determining factor in poor and imbalanced bone formation observed in diabetes [3]

2.1.5 Remodelling

Endothelial cells, osteoclasts, osteoblasts, and osteocytes make up the bone remodelling unit (BRU) or basic multicellular unit (BMU) that maintains mature bone homeostasis. The process of bone remodelling is central to bone health and many of the most prominent diseases. While osteoblasts and osteoclasts are the effectors of bone remodelling, osteocytes are the orchestrators; sensing externally applied loads

and transducing them though biochemical signalling to control osteoblast and osteoclast activity [85]. In section 2.1.2, how these cells execute remodelling was described, In this section the crosstalk between cells, and the key molecular players that transduce these signals are discussed.

Osteocytes adapt bone tissue to be consistent with its externally applied loads. To achieve this, osteocytes use an array of molecular tools to orchestrate when bone is formed, and when it is resorbed (Figure 2.6). Of these, the most critical are sclerostin, Dickkopf-1 (DKK1), RANKL and osteoprotogerin (OPG). Though sclerostin is one of the better known proteins involved in inhibition of bone formation, the molecular mechanisms through which SOST is mechanically regulated in osteocytes is still unknown, though FAK/HDAC5 [99] and Piezo1-Akt [100] have been suggested. The mechanism by which DKK-1 is upregulated is also unknown, although it is also downregulated in response to mechanical stimulation. Finally, a number of other osteocyte secreted proteins, such as nitric oxide (NO), prostaglandin E_2 (PGE2), and insulin-like growth factor (IGF) are also secreted and positively regulate osteoblast activity.

It was previously stated that bone resorption is carried out by osteoclasts, thus regulation of resorption entails regulation of osteoclast activity. The primary pathway that drives osteoclastogenesis, and governs osteoclast activity is the RANK/RANKL OPG pathway [101]. This pathway is activated by binding of RANKL with its receptor RANK on the osteoclast membrane, leading to NF-κB activation, and transcription of osteoclastic genes through transcription factor nuclear factor-activated T cells c1 (NFATc1). Activation leads to transcription of the cellular machinery needed for bone resorption, such as Cathepsin K, MMP-9 and TRAP [102]. Both osteoblasts and osteocytes modulate this pathway through secretion of a RANKL decoy receptor,

osteoprotogerin (OPG), which binds RANKL and prevents binding to RANK, inhibiting osteoclastogenesis [103]. A number of other, more indirect pathways exist for modulating osteoclastogenesis. For example, though osteoclasts lack a PTH receptor, hyperparathyroidism is associated with increased osteoclast activity and bone resorption. Furthermore, many cell sources upregulate RANKL and M-CSF such as hypertrophic chondrocytes, BMSCs, osteoblasts, and osteocytes [104]. Additionally, activation of the WNT signalling pathway on osteoblasts, inhibits osteoclastogenesis by downregulating RANKL and upregulating OPG [105].

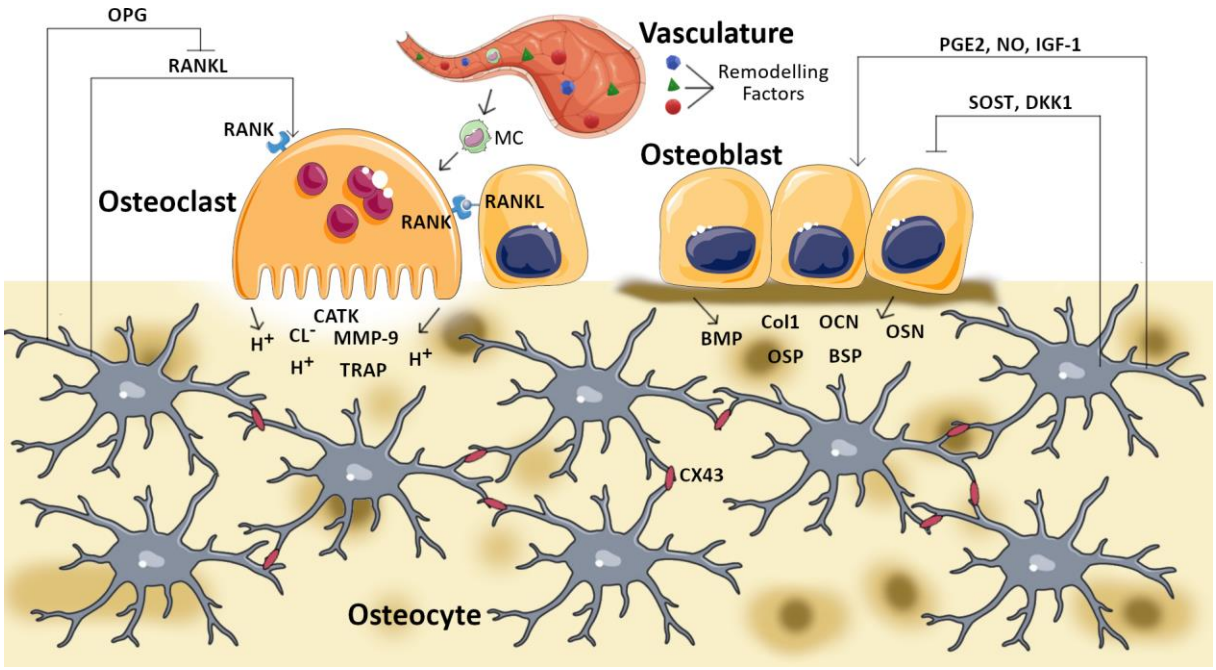

Figure 2.6: Schematic of bone remodelling and the key governing molecular mechanisms. (B). Vasculature adjacent to the remodelling site supplies osteoclast precursors and systemic factors such as PTH and vitamin D, that are involved in bone remodelling [3]. Osteoclast activation is identified by polarization and forming a ruffled border (shown), releasing hydrogen ions (H+) cathepsin K (CATK), matrix metalloproteinase-9 (MMP-9), and tartrate-resistant acid phosphatase (TRAP) that degrade the organic matrix. This catabolic activity is activated by osteoblast (OB) and osteocyte (OC) secreted and membrane bound RANKL. OB and OC can also dampen this activity through secretion of the soluble RANKL decoy receptor OPG. OB deposit collagen type (Col1) and non-collagenous proteins such as osteocalcin (OCN), osteonectin (OSN) osteopontin (OSP), bone sialoprotein (BSP), and bone morphogenetic proteins (BMP). The anabolic activity of osteoblasts is activated by factors osteocyte factors protoglandin E_2, Nitric Oxide (NO), and insulin like growth factor 1 (IGF-1) secreted by osteocytes. OB activity is also dampened by OCs through the secretion of WNT inhibitors sclerostin (SOST) and Dickkopf-related protein 1 (DKK-1). OC cytoplasmic processes cross canaliculi to make connection with other neighbouring osteocytes by connexin 43 (Cx3), which has a central role in mechanotransduction.

2.1.6 Endocrine Function

The study of bone tissue and its resident cells has largely been confined to the transduction of external forces to molecular signals that govern bone remodelling. However, recent studies suggest that bone also has an endocrine function; effecting diverse biological processes such as glucose metabolism [18] and fertility [37]. This work has been pioneered by the lab of Gerard Karsenty using mice as a model organism. They have shown that the osteoblast secreted factor osteocalcin (OCN) has effects on distant organs; specifically the pancreas, where it induces proliferation of beta cells [17], and in the testes, where it binds to receptors on Leydig cells to induce testosterone production [37]. Osteoblasts secrete both this circulating undercarboxylated OCN, and the mineral bound, vitamin K dependent γ-carboxylated OCN that remains in bone tissue due its high affinity for bone apatite [106, 107]. Undercarboxylated osteocalcin is released into the circulation, however γ-carboxylated OCN is only released once it becomes undercarboxylated, which takes place in the acidic environment of the osteoclast resorption lacunae [106]. This particular mechanism of osteocalcin release is counterbalanced by leptin signalling; when undercarboxylated OCN activates leptin signalling on adipocytes, which drives carboxylation of osteocalcin on osteocytes by the sympathetic nervous system [16]. Notably, in obese individuals, both fat mass and leptin levels have a inverse correlation with osteocalcin levels, suggesting an inverse relationship between osteocalcin and fat mass, and that leptin may be the link between the two. Thus, the mechanisms of osteocalcin decarboxylation, and hence activation, are tightly coupled to bone remodelling.

The link between bone and glucose metabolism has long been suggested. This relationship was first thought to be unidirectional; with metabolic disorders such as

diabetes effecting bone quality, resulting in patients with diabetes having increased risk of fracture [16]. However, it is now known that this relationship is more complex, and may indeed be bidirectional. Bone derived chemokines such as osteocalcin, bone morphogenetic protein, and osteoprotogerin have been shown to modulate glucose homeostasis [108]. These findings has lead to the paradigm that bone and glucose metabolism are strongly interrelated, however the specifics of this interrelation have yet to be fully defined. Nonetheless, the fact that bone has a key role to play in glucose metabolism is an exciting paradigm given it is relatively unexplored as a treatment for disorders such as diabetes. Osteocalcin is the most prominent of these bone derived chemokines, and was first suggested to be involved in energy metabolism when experiments generating osteocalcin deficient mice produced a phenotype with an abnormal amount of visceral fat [109]. Subsequent experiments revealed that these osteocalcin deficient mice are in fact hyperglycaemic, hypoinsulinemic, and have decreased β-cell mass. Interestingly, administration of osteocalcin to wild-type mice stimulates β-cell proliferation, insulin production, and increases energy expenditure, and protects against diet-induced obesity [18].

It has been known for a long time that bone metabolism is regulated by the gonads [110]. However, the extent to which gonad function is modulated by bone and its component cells has only recently been studied. Osteocalcin deficient mice breed poorly, and it has been shown *in vitro* that osteoblasts secrete factors that drive testosterone production in testis explants and isolated Leydig cells [37]. In addition, osteocalcin deficient mice have decreased testes, epidydimedes and seminal vesicle weights, and lower sperm counts [37]. This phenotype is also observed in specifically osteoblast secreted osteocalcin deficient mice. The identification of a bone derived hormone begs the question of what receptor is triggered in the organs it effects. In

both pancreatic β cells and Leydig cells, osteocalcin binds to GPRC6a to exert its function, with GPRC6a deficient mice showing the same phenotype as osteocalcin negative mice [111]. Furthermore, the effects of osteocalcin on fertility are independent of the hypothalamo-pituitary axis; the canonical system controlling male fertility.

These studies showing the influence of bone in distant organ function suffer from one main inherent limitation: the data is derived from mice. Firstly, *in vitro* testing has confirmed that osteocalcin does stimulate insulin secretion and β-cell proliferation in cultured human islets [112]. Clinically, higher serum levels of total osteocalcin, are associated with lower plasma glucose levels, improved glucose tolerance, b-cell function, and insulin sensitivity in both normal subjects and patients with T2D, prediabetes, gestational diabetes, or metabolic syndrome [113]. Furthermore serum osteocalcin levels are negatively associated with total and visceral fat [114], and increase significantly during weight loss. Longitudinal studies have found, overall, that serum osteocalcin levels are positively associated with β-cell function, but negatively associated with insulin resistance, and the subsequent development of T2D [115-117]. Additionally, as bone resorption is a mechanism by which osteocalcin is released into the circulation, one concern is that antiresorptive agents such and bisphosphonates and biologics could potentially interfere with osteocalcin, and hence energy metabolism. More research in this area is needed, as reports have shown both no change in glucose metabolism [118], or substantial increase in type 2 diabetes risk with use of antiresorptive medication [119].

2.2 Bone Pathophysiology

The focus for this thesis, and this chapter up to this point, is recreating and better understanding bone physiology. However, while *in vitro* systems facilitate the essential

pursuit of understanding biological fundamentals, the pertinent application of these systems is to inform approaches to treat bone pathology. Thus, review of the prominent pathologies that involve bone developmental processes and mature bone function is prudent and are discussed briefly below.

2.2.1 Impaired Endochondral Ossification

Developmental failures of the skeleton, as a group of conditions, are collectively prevalent, despite being individually rare. Skeletal deformities, known collectively as osteochondrodysplasias, are always due to disorders of growth, and the majority are linked to impaired of EO [120]. In many cases, chondrocyte proliferation and differentiation are effected; with IHH, PTHrP, and FGF signalling all implicated [121]. Osteochondrodysplasias are genetic disorders that occur in around 1 in 4000 births where mutations in PTHrPR, COL2A1, FGFR3, and DTDST disrupt endochondral ossification in the growth plate [122], resulting in phenotypes from mild to lethal. These genetic conditions are only partially understood, and no curative treatment exists. Additionally, conditions such as osteochondrosis result from impaired vascular invasion; the critical process that initiates bone formation in bone development (Section 2.1)

Dysregulated EO is comparatively more prominent in fracture healing of developed bone. Failures in EO can manifest in fracture non-union; fractures can exhibit delayed healing, heal in incorrect anatomical positions, or exhibit complete non-union [123]. Risk of fracture non-union is around 1.9% in the general population, but, interestingly, can increase to as high as 9% in tibial and clavicular fractures in young and middle ages adults [124]. It has also been reported the 10% of fractures do not heal properly [57]. In the UK, it is estimated that treatment for fracture non-union can cost in the

range of €8000 to €91,000 [124, 125]. The aetiology of fracture non unions isn't known, however the empirical risk factors include extent of trauma, aging, diabetes, surgical procedure, fracture type, smoking, infection, vascularisation of the fracture area, and peripheral vascular disease [126]. Current clinical treatments range from non-invasive bone stimulation [127], to surgical bone grafting and fixation [123]. More advanced therapies include platelet-rich plasma (PRP) and BMP administration, which have shown to be safe alternative to autografting [123]. Improved understanding of the mechanisms that underpin fracture healing may bring about improved outcomes in the case of non-union. As it stands, few pharmacologic interventions are available for fracture repair; despite years of candidate therapeutic testing in animals, few treatments are translated into humans [128].

Osteochondrosis is another condition effecting the growth plates in fast growing organisms, including humans, but also horses [129] where the stage of vascular invasion at the ossification front, and regression at the chondrification front during growth is dysregulated [130]. As a local failure of endochondral ossification, this condition can cause failure of chondrocyte proliferation, bone necrosis, and with persistent inadequate vascular supply, can progress to osteochondritis dessicans, where fragmentation of the necrotic tissue as a result of poor vascularisation is released into the joint. The underlying cause is unknown, but potentially may be modulated by IHH/PTHrP signalling [129], and surgery and replacement of the affected joint / tissue is often necessary.

2.2.2 Impaired Bone Remodelling

Impaired bone metabolism is the most clinically prevalent disease of bone tissue. This imbalance of bone formation and resorption is traditionally thought to be reserved for the aging population, but also effects young patients [131]. The most common

metabolic bone diseases, and of most clinical relevance, are osteoporosis, chronic kidney disease – metabolic bone disease (CKD-MBD), and Paget's disease [132]. These metabolic bone diseases are typically characterised by excessive bone resorption and incomplete or disorganised bone formation. However, each of these conditions has its own nuances. In osteoporosis for example, the loss of oestrogen in postmenopausal women is one of the key factors in osteoporosis, as it suppresses RANKL expression in marrow cells and increases OPG expression in osteoblasts [133]. In CKD, high serum phosphate is balanced by increased osteocyte secreted FGF23 in attempt to regain balance in serum phosphate levels. In addition to enhancing phosphate excretion, FGF23 suppresses 1,25(OH)2 vitamin D, which decreases intestinal calcium absorption. This chain of biological events promotes excessive PTH excretion, which leads to dissolution of calcium, and subsequent weakening of the bones [134]. Finally, Paget's disease of bone manifests as discreet areas of pathological increased bone turnover, effecting approximately 8% of men and 5% of women by the time they are 80 years of age [135]. Genetic factors have an important role, particularly those that effect the aforementioned NF-κB pathway that is involved in osteoclastogenesis [136]. Additionally, NF-κB has also been shown to be modulated by the inflammation associated with aging, termed inflammaging, and a driver of osteoclast activity in the elderly population [137] Focal Pagetic lesions are characterised by increased osteoclastic bone resorption, and increased but disorganised bone formation, leading to a loss in mechanical integrity of the tissue [138].

Combating the imbalanced bone resorption in these conditions usually mandates adequate diet and exercise, however, in many cases, therapeutics are necessary to maintain bone health. Treatment can involve targeting the underlying cause, if it is

known. For example, oestrogen therapy, or selective oestrogen receptor modulators (SERMs), or recombinant PTHrP are used as anti-resorptive treatment for osteoporosis, however are associated with off target effects in other organs [139, 140]. For excessive bone resorption, bisphosphonates are typically the therapy of choice. Bisphosphonates inhibit bone resorption by binding to bone surfaces and inhibit farnesyl pyrophosphate synthase production, leading to osteoclast apoptosis [12]. Latest generation bisphosphonates target inhibition of the RANK/RANKL/OPG pathway [13] leading to decreased bone resorption. Bisphosphonates are widely used, but are correlated to a number of side effects, such as gastrointestinal irritation, post-infusion syndrome, osteonecrosis of the jaw, and atypical fractures [141]. Biologic treatments are the most recent addition to therapies that combat aberrant bone turnover. Monoclonal antibodies against sclerostin (Romosozumab) and RANKL (Denosumab) both target reduced bone resorption, however they are associated with off-target side effects [1, 22].

A number of therapies exist for treatment of impaired bone turnover, however they are associated with adverse and off-target effects. Additionally, medications for other conditions, such as diabetes [23], epilepsy [24], and androgen therapy [142] carry warning statements for their adverse effects on bone tissue. Thus, while these conditions, or their symptoms, are treatable, we still don’t fully understand their reciprocal relationship with other tissues and organs. The adverse effects associated with bone and other medicines, and future medicines, will continue to carry unseen risk until our knowledge and models of human physiology improve.

2.2.3 Impaired Bone Endocrine Function

Bone has two primary endocrine roles. The first is comparatively more established; osteocytes and osteoblasts secrete FGF23, which partakes in the PTH/Vitamin

D/FGF23 axis by interacting with the Klotho receptor in the proximal tubule of the kidney to increase phosphate secretion and supress serum levels of vitamin D [143]. The second, less explored role is osteocalcins's role in glucose metabolism.

The FGF23 hormone secreted by osteoblast and osteocytes is a relatively new addition to the molecular control of mineral homeostasis [144]. Its expression is increased in a number of bone diseases, such as CKD, rickets, and tumour induced osteomalacia [145]. Thus, in each particular condition, it is difficult to discern if FGF23 has a cause or effect role in disease. Despite this, targeting FGF23 to increase phosphate reabsorption is a reasonable therapeutic strategy. This concept lead to a number of new therapies aiming to dampen this excess FGF23 to allow phosphate reabsorption. One particular strategy, modulation of FGF23 with monoclonal antibodies, has been developed to the point of FDA approved for treatment of X linked hypophosphatemia [146]. Given the therapeutic efficacy of FGF23 modulation for XLH, FGF23 modulation may prove therapeutically useful for other conditions where its overexpression is implicated. However, care must be taken in pre-clinical evaluation, as elevated FGF23 is associated with left ventricular hypertrophy [147].

The role of osteocalcin as a therapy for dysregulated glucose metabolism is backed by a wealth of evidence but is still not fully understood. The first mouse models clearly demonstrated a therapeutic effect from osteocalcin administration, as it could rescue a diabetic phenotype [18]. However, human data both supports and refutes osteocalcin's endocrine function. The most recent data suggests osteocalcin correlates with a number of readouts of metabolic syndrome readouts; such as diabetes risk, insulin sensitivity, body mass index, triglyceride concentrations and insulin resistance [148]. However there is also evidence to the contrary; with osteocalcin knockout mice with CRISPR showing no glucose handling issues [149].

Thus further study of the role of osteocalcin may lead to therapeutics not only for diabetes, but also fertility [37] and cognitive function [150], which it is suggested to have a role.

2.3 Models of Bone Physiology / Pathology

Section 2.2 detailed the ways in which bone development, remodelling and endocrine function can become pathological. In order to understand the basis for this pathological transition, model systems analogous to the *in vivo* condition must be employed. Both developmental and mature bone can be modelled in simplified *in vitro* models; hence a number of cell lines, and methods for isolating primary cells have been established. In addition, in order to study how these pathologies manifest at an entire organism level, numerous animal models have also been established

2.3.1 *In vitro*

In vitro systems are critical to further our understanding of how tissues and organs work *in vivo*. Though there is some overlap in the cellular composition of developing and mature bone, modelling these tissues will have different cellular requirements. Thus, the candidate cells for building *in vitro* models of these tissues will be discussed separately.

Development

The chondrocyte is the main functional cell in developing and regenerating bone. Both cell lines and primary cells are available for modelling chondrocytes. However, each have advantages and disadvantages.

ATDC5

In contrast to osteoblasts and osteocytes, very few cell lines exist for modelling the chondrocyte in developing bone. The ATDC5 cell line, derived from mouse

teratocarcinoma fibroblastic cells [151], can under sequential chondrogenic differentiation; undergoing cellular condensation, accumulation of type II collagen and aggrecan, and finally progression into hypertrophy marked by mineralisation and collagen type X expression [152]. Thus these cells are seen as good models of the hypertrophic progression seen in chondrocytes during endochondral bone formation [153]. While these cells may be suitable for many biological applications, their non-human origin is a major limitation.

Primary Chondrocytes

Primary chondrocytes are a natural candidate for developing *in vitro* models of the bone development process. However, human cartilage tissue will typically come from patients with disease tissue that is being replaced, which may be applicable in some applications, but osteoarthritic and healthy chondrocytes differ at a molecular level [154], and therefore may not be appropriate for modelling developmental chondrocytes. Other sites, such as the growth plate can be accessible in some cases, such as surgical excision in joint replacement, however, again the diseases origin of these cells may not be applicable to modelling healthy developing chondrocyte.

Bone Marrow Stromal Cells

Bone marrow stromal cells are a natural candidate cell as they are the progenitor cell of chondrocytes [77], can be easily accessed and expanded, can be of human origin, and undergo the appropriate stages of chondrogenic differentiation and hypertrophy [155]. Additionally, given their accessibility, MSCs can be isolated from donors with different disease conditions as models of a specific disease phenotype [156].

Mature Bone

A number of cell sources are available for the study of the cells of mature bone. Specifically, osteoblasts and osteocytes have a number cell lines that are used to study their function. While osteoclasts have a crucial role in bone homeostasis, osteoblasts and osteocytes are more pertinent to roles in disease modelling, as they are the source and modulators of the chemical entities that are targeted clinically in many diseases, and for the control of many physiological processes. Thus, the subsequent section will focus on *in vitro* models of osteoblasts and osteocytes

Primary Osteoblasts and Osteocytes

Osteoblasts reside on the bone surfaces and account for between 3-5% of bone cells, thus are difficult to isolate in significant numbers. Osteocytes, however, represent over 90% of the cells in bone, but are buried in a dense mineralised matrix. The study of primary osteocytes has been hampered by their lack of proliferation, difficulty in isolation [96], and their tendency to de-differentiate when cultured outside of 3D mineralised matrix [157]. In addition, any contaminating fibroblastic cells will overgrow the mitotically inactive osteocytes, allowing only for short term experiments [158]. Thus, alternatives to differentiated primary cells are often used due to these limitations.

Marrow Stromal Cells

Bone marrow stromal cells are a population of clonogenic, plastic adherent cells that reside in the bone marrow and have proven ability to generate whole bone organs, including osteoblasts and osteocytes, in functional transplant assays [159]. The ability of BMSC to differentiate into osteoblasts *in vitro* is well recognised. When exposed to dexamethasone (or vitamin D_3), ascorbic acid, and β-glycerophosphate *in vitro*, BMSCs secrete a collagen 1 rich matrix mineralised with hydroxyapatite crystals; indicative of osteogenic differentiation [160]. In addition, these BMSCs express

RUNX2 [160], tissue non-specific alkaline phosphatase (TNAP) [161], Osteocalcin [162], osteopontin [163], and collagen 1 [162], which are all expressed by osteoblasts *in vivo* [94, 164].

While there is clear evidence that MSCs can differentiate into osteoblasts, the extent to which they can further differentiate into osteocytes is less explored. In mice, 2D cultures of C57BL/6 BMSCs have been shown to express osteocytic genes after 2 weeks in osteogenic media, secrete the WNT inhibitor sclerostin, and be responsive to PTH and mechanical stimulation [165]. Monolayer MSCs derived from adipose tissue also show osteocytic gene expression after 3 weeks when cultured in osteogenic media supplemented with epidermal growth factor (EGF) [166]. Osteocytes however, reside in a 3D mineralised matrix, which research suggests is crucial for their differentiation and maintenance. 3D matrices have also been employed to drive osteocytic induction of BMSCs; Thrivikraman *et al.* cultured human BMSCs in collagen matrices in medium supersaturated with calcium and phosphate ions, which are prevented from spontaneously mineralising with osteopontin [167]. These cells expressed osteocalcin, and osteocyte gene markers DMP-1 and E11 after 21 days in culture [168]. Thus, evidence supports the potential for obtaining functional osteocyte cultures through optimised MSC differentiation, and this would fill a critical need for *in vitro* models of osteocytes.

MLO-A5

MLO-A5 is a late osteoblastic / preosteocytic cell line that is isolated from the long bones of transgenic mice in which the oncogene SV40 is expressed under the control of an osteocalcin promoter [169]. These cells represent early osteocytes embedded in osteoid; expressing high osteocalcin, alkaline phosphatase (ALP), collagen type 1, parathyroid hormone/parathyroid hormone–related peptide (PTH/PTHrP) receptor,

and bone sialoprotein (BSP). At this differentiation stage, early osteocytes begin to generate cell processes, which is modulated by E11/gp38/PDPN, and this process is reproduced by MLO-A5 cells in culture [170].

MLO-Y4

MLO-Y4 is a mature osteocyte cell line derived from the same transgenic mouse as the MLO-A5. The process for isolation is almost identical for both cells, only MLO-Y4 cells are isolated from the bone digestion, and MLO-A5 cells are isolated from the bone chips resulting from the digestion. MLO-Y4s have been essential in studies of osteocyte apoptosis and mechanotransduction. However, as with MLO-A5s, these cells are murine derived, don't mineralise or produce sclerostin [171].

IDG-SW3

The IDG-SW3 cell line is a more recent osteocyte analogue and is derived from long bones of mice expressing a thermolabile SV40 Large T antigen that is regulated by interferon γ crossed with mice carrying a DMP-1 driven GFP mutation [172]. This allows these cells to proliferate at 33˚C and resume their osteogenic phenotype at 37-39˚C. The IDG-SW3 cell line represents the late osteoblasts that can mature into mature osteocyte like cells. These cells produce mineralised matrix, and express many osteocyte related genes after 3-4 weeks of culture, such as DMP-1, MEPE SOST, and FGF23 [171]. Furthermore, these cells exhibit a dendritic morphology and are responsive to parathyroid hormone treatment [172]. This cell line has been used to study the osteoblast to osteocyte differentiation process [173], mechanosensitivity [174], osteocyte response inflammation [175]. One of the key differentiating features of IDG-SW3 cells from MLO-Y4 and MLO-A5 cells is their higher expression of FGF23. Although initially absent, FGF23 rises to detectable levels post differentiation, thus this cell line have been used in a number of studies to study FGF23 in osteocytes [175-

177]. However, as this cell line is a mixture of osteoblasts and osteocytes at various differentiation stages, fluorescence activated cell sorting (FACS) would be required for enriched osteocyte cultures [171].

OCY454

OCY454 is another murine derived osteocyte-like cell line that was developed to express and secrete sclerostin at early time points in the absence of differentiation factors [178]. OCY454 are also mechanosensitive, adjusting their sclerostin expression in response to fluid flow, and making them a candidate cell for studying crosstalk between osteocytes and other cells. For example, OCY454 have been used to study the influence of osteocyte mechanostimulation on bone remodelling cells [179, 180]. In addition, OCY454s have been used to study the effects of osteocyte secretions on skeletal muscle differentiation [181].

OMGFP66/10

OmGFP66 and OmGFP10 are two very recent cell lines that show striking morphological similarity to *in vivo* osteocytes. Cells from the calvaria of DMP-1-GFP mice are isolated and immortalised by transfected to express the SV40 T-antigen. OMGFP66 and OMGFP10 are specific clones of these isolated cells, selected based on high GFP expression and ability to mineralise in 2-3 weeks [182].

Vascular Cells

Bone is highly vascularised and contains a dense network of vessels both in the soft marrow and hard mineralised tissue. The relevance of vasculature in bone physiology has already been discussed, thus endothelial cells are a necessary consideration for physiologically accurate *in vitro* bone models. Endothelial cells (ECs) are a heterogeneous population, with phenotypes that reflect their *in vivo* niche. Bone

microvascular ECs would naturally be an ideal candidate for bone models, however while a bovine clonal EC line has been reported [183], it has not been used extensively, and no cells from human origin exist. However, it must be noted that bone ECs have shown to be sensitive to hormones involved in bone homeostasis, such as parathyroid hormone (PTH), where ECs from other sources have not [183], and bone ECs have been shown to express oestrogen receptors, and to proliferate and show inhibited PTH responsiveness when treated with oestrogen [184]. Despite this, primary human cells, such as HUVECS and HMVECs are ubiquitous as the endothelial component in engineered vasculature for *in vitro* organ systems [33, 185].

2.3.2 *In vivo*

Animal models are the gold standard for both basic and applied bone research. *In vitro* models excel in their simplicity, resource requirements, and the extent to which they can be controlled, however, *in vitro* systems cannot reproduce an entire organism response, thus *in vivo* animal models are essential tools for studying the role of endogenous proteins or therapeutics at the level of the entire organism, and are required for validation of new therapeutics [20].

There are a number of established animal models of human bone disease that are deemed adequate models [10]. For example, ovariectomised mice, rats and non-human primates recreate the serum biochemical, histological, and densitometry findings in adult female humans [10]. Mice and dogs serve as models for skeletal metastasis [12], however given the heterogeneity, there is a plethora of non-standardised models are used for the various presentations of the disease. Other models, such as hindlimb suspension, is a common model of disuse induced bone loss that is a common side effect of many conditions [8]. However, like with models of

skeletal metastasis, the heterogeneity of disuse induced bone loss, the models themselves, or the functional outcomes are not standardised. Genetic knockout tools can be used to produce a specific disease phenotype, such as the $OCN^{-/-}$ mouse that recreates the diabetic phenotype [18], or $SOST^{-/-}$ mouse as a model of sclerostosis [186]. The combination of more traditional experimental models, such as hindlimb suspension, and genetic tools is promising for the development of new *in vivo* models.

Though *in vivo* models are critical for basic research, there are still some major limitations. Firstly, the species mismatch is one of the most critical limitations of animal models. Despite the efficacy of animal models in recreating a specific disease phenotype, many critical biological functions in humans and animals are distinctly different. For example, mice can recreate the symptoms of multi system inflammatory responses in conditions such as sepsis and acute respiratory distress syndrome, the mechanisms that drive these processes in mice are distinctly different to humans [187]. A similar phenomenon exists with Alzheimer's disease [19]. In a bone context, mice do not present haversian remodelling or closure of the epiphyseal growth plate as occurs in humans [188]. Additionally, bone composition is different between species [189]. Though animal models may be able to recreate a phenotype indicative of bone disease, the above evidence suggests the governing molecular processes may differ, thus leading potential false indicators of treatment for human disease.

2.3.3 Clinical predictivity of bone models

These *in vitro* and *in vivo* models are used for both basic, and applied research. However, for applied research, models have the unique requirement of being evaluated for their predictivity of human response. Specifically, the success of a pre-

clinical model is measured by its ability to predict human response at the population level. The only indicator of this is the clinical attrition rate of the therapeutics targeting molecular processes identified in pre -clinical systems. The statistics in this regard are bleak, with 8 out every 9 candidate therapies identified in pre-clinical evaluation ultimately failing [21]. This failure can arise from unidentified differences in disease mechanisms between animals. For example, In Alzheimer's Disease, mice that are engineered to develop neurofibrillary tangles, a hallmark of the condition, have not translated well into humans, due to differences in the underlying mechanisms, despite the disease phenotype being similar between species [19]. In a bone context, a number of disease modifying osteoarthritis drugs (DMOAs) that showed potential in pre-clinical results showed uninspiring efficacy once they reach the clinic [10]. Furthermore, next generation osteoporosis drugs, such as the anti-sclerostin monoclonal antibody romosozumab showed adverse cardiac events in the clinic [1]. Additionally, other osteoporosis [22], diabetes [23], and epileptic [24], and acid reflux [25] medications have all shown negative bone health consequences post marketing, thus indicating the interactions of other medications with bone tissue are not adequately accounted for in pre-clinical models. Clearly, development of improved models of human bone physiology are needed to improve basic understanding and hence improve therapeutic efficacy.

2.4 Microphysiological Systems (MPS)

Current pre-clinical models of bone are clearly producing a low number of therapeutic products with a higher risk profile that would otherwise not exist with optimal models. One of the most promising solutions to this problem is developing more sophisticated *in vitro* models that are more representative of tissue and organ physiology. Microphysiological systems (MPSs), or organ-on-chip systems are one such

application that are advanced models of human tissues and organs that recreate biological function at the microscale, and are a potential platform to augment both basic biological research and the drug development process [190]. MPS systems can be designed to include complex geometries, real time analyte sensing, mechanical loading, and tissue vascularisation [191], and are thus an ideal platform on which to develop advanced models of bone physiology and pathophysiology.

2.4.1 Fabrication and Design

MPSs require the fabrication of small channels, most typically in the region of tens of microlitres, for media and hydrogel injection for cell culture. The most common technique to achieve this is replica moulding; a process for shaping pliable polymer materials using a micropatterned rigid frame, or master. Casting curable polymers on to the master, allowing to set, and removing from the master can be repeated to make multiple replica moulds. These moulds are then typically bonded to a glass coverslip substrate for imaging purposes and sterilised for cell culture (Figure 2.7).

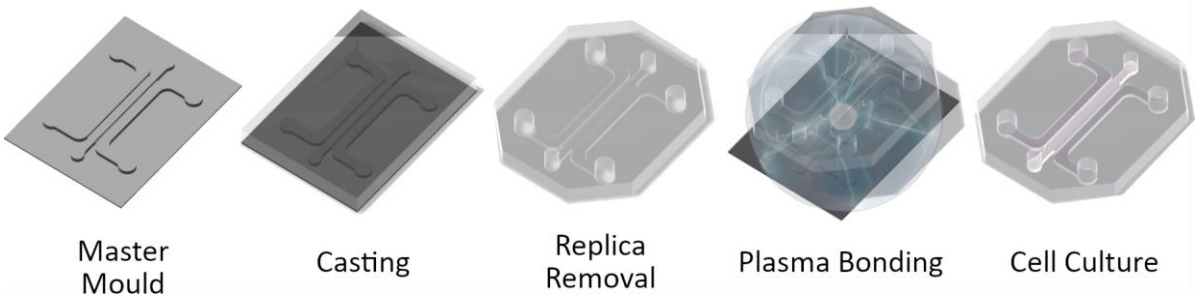

Figure 2.7: General microphysiological system fabrication process. MPS devices are fabricated through first generating a positive master mould. Then, a moulding material is cast on to the master and allowed to cure. Once cured, the imprinted replica is removed from the master, plasma treated to impart hydrophilicity to the surface, and bonded to a coverslip before sterilisation and subsequent cell culture.

The above figure depicts a generalised method for fabricating MPS devices. There are however, a number of fabrication methods used to make MPSs, by far the most common of which is soft lithography; a set of techniques encompassing making

moulds using photolithography, replica moulding using elastometric polymers such as polydimethylsiloxane (PDMS), and functionalising surfaces for biological applications [192]. Although soft lithography is most widely used technique for MPS fabrication, with the number of groups beginning research in the area of MPSs, a number of non-lithographic, more accessible methods of master fabrication have now been reported [193]. For example, laser cutting and micromachining can create features in polymers down to tens of microns; suitable for microfluidic applications.

The design and geometry of MPS systems vary considerably depending on the final application. For example, MPS devices can have multiple channels to incorporate multiple tissues (Figure 2.8A). Mechanical integration can also be achieved through addition of vacuum channels; facilitating biologically relevant mechanical stimuli such as gut peristalsis, or cartilage compression (Figure 2.8B). Additionally, perfusable, physiologically relevant vasculature networks can be engineered into MPSs to model processes where vasculature has a critical role, such as tumour cell extravasation [30], or vascularisation of a cartilage template in EO [14] (Figure 2.8C). Among the most exciting and unique prospects of MPS systems is the integration of multiple organs in 'body-on-chip' or 'physiome-on-chip' applications. This can be achieved, with integration of multiple organ systems in to one MPS device, or the fluidic coupling of a number of MPS systems with liquid handling technology [32] (Figure 2.8D). This function is critical for making closer approximations to human physiology at the entire organism level.

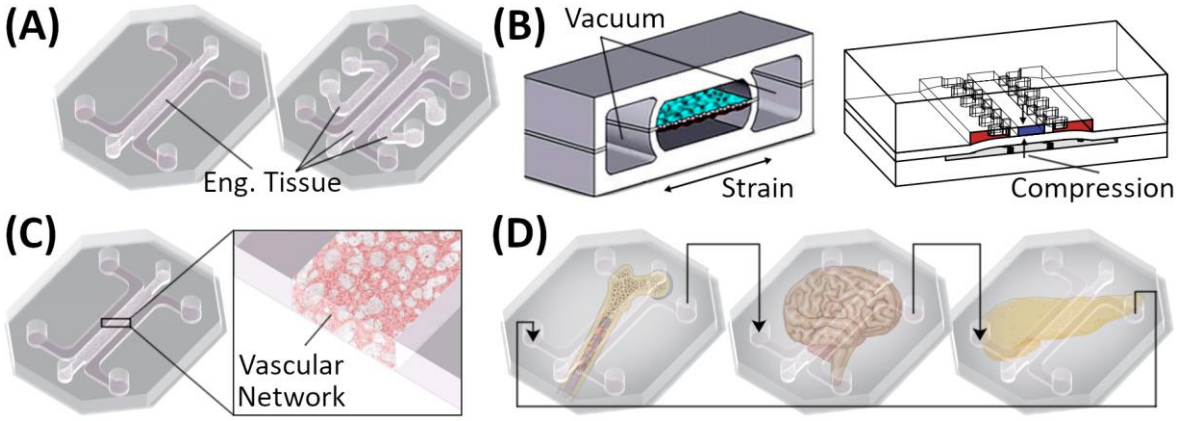

Figure 2.8: MPSs integrate physiologically relevant functions for advanced *in vitro* modelling. (A) MPSs geometry can be varied to include numerous fluidic channels for engineered tissues and media. **(B)** Mechanical stimulation integrated into MPS devices through integration of pneumatic channels that stretch or compress tissues [31]. **(C)** Perfusable vascular networks can be engineered into MPS devices for more physiologically relevant engineered tissues. **(D)** Fluidic coupling of multiple MPS organs to closer approximate the entire organism by modelling multi-organ interactions.

2.4.2 Applications in Drug Discovery

The primary motivating force for the funding and development of MPS systems was the lack of efficacy of animal models in recreating human physiology and predicting drug responses. Despite the nascency of the field, MPS systems have already revealed findings that were not observed in animal models. For example, lung MPS systems subjected to cigarette smoke could identify ciliary abnormalities and exhibited a COPD specific lung phenotype, which could not be achieved as effectively in animal models [194]. Additionally, replication of host cytokine and immune cell responses, and clinical responses in an MPS of human influenza virus has been achieved that is incredibly difficult to replicate in animal models [195, 196]. Finally, a human kidney MPS model system unveiled a unique mechanism by which an the antibiotic polymyxin induces kidney damage [197]. Thus, MPS systems, despite their recently short history, have and are contributing valuable biological knowledge to the scientific community on which advances in medicine can be made.

Research articles are an indicator of the utility of any novel technology, and in this context, MPS systems indeed look very promising. Initial publications in the early

2000s focussed primarily on microfluidic fabrication techniques, but since the publication of the first lung on a chip article [198], MPS and organ on chip related publications have been increasing, resulting in a 46% compound annual growth rate between 2007 and 2017 [199] (Figure 2.9). However, this potential must materialise; specifically through the adoption and integration of MPS technologies by pharmaceutical and government agencies. There is plenty of evidence that this is the case. The FDA is already adopting MPS systems for study of toxicology [200] and radiation countermeasures [201]. In a pharmaceutical context, large manufacturers, such as Roche [202], and AstraZeneca [29, 203] are working with MPS systems. Thus, the efficacy of MPS systems in biological research has initiated widespread adoption is slowly starting to percolate into commercial settings.

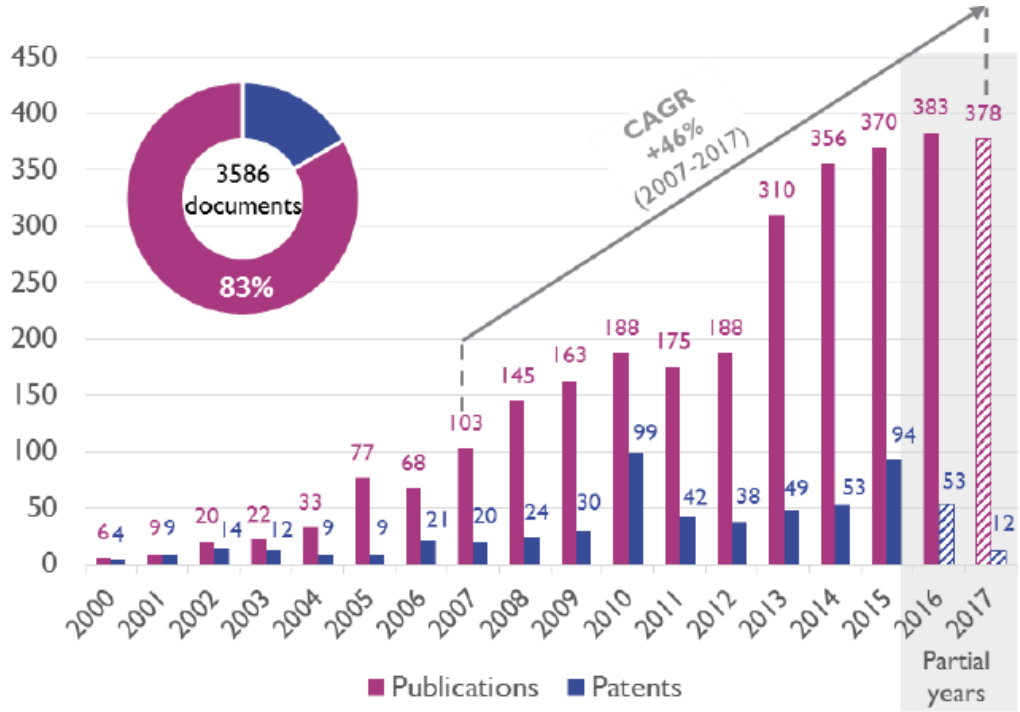

Figure 2.9: MPS and organ on chip related scientific publications and patents from 2000-2017. Reproduced from [199].

Finally, one of the key considerations for further wider adoption of MPS systems is integration of MPS systems into current infrastructure. The vast majority of MPS

systems exist as PDMS replicas bonded to a coverslip (as per Figure 2.7), and while liquid handling robots can automate the processing of these devices [32] (Figure 2.9A), this type of resource requirement is inhibitive in the context of adoption of new laboratories and integration into existing systems. However, companies such as MIMETAS, have taken an innovative and alternative approach by integrating organ systems into conventional 96 and 384 well plates (Figure 2.9B), which have been adopted by pharmaceutical manufacturers for drug discovery research. Innovations such as this that integrate the MPS concept with current laboratory and R&D infrastructure will be essential in ensuring adoption of MPS technology.

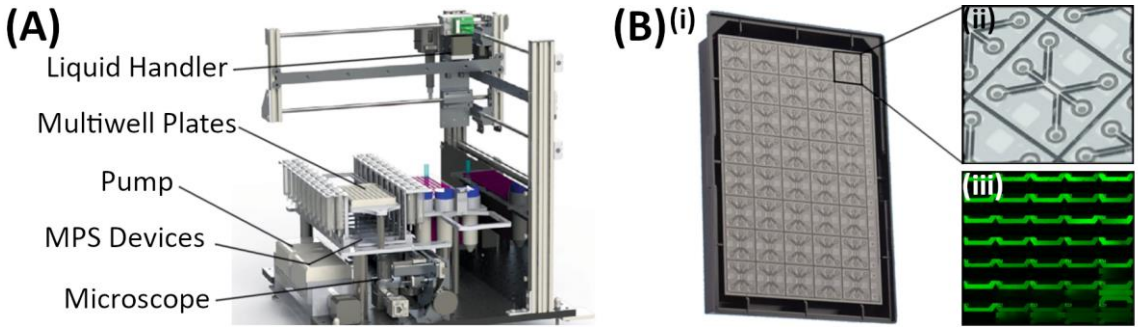

Figure 2.10: Towards translation and adoption of MPS technology. (A) Liquid handling devices have been developed to fluidically couple MPS devices. **(B)(i)** MPS technology in standard multiwall plate format containing **(ii)** 3 channel devices that can accommodate testing **(iii)** multiple experimental groups in one plate.

One of the final key challenges for the translation of MPSs is the lack of defined quality standards. Medical devices and pharmaceutical products have quality standards that define the requirements for how products are designed and manufactured to be in compliance with FDA and medical device regulation. While these specific standards can provide a framework for standardisation for MPSs, specific standards are required to cover standardisation of materials, manufacturing, test methods, and validation for example [204]. Establishment of quality standards for MPS development, manufacture and validation will be essential for regulation of these products.

2.4.3 Applications in Modelling Bone

MPS application have typically focussed on engineering organs primarily involved in drug metabolism and toxicity: intestine, lungs, liver, and kidney. Firstly, a complete model of drug metabolism *in vitro* will require models of secondary tissues, such as bone, that are not canonically involved in these processes, but can be the target of drug side effects [205]. Secondly, separate to drug discovery, the integration of physiological functions in MPSs such as mechanical stimulation, vascularisation, and multi organ coupling make it an ideal platform to develop models of specific bone pathologies and biological processes.

The most prominent area of bone research using MPS technology is in cancer research. Circulating tumour cells that have disseminated from a primary tumour commonly migrate to bone tissue and form a secondary tumour; particularly in breast and prostate cancer [206]. This clinical finding has motivated the development of models of bone metastasis using tissue engineering principles to try and better understand this process. Bersini et al. osteogenically pre-differentiated BMSCs in monolayers before embedding them within a collagen matrix in an MPS as an analogue of bone tissue [33]. This model was vascularised by adding HUVECs to form an endothelialised channel parallel and adjacent to the bone channel. Breast cancer cells were found to extravasate through the endothelium into the bone matrix channel at higher rates compared to a control matrix; with receptor CXCR2 and chemokine CXCL5 playing a major role in this process. A similar study followed with an alternative MPS design, this time incorporating a physiologically relevant, self-assembled vascular network perfused with tumour cells. Again, this system showed that the bone mimicking environment favours metastasis, and additionally showed that adenosine is

a key modulator of metastasis in skeletal tissues [207]. Hao et al. created a similar model by using an osteoblast cell line, MC3T3-E1, to create osseous tissue within an MPS system, then seeded this with MDA-MB-231 and MDA-MB-231-BRMS (metastasis suppressed) breast cancer cells to monitor colonisation of the osseous tissue [208]. Using this model, they found that metastasis suppressed cells actually colonise the osseous tissue more aggressively, but that metastasis is more frequently single cells, rather than micrometastatic cell clusters. Marturano-Kruik *et al.* also created a vascularised bone model; seeding demineralised bone matrix (DBM) with undifferentiated hBMSCs and HUVECS [209]. HUVECs self-assembled into vascular networks on the DBM, which was subsequently perfused with MDA-MB-231 breast cancer cells. These cancer cells assumed a slow proliferative, drug resistant phenotype when cultured with interstitial flow. Thus, MPS of vascularised bone can, and have been, employed to make significant contributions in cancer research.

Very few other areas of bone physiology or pathophysiology have been modelled using MPS technology. For MPSs to make contributions significant advances in bone research, creating predictive models of both bone development and remodelling will be essential. The main diseases that affect bone either target growth and development, or effect remodelling of developed bone. At the time of writing, no applications have been published in the area of bone development in an MPS. Furthermore, MPSs of bone regulatory function in a remodelling or endocrine context have been scarcely reported. George *et al.* fabricated remodelling on chip applications using a PDMS device that could mechanically stimulate osteocytes and subsequently flow conditioned media to cultures of osteoblasts and osteoclasts [210]. Despite the relatively low number of published MPS applications in bone remodelling, this field is intensely studied using conventional *in vitro* methods [211, 212]. Predictive models of

bone development and its regulatory function would be a significant benefit to biomedical research, and MPS technology is a potential platform to facilitate these applications.

From the above, it is clear that MPS technology has potential as a platform to build advanced models of human bone and accelerate progress in both basic research and drug discovery. In light of this, the proceeding chapter focusses on incorporating vasculature into MPS devices given the critical role of vasculature in bone development, physiology and repair. More specifically, it investigates the ability of human bone progenitor cells to support endothelial cell vascular network formation within MPS devices.

Chapter 3: Vascularised MPS Templates for Bone Research Applications

3.1 Introduction

Vasculature has the canonical role as a conduit for the exchange of nutrients, signalling molecules and metabolites for tissues and organs. In addition, it also has key roles to play in tissue specific processes and pathologies. In bone, vasculature is essential in development and fracture repair [15], bone remodelling [213], and maintenance of the skeletal stem cell phenotype [97]. In a pathological context, vascular disruption is a hallmark of a number of prominent pathologies [2]. For example, impaired angiogenesis and vascularity correlates with increased bone loss in osteoporosis [214-217]. Additionally, systemic diseases such as diabetes mellitus leads to the development of microangiopathy [217], and impaired blood flow in long bones [218], which correlates with altered bone microstructure and higher risk of fracture [219]. Fractures are also induced in avascular necrosis of the femoral head (ANFH) when vascular supply is disrupted, which can be for traumatic and non-traumatic reasons [220]. Vasculature clearly has diverse roles in both bone function and disease, and thus is a necessary component within for analogues of bone.

Until recently, three dimensional, perfusable, physiologically relevant vasculature could not be easily recreated *in vitro*. However, MPSs have been reported that facilitate engineering these vascularised tissues [221]. Such MPS systems may facilitate engineering more physiologically relevant bone models, potentially leading to significant discoveries and the development of new therapeutics. There are, however, few examples of MPSs being utilised in bone applications, despite their significant potential for the accurate modelling of bone physiology. One area where MPS have

demonstrated their utility is in the study of breast cancer metastasis to bone; metastasising cancers of the breast and prostate have an affinity for bone tissue, with post-mortem examination showing 70% of patients have bone metastases [222]. This has motivated the development of vascularised bone systems to model breast cancer cell extravasation through the vasculature into the bone niche [33, 207].

Endothelial cells require a support cell form stable blood vessel networks [223]. The vast majority of vascularised MPS applications use stromal cells as a support cell to facilitate HUVEC vasculogenesis, such as normal human lung fibroblasts (NHLFs) and dermal fibroblasts [30, 185, 221, 223, 224]. However, bone applications warrant a stromal cell relevant to the bone niche. Bone marrow stromal cells (BMSCs) are progenitor stromal cells that reside in the bone marrow that have demonstrated angiogenic potential [225, 226].

This chapter describes the development of templates for developing perfusable vascular networks within MPS devices using bone marrow stromal cells (hBMSCs) as support cells to human umbilical vein endothelial cells (HUVECs). Specifically, the goal is to engineer perfusable interconnected vascular networks within a microfluidic chip using hBMSCs to support HUVEC vasculogenesis. hBMSCs are the canonical bone progenitor cell, used as models of chondrocytes [227], osteoblasts [228] and osteocytes [228], and are of human origin. They can therefore potentially play two roles within an MPS of bone; firstly, to support HUVEC vasculogenesis, and secondly as a progenitor cell for the development of cartilage or bone tissue within the MPS. Herein the development of two vascularised MPS platforms is described using two cellular arrangements in two separate microfluidic devices, that can be applied to developing advanced MPS models of bone tissue.

3.2 Methods

3.2.1 Device Fabrication

Microfluidic Devices were fabricated using replica moulding. Master moulds were obtained from the MECBIOMED lab at University College London department of mechanical engineering. Master moulds were fabricated by laser cutting the channel geometries from 1mm thick poly(methyl-methacrylate) (PMMA) sheets and adhering to 30mm diameter PMMA plates using acrylic glue (Scigrip 4SC, USA). Master moulds were then glued to the bottom of 100 mm diameter petri dishes. To create microfluidic chips, sylgard 184 (poly)dimethylsiloxane (PDMS) (Dowsil, USA), was mixed at 10:1 (polymer : catalyst), degassed under 40 mbar vacuum for 10 minutes and poured on master moulds. PDMS was allowed to cure overnight at 80˚C. Once cured, PDMS replicas were removed by cutting around the circumference of the mould and removing with a spatula. PDMS replicas were then trimmed and cleaned using adhesive tape. To form the microfluidic devices, PDMS replicas and #1.5 thickness glass coverslips (160-190µm) were plasma treated with corona plasma (Corona SB, BlackHole Labs, Paris) for 1 minute each and pressed together. Devices were then placed in an oven overnight at 60˚C for hydrophobic recovery. Finally, devices were sterilised using ethylene oxide and allowed to air for 2 days before culture. 3 Channel device features are shown in Figure 3.1. 5 channel devices have additional channels and the hydrophobic barrier is provided by PDMS pillars.

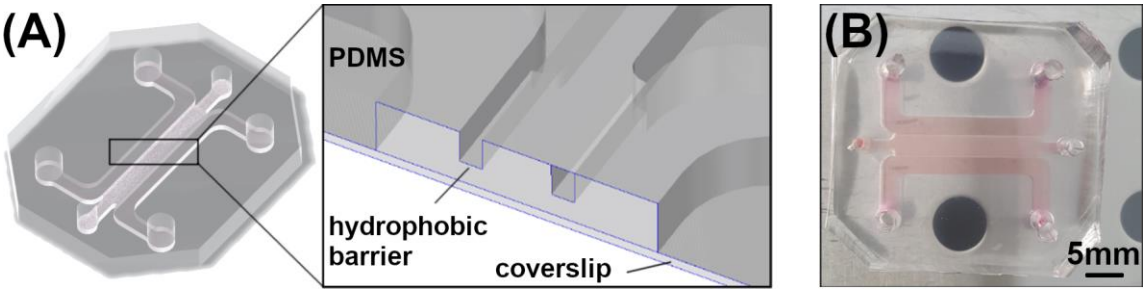

Figure 3.1 Features of the microfluidic devices. (A) Microfluidic devices consist of a PDMS master bonded to a glass coverslip, individual channels are separated by a PDMS partial wall, which acts as a hydrophobic barrier, allowing hydrogel to flow through the channel when injected into the device without leaking into the adjacent media channels. **(B)** Image of the microfluidic device.

3.2.2 Cell Culture

Media Formulations

Expansion Medium (XPAN): XPAN medium was used for monolayer expansion. XPAN medium consisted of high-glucose GlutaMAX Dulbecco's modified Eagle's medium (DMEM) supplemented with 10% v/v fetal bovine serum (FBS), 100 U/ml penicillin, 100mg/ml streptomycin (all Gibco Biosciences, Dublin, Ireland) and 5 ng/ml FGF-2 (Peprotech, UK).

Endothelial Growth Medium 2 – Microvascular (EGM)

EGM-2MV (herein referred to as EGM) was used for HUVEC expansion and MPS culture. Endothelial Basal Media (CC-3156, Lonza) was fully supplemented with EGM™-2 MV Microvascular Endothelial SingleQuots™ Kit (CC-4147) as per the manufacturer's instructions.

Cell Culture

Human Bone Marrow Stromal Cells (hBMSCs)

Whole human bone marrow (Lonza, USA) was purchased and hBMSCs were isolated. Whole bone marrow was plated at 2000 cells/cm^2 and expanded in XPAN for one week at 37°C, 5% O_2 and 5% CO_2. Once colonies had formed, cells were trypsinised

and subculutred until sufficient cell numbers were achieved, cells were then frozen down and stored in LN_2 before use. The donor used was evaluated for osteogenic, adipogenic, and chondrogenic capacity. For experimental expansion, hBMSCs were plated at 5000 cells/cm^2, expanded in XPAN until confluent and passaged at 80% confluence. hBMSCs at P4 were used for all experiments.

Human Umbilical Vein Endothelial Cells (HUVECs)

Green fluorescent protein expressing human umbilical vein endothelial cells, herein referred to as HUVECs, were purchased from Angio-proteomie. HUVECS are transduced with a lentiviral vector carrying a GFP transgene at P1 and theses transduced cells are selected for puromycin resistance. Transfected cells are HUVECs were expanded in microvascular endothelial growth media (EGM-2MV, Lonza) on rat-tail collagen coated T75 flasks at 10µg/cm^2. HUVECs were used at passage 8 for all experiments.

Microfluidic Device Culture

Microfluidic devices were seeded with a co-culture of hBMSCs and HUVECs. Each channel holds 100 µL of hydrogel. hBMSCs and HUVECs were trypsinised and separately resuspended in medium containing with 4U/ml thrombin (Sigma Aldrich, Ireland) at 4X the desired final concentration. Equal parts of the hBMSC and HUVEC cell suspensions were mixed, and 50µL of this combined suspension was mixed with 50 µL of 6mg/ml bovine fibrinogen (Sigma Aldrich, Ireland), mixed and quickly pipetted into the microfluidic devices. Fibrin was allowed to clot for 40 mins in a humidified incubator, after which EGM-2MV is added to each device. Media was exchanged daily.

3.2.3 Design of Experiments

Fractional factorial design of experiments (DOE) was used as a tool to optimise vascular network perfusability [229]. Specifically, in some vascularised templates, a number of factors identified from the literature were tested to ascertain their effects on improving network perfusability. These factors were; addition of HUVEC monolayers to the media channels at $1x10^6$ cells/ml [230], supplementing the EGM-2MV with additional 50ng/ml vascular endothelial growth factor (VEGF) [30], varying fibrin concentration at 3mg/ml and 10mg/ml [231-233], supplementing the EGM-2MV with additional 250 nM sphingosine-1-phosphate [234], and varying oxygen tension at 5 and 20% [235]. The resulting DOE used to explore these factors is shown in Table 3-1.

Table 3-1 Groups Explored in DOE experiment

Group Number	**Channel ECs**	**VEGF**	**Final Fibrinogen Concentration**	**Sphigosine-1-Phosphate**	**Oxygen**
1	None	0	3	250	20
2	Present	0	3	0	5
3	None	50	3	0	20
4	Present	50	3	250	5
5	None	0	10	250	5
6	Present	0	10	0	20
7	None	50	10	0	5
8	Present	50	10	250	20

3.2.4 Characterisation of Network Morphology

Overall Network

Entire constructs were imaged to analyse vascular formation. Images were analysed using a custom macro to automate processing in Fiji is just ImageJ (FIJI) [236] (Appendix 1). Images were cropped into user defined regions of interest (ROIs), despeckled, and contrast adjusted to increase signal to noise ratio. Images were then gaussian blurred and thresholded using FIJI's Li algorithm. Finally the resulting binary image was skeletonised and analysed using FIJI's analyse skeleton function [237]. Automated thresholding was checked against the original image.

3.2.5 Perfusion

Vascular network perfusion was evaluated by perfusion of fluorescent dextran. 10kDa dextran (Sigma Aldrich, Ireland) was diluted in PBS to 2mg/ml, vortexed and stored at 4˚C protected from light. Media was removed from both channels and device placed on a Leica SP8 scanning confocal microscope stage. Once positioned for imaging, dextran was introduced to one channel and filled to the top of the feeding port of each device to create a hydrostatic pressure gradient across the vascularised hydrogel. Images were taken immediately to avoid excessive diffusion of dye across the bulk hydrogel.

Vasculature-Media Interface

Vasculature at the gel-media interface was analysed to asses dextran accessibility to vascular network. At day 7, devices were perfused as per section 3.2.5, and confocal z stacks were taken at the vessel-perfusate interface. Diameter of vessels in the perfusion direction (orthogonal/perpendicular to the Z stack direction were analysed using FIJI.

3.2.6 Statistical Analysis

Fractional factorial experimental set up and analysis was performed using Minitab statistics package (Minitab, USA). For analysis, main effects plots and pareto charts were generated. The standardised effect of each factor was considered significant at $\alpha=0.05$. Comparisons made between 2 groups, or multiple groups were analysed using GraphPad Prism (GraphPad, USA) using student's t-test or one-way ANOVA respectively. Non-parametric tests were used where assumptions of normality could not be justified. Graph notation for deemed significance is as follows: * $p<0.05$, ** $p<0.01$, *** $p<0.001$, **** $p<0.0001$.

3.3 Results

3.3.1 A direct co-culture of HUVECs and a low number of hBMSCs supports the development of perfusable vasculature within an MPS device

Direct vascularisation, combining GFP-HUVECs and hBMSCs together in a fibrin hydrogel, as a template for MPS device vascularisation was first explored (Figure 3.2A). The effect of hBMSC number on the formation and perfusability of the formed vascular networks was initially assessed. A total cell number of 600,000 (400,000 HUVECs; 200,000 MSCs; 33%) was initially maintained within the central chip channel, as this percentage of non-endothelial cells has previously proven successful for engineering perfusable networks [230]. The highest relative numbers of hBMSCs (33% and 10%) evaluated were found to facilitate the formation of vascular networks, with decreased branching and larger vessels correlating with decreased relative proportions of hBMSCs, however networks were not perfusable (Figure 3.1B). Further decreasing hBMSCs to 5% (of total cell number) induced perfusability, but vascular

networks do not form. By maintaining this absolute number of hBMSCs (30,000) within the channel, but reducing the total number of HUVECs to 400,000, it was possible to promote both vascular network formation and perfusability (Figure 3.1C). Quantification of the formed vasculature substantiated the qualitative evidence, with decreases in branch density and increases in the percentage of perfusable devices observed with reductions in the proportion of hBMSCs within the MPS device (Figure 3.1D).

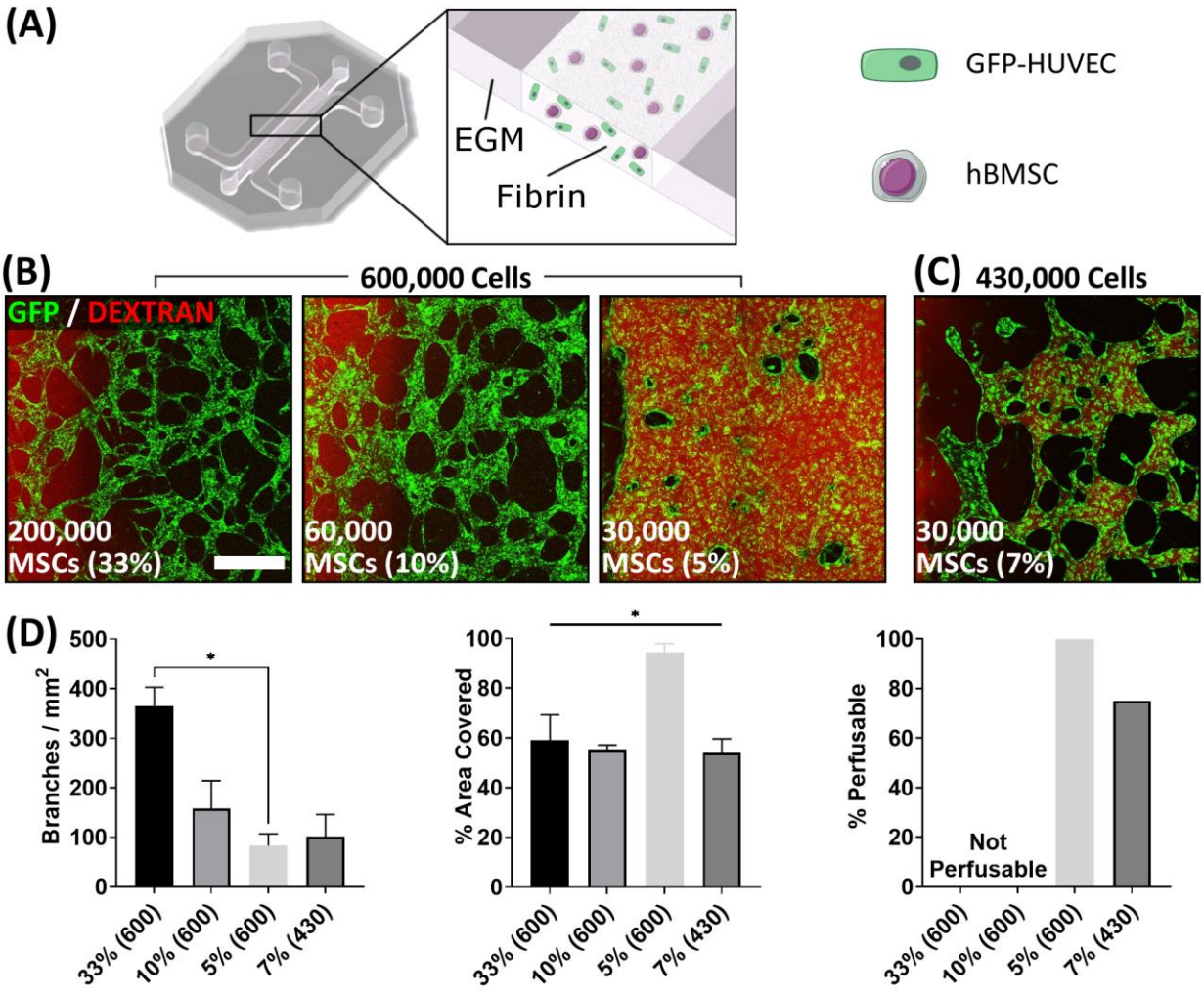

Figure 3.2: Direct vascularisation in a MPS device using hBMSCs and HUVECs facilitates vasculogenesis and perfusability at low cell numbers. (A) Schematic showing the direct hBMSC vascularisation approach in a MPS device **(B)** For a fixed total number of cells within the channel (600,000), decreasing fractions of hBMSCs induces perfusability but inhibits vascular network formation. Scale bar = 200µm. **(C)** By decreasing the total number of cells within the channel to 430,000, whilst maintaining a lower proportion of BMSCs (7%), an interconnected and perfusable vascular network can be established. **(D)** Quantification of vascular branch density, % area vascularised, and % of devices perfusable. n=4 for all groups * p<0.05

3.3.2 Increased fibrin concentration increases vessel diameter at the perfusate-vascular network interface

Recognising that certain applications of MPS might require higher numbers of hBMSCs, it was next sought to optimise the direct vascularisation MPS template for perfusability using higher numbers of hBMSCs. With 33% hBMSCs, a number of factors for their influence on perfusability were screened. We used a fractional factorial experimental design [229, 238] to explore 5 different factors: presence of an endothelial monolayer in the media channels, EGM supplementation with VEGF, increased fibrin concentration, EGM supplementation with sphingosine-1 phosphate (S1P), and oxygen tension, as outlined in section 3.2.3, with 8 experimental groups. As vascular networks were not previously perfusable in this configuration, an alternative readout for the experiment was required. For this, luminal area at the perfusate-vascular network interface was used to gauge the accessibility of the perfusate to the vascular network. Fibrin concentration was the only significantly influential factor (Figure 3.2A(i)), with increased fibrin concentration attributed to an increase in luminal area (Figure 3.2A(ii)). Segregation of the groups by fibrin concentration demonstrates smaller vessels at the interface at the gel matrix interface in 3mg/ml groups (Figure 3.2B(i)) compared to 10mg/ml groups (Figure 3.2B(ii)). Thus, fibrin concentration can be used to increase luminal area at the interface of the vascular network and the medium, suggesting it may be used to promote network perfusability.

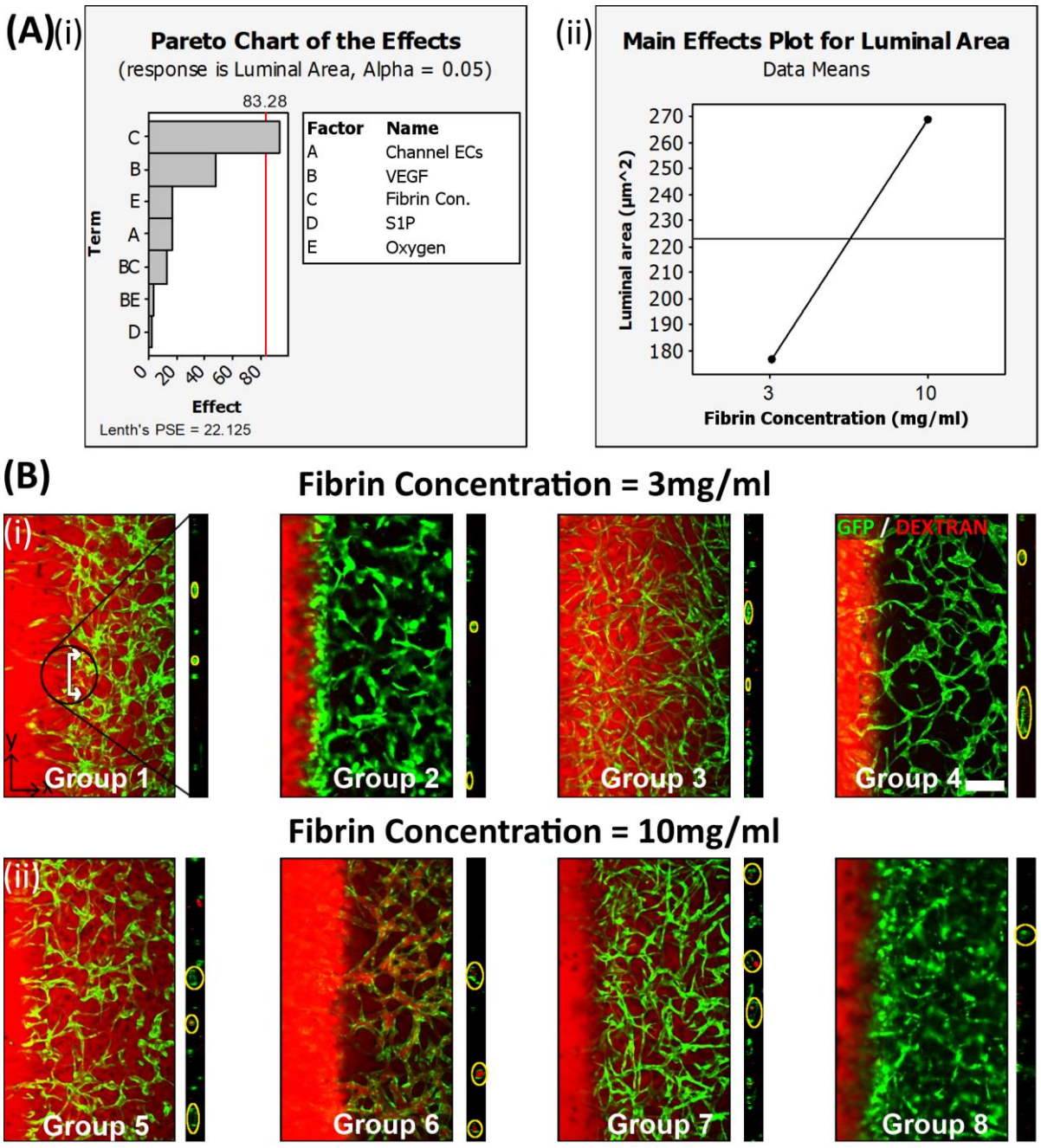

Figure 3.3: Increased fibrin concentration increases vessel diameter at the perfusate-vascular network interface (A) (i) Pareto chart showing fibrin concentration is a significantly influential factor and that **(ii)** increased fibrin concentration correlates with increased luminal area; average 180 µm^2 for 3mg/ml fibrin hydrogels (7.57µm equivalent lumen diameter) and 270µm^2 9.27µm (equivalent lumen diameter) **(B)** Luminal area is evaluated at the vasculature-media interface. All groups with **(i)** 3mg/ml fibrin have smaller area vessels than **(ii) all** groups with 10mg/ml fibrin, irrespective of the other parameters. Group numbers references are those as described in Table 3-1. Scale bar = 100µm.

3.3.3 Increased fibrin concentration regulates vascular morphology in direct vascularisation, but does not induce perfusability

Having identified fibrin concentration as a means to modulate vessel diameter at the network interface, fibrin concentration was next increased to facilitate perfusability at higher hBMSC numbers in the direct vascularisation template. A similar trend to 3mg/ml hydrogels was observed in the 10mg/ml hydrogels when analysing network formation and perfusability for each percentage of hBMSCs (Figure 3.1A); with decreased branching and larger diameter vessels observed with reduced percentage of hBMSCs. However, no perfusability was observed in any of the groups. Quantification of the formed vascular networks (Figure 3.3B) indicted a significant decrease in branch density, and significant increases in area vascularised in low hBMSC density groups. Based on these observations, it would appear that perfusable networks can only be engineered using direct co-cultures of hBMSCs and HUVECs when using low relative numbers of hBMSCs.

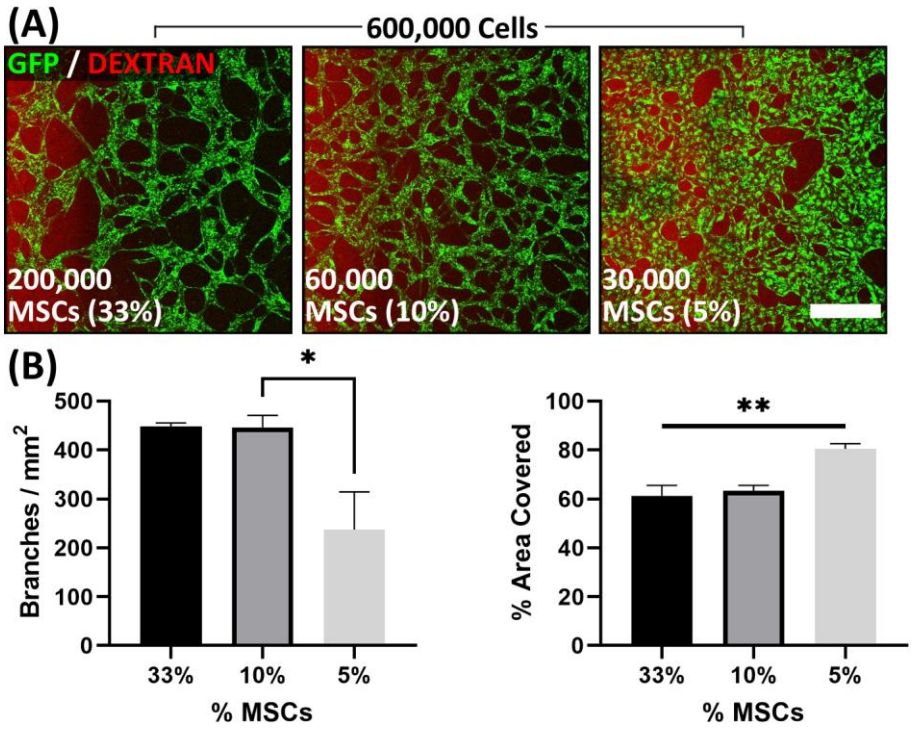

Figure 3.4: Higher Fibrinogen content influences vascular morphology without inducing perfusability. (A) In 10mg/ml fibrin gels, decreased relative fraction of hBMSCs modulates vascular network morphology, but does not induce network perfusability. Scale bar = 100µm **(B)** Quantification of the formed vascular networks indicted a significant decrease in branch density ($p<0.05$), and significant increases in area vascularised ($p<0.01$) in low hBMSC density groups.

3.3.4 An indirect co-culture of HUVECs and hBMSCs supports the development of perfusable vasculature within an MPS device

Given that the direct vascularisation MPS template could only facilitate both network formation and perfusability at low cell numbers, which may not be suitable for many applications, an alternative MPS template was explored. The concept of indirect vascularisation of the MPS device using hBMSCs as a support cell is shown in Figure 3.4A, with 400,000 HUVECs in a central channel with two adjacent hBMSC channels. hBMSCs were seeded at 1:1 or 2:1 ratio (total hBMSCs: total HUVECs) in a fibrin gel (3mg/ml) and cultured in either 20% or 5% O_2. Perfusability was observed in all devices, along with striking differences in vascular network formation (Figure 3.4B). Interestingly, a higher ratio of hBMSCs (2:1) induced formation of more interconnected

vasculature, while a lower ratio induced less interconnected vasculature, with a 1:1 ratio not inducing any vascular network formation at 20% oxygen. Oxygen tension also clearly effected vascular network formation; with interconnected vasculature forming in both groups at 5%, even at the lower 1:1 hBMSC ratio. Critically, indirect vascularisation induced perfusability in all groups (Figure 3.4B and Figure 3.4C). However, the percent of devices perfusable was higher at lower ratios of hBMSCs to HUVECs (1:1); with all devices perfusable at both 5% and 20% O2. Reduced oxygen tension increased the number of perfusable devices for the higher 2:1 ratio of hBMSCs to HUVECs.

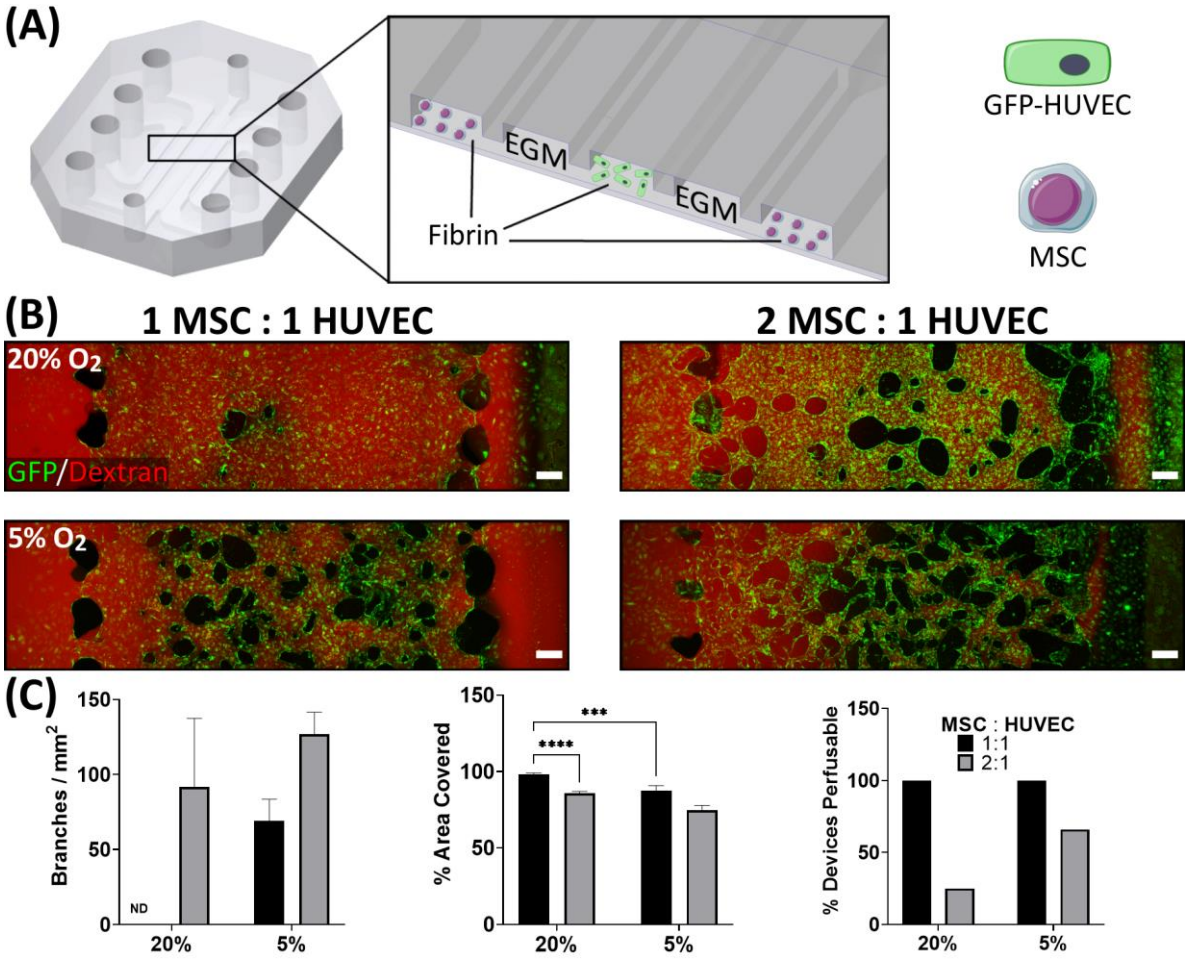

Figure 3.5: Indirect vascularisation of hBMSCs facilitates vasculogenesis and perfusability at high cell ratios. (A) Schematic showing indirect hBMSC vascularisation in MPS device (shown is a 2:1 MSC:HUVEC ratio). **(B)** Vascular network formation at high (2:1) and low (1:1) hBMSC ratio, and at 20% and 5% oxygen. Scale bar = 200µm **(C)** Quantification of formed vascular networks

3.4 Discussion

MPSs represent a promising technology for the *in vitro* study of tissue and organ function. MPSs have been applied to modelling tissues such as gut [239], brain [240] and lung [198] in ways not possible in traditional 2D culture. Despite significant progress in the field, few applications have been developed for skeletal tissues such as bone. Particularly, models of vascularised bone tissue have the potential to advance our understanding of bone physiology and prominent skeletal diseases. In light of the application gap, we have engineered vascularised MPS templates to

facilitate and expedite the development of advanced models of bone function and pathology.

To realise these templates, a MPS device was vascularised using hBMSCs as a support cell to HUVECs. hBMSCs were chosen as they are the canonical human bone cell used therapeutically and in human models of bone function. The first template, the direct vascularisation template, incorporated hBMSCs and HUVECs in one hydrogel. The findings that high concentration of hBMSCs inhibit vascularisation have been observed in other studies [230], as is the observation that lower concentrations better facilitate vascularisation [207]. Interestingly, vasculature formed in these non-perfusable devices is patent throughout, but the network is inaccessible at the medium interface. Interestingly, similar MPS configurations produce perfusable vasculature with fibroblasts [30, 221], thus the anti perfusability effects that hBMSCs have are likely to be both cell specific and dose dependent. Oxygen, nutrient or signalling factor gradients that exist between the tissue centre and media interface may induce hBMSC behaviour that varies spatially, with a phenotype at the edges that ultimately inhibits tubulogenesis. Additionally, fibroblasts and MSCs from different tissues drive ECs to use different proteolytic mechanisms to remodel their matrix during vasculogenesis [241-243], thus perhaps resulting alternative vascular phenotypes with different perfusabilities. Despite this, perfusable vasculature can be achieved in the direct vascularisation template, albeit with low hBMSC cell density, which would still facilitate a number of analytical methods.

An alternative approach, indirect vascularisation, produced perfusable vascular networks using higher numbers of hBMSCs for detection of secreted factors, extraction of RNA, or extraction of intracellular protein for molecular analysis. It was found that indirect vascularisation readily produced perfusable vascular networks, and

that the vascular network morphology and percentage of perfusable devices was influenced by both the number of hBMSCs and oxygen tension. Increased number of hBMSCs correlated with vascular network formation and increased vascular branching. hBMSCs have been shown to have a pro-angiogenic secretome [225], which, like many cells, is regulated by HIF-1 activation at low oxygen [244]. This, along with increased secretome concentration at higher hBMSC densities may account for this observation, which has also been shown in fibroblasts [234]. Interestingly, though all groups were perfusable, increased hBMSC numbers again inhibited perfusability, although this was only observed at higher oxygen tensions. The data suggests that there may be an optimal nutrient/oxygen milieu that drives hBMSCs to secrete adequate factors supportive of the formation of a perfusable vascular network. This vascularised hBMSC template would be particularly suitable in applications were ECM parameters that drive osteogenesis and angiogenesis, such as matrix stiffness [245], or high mineral content [185] are incompatible, and can be simply decoupled through separate gels.

One limitation of the templates is the low cell numbers required for direct co-culture. The low number of cells would limit molecular techniques available where direct co-culture would be required, such as for a bone peri-vascular niche. Additionally, traditional MPS systems are small devices, with gel volumes around 10-20µl. The MPS device used is designed for application in non-specialised labs, negating the need for specialised processes such as lithography. Thus, the volume of gel is larger, 100µl, which could be reduced through optimisation for cost savings.

This chapter details the development of two vascularised MPS templates, indirect and direct, for application in bone physiology and disease. In the short term, development of media formulations to facilitate study of angiogenic-osteogenic coupling would be

an immediate application where these models could add value to the bone research community. Similarly, the reduced perfusability and angiopathy observed clinically in osteoporosis and diabetes mellitus could be modelled with hBMSCs from those patients. Longer term, integration of a bone MPS within a larger body on chip system is a prudent long-term objective in the community for modelling inter-organ communication and modelling the endocrine effects of bone tissue.

3.5 Conclusion

This chapter details the development of vascularised MPS templates for bone research applications. Vascular impairment correlates with a number of the most prominent skeletal diseases, such as osteoporosis. Additionally, vasculature is central to bone development, repair and regeneration. Despite this, vascularised models of bone tissue are underutilised. To this end, two methods of vascularising tissues within MPS using hBMSCs were developed: direct and indirect co-culture systems. The direct system only produces perfusable networks at very low hBMSC numbers, which greatly limits the possibility of using this cell population as the precursor for bone tissue development within the MPS. In contrast, the indirect system facilitates the development of perfusable vascular networks using higher numbers of hBMSCs, which in turn may facilitate the use of specific assays and system readouts. These systems are templates that can be adopted for building models of vascularised bone for MPS applications.

The physical separation of cells in the indirect vascularisation approach limits the interaction between hBMSCs and HUVECs to solely paracrine mechanisms. An optimal vascularised MPS for the study of bone development and/or (patho)physiology would permit both paracrine and physical interaction between the cell types. As

already discussed, the direct vascularisation approach only permits this at very low hBMSC numbers, which limits both the analytical methods that could be applied and the possibility that this cell population could be used as the precursor for bone tissue development around the vascular network. As part of the next chapter, we will address this challenge by engineering bone precursor organoids separately before integration into a vascularised MPS device.

Chapter 4: Development of a Microphysiologcal Model of Endochondral Ossification

4.1 Introduction

Endochondral Ossification (EO) is a process critical to the development, post-natal growth, and healing of the long bones of the human skeleton. During EO a cartilage template matures to hypertrophy; initiating a pro-angiogenic program resulting in vascular invasion that initiates the transformation of cartilage to bone. The specifics of how bone develops in this way, and specifically how vasculature initiates the cartilage to bone transformation is still not fully understood. A deeper understanding of EO will bring about not just an improved basic understanding of this key aspect of bone biology, but could also improve treatment of a number of skeletal diseases, such as fracture non-unions [123], chondrodysplasias [122], and osteochondrosis [130]. More indirectly, given that EO is specifically concerned with cartilage to bone transition, discoveries may lead to treatments for conditions involving aberrant cartilage to bone transformation, such as osteoarthritis [246].

Advancements in our understanding of EO biology may also improve the treatment of large bone defects. At present, autografting is the current gold standard approach for large bone defect repair, but has inherent drawbacks such as donor site morbidity and limited supply [247]. As EO is central to long bone development and secondary fracture healing, recapitulating this process is forming the basis to emerging alternative strategies to repair large bone defects [155, 248]. The EO approach involves implantation of a pre-cultured cartilaginous or hypertrophic tissue to stimulate the healing process and drive regeneration [249]. Such developmentally inspired tissue engineering implants have the advantage of scalability over autografting, and would

be less prone to donor site morbidity as smaller biopsies are required to extract cells for such tissue engineering applications.

To advance understanding of EO, and in turn improve the design of therapeutics aimed at modulating this process, adequate experimental models are needed. Currently, rodent models are the gold standard for probing EO in both developmental [67] and regenerative contexts such as fracture healing [14]. These animal models are essential for research, as no *in vitro* system can replicate the complexity of an entire organism. However, rodents do not present haversian remodelling or closure of the epiphyseal growth plate as occurs in humans [188, 250], and therefore the underlying mechanisms of EO may differ between the species. Alternatively, *In vitro* models are less expensive, potentially of human origin, and can produce more specific, higher resolution information than animal models. A number of *in vitro* systems exist to model EO; for example, the murine-derived ATDC-5 cell line can undergo cellular condensation, proteoglycan synthesis, collagen type II secretion [251], and hypertrophic mineralisation [152, 252], and have been used as model cells for EO research. Additionally, *ex vivo* mesenchymal micromass cultures from the developing limb bud [253], isolated chondrocytes [254] and growth cartilage explants [255] are other common model tissues for EO research. The drawback of these models is that they are typically not of human origin, which in itself can result in poor predictive ability [256]. Additionally, these systems lie on either end of a spectrum of *in vitro* biological complexity; exhibiting a substantial trade off in experimental control and physiological relevance.

Next generation *in vitro* models of EO should exist in the centre of this spectrum, incorporating more physiological relevance to *in vitro* models to facilitate advanced study of this key developmental and regenerative process. MPSs are a candidate

platform on which to build these next generation models. MPSs can incorporate EO relevant biological functions such as mechanical stimulation. However, a more pertinent feature of MPS technology is the ability to generate 3 dimensional tissues with physiologically relevant vasculature [221], which, if incorporated into an *in vitro* model of EO, could facilitate probing the essential role of vasculature in EO progression.

The aim of this chapter was to develop and validate a MPS model of EO. More specifically, the aim is to develop a MPS to model the vascular invasion of cartilage during EO in developing bone. Thus, to further understand this developing bone – vasculature crosstalk, developing bone organoids (µDBO) that represent stages along the endochondral pathway were vascularised in an MPS device, and their response to vascularisation at the tissue and gene level was characterised. The model captures the antiangiogenic properties of mature cartilage, and the vascular induced activation of pluripotency associated genes in chondrocytes. This system represents an advanced in vitro platform to further EO research, and may also serve as a modular unit to monitor drug metabolite responses on EO in a multi-organ system.

4.2 Methods

4.2.1 Cell culture

Media Formulations

Expansion Medium (XPAN): XPAN medium was used for monolayer expansion. XPAN medium consisted of high-glucose GlutaMAX Dulbecco's modified Eagle's medium (DMEM) supplemented with 10% v/v fetal bovine serum (FBS), 100 U/ml penicillin, 100mg/ml streptomycin (all Gibco Biosciences, Dublin, Ireland) and 5 ng/ml FGF-2 (Peprotech, UK).

Basic Chemically Defined Medium (CDM-): CDM- medium was used for undifferentiated µDBO µwell culture. Chemically defined medium was prepared by adding 100 U/ml penicillin, 100mg/ml streptomycin (all Gibco Biosciences, Dublin, Ireland), 100 µg/ml sodium pyruvate, 40 µg/ml, L-proline, 50 µg/ml and 1.5 mg/ml bovine serum albumin (Sigma Aldrich, Ireland) to DMEM.

Fully Supplemented Chemically Defined Medium (CDM+): CDM+ medium was used for early cartilage (EC) and mature cartilage (MC) µDBO µwell culture. CDM- was supplemented with; 4.7 µg/ml L-ascorbic acid-2-phosphate, 4.7µg/ml linoleic acid, 10 mg/ml insulin, 5.5 mg/ml transferrin, 6.7 µg/ml selenium (Gibco), 100 nM dexamethasone (Sigma–Aldrich, Ireland), and 10 ng/ml of human transforming growth factor-b3 (TGF-b3) (Peprotech, UK)

Hypertrophic Medium (HYP): HYP was used for hypertrophic cartilage (HC) µwell culture, CDM- was supplemented with 4.7 µg/ml L-ascorbic acid-2-phosphate, linoleic acid, 10 mg/ml insulin, 5.5 mg/ml transferrin, 6.7 µg/ml selenium (Gibco), 100 nM dexamethasone (Sigma–Aldrich, Ireland), 7.5mM β-glycerophosphate, and 25 ng/ml L-Thyroxine (Sigma Aldrich, Ireland).

Endothelial Growth Medium 2 – Microvascular (EGM)

EGM-2MV (herein referred to as EGM) was used for HUVEC expansion and MPS culture. Endothelial Basal Media (CC-3156, Lonza) was fully supplemented (CC-4147) as per the manufacturer's instructions.

Cell culture and Expansion

Human Bone Marrow Stromal Cells (hBMSCs)

Whole human bone marrow (Lonza, USA) was purchased and hBMSCs were isolated. Whole bone marrow was plated at 2000 cells/cm^2 and expanded in XPAN for one

week at 37°C, 5% O_2 and 5% CO_2. Once colonies had formed, cells were trypsinised and subculutred until sufficient cell numbers were achieved, cells were then frozen down and stored in LN_2 before use. The donor used was evaluated for osteogenic, adipogenic, and chondrogenic capacity. For experimental expansion, hBMSCs were plated at 5000 cells/cm^2, expanded in XPAN until confluent and passaged at 80% confluence. hBMSCs at P4 were used for all experiments.

Human Umbilical Vein Endothelial Cells (HUVECs)

Green fluorescent protein expressing human umbilical vein endothelial cells, herein referred to as HUVECs, were purchased from Angio-proteomie. HUVECs were expanded in microvascular endothelial growth media (EGM-2MV, Lonza) on rat-tail collagen coated T75 flasks at 10µg/cm^2. HUVECs were used at passage 8 for all experiments.

µDBO formation and harvesting

µDBOs were formed by seeding hBMSCs on an a 401 µwell agarose mould. Custom designed master stamps were 3D printed (Form 3, Formlabs, USA), and sterilised with ethylene oxide before moulding. To create the multiwell moulds, 3 mls of 4% molten agarose (Sigma, Ireland) was pipetted into each well of a 6 well plate, stamps inserted, and agarose allowed to cool. Upon removal of stamps, 3 mls of media is added and exchanged daily for two days to allow media contents to equilibrate in the agarose.

To form µDBOs, hBMSCs were pipetted on to the agarose mould, allowed to settle for 30 mins in an incubator and centrifuged at 700g for 5 mins. 3 mls of media was then exchanged every other day for the duration of culture. 4 different organoids were fabricated to represent increasing cartilage tissue maturity: undifferentiated (UD) µDBOs (-ve control) were cultured in CDM- at 5% O_2 for 7 days, early cartilage µDBOs

(EC) were cultured in CDM+ at 5% O_2 for 7 days, mature cartilage µDBOs (MC) were cultured in CDM+ at 5% O_2 for 21 days, and hypertrophic cartilage (HC) µDBOs were cultured for 21 days in CDM+ at 5% O_2 and a further 7 days in HYP media at 20% O_2.

To harvest µDBOs, high media flow from a 20ml syringe and 20g needle was used to release µDBOs from each individual well. Suspended µDBOs were then harvested directly from the medium, while µDBOs remaining in the well were removed by flipping the agarose moulds into a fresh 6 well plate and centrifuging for 600g for 5 mins and collecting in media. µDBOs were passed through a 500µm filter to remove fused µDBOs and agarose fragments.

4.2.2 µDBO Diameter

µDBO diameter was determined using image analysis. Images of µDBOs were taken during culture with a brightfield microscope and images were measured manually using FIJI software [236].

4.2.3 Biochemical Analysis

After µwell culture, µDBOs were washed in PBS and frozen in liquid nitrogen and stored at -80˚C. Each construct was digested with papain (125 µg ml -1) in 0.1M sodium acetate, 5mM L-cysteine–HCL, 0.05M ethylenediaminetetraacetic acid (EDTA), pH 6.0 (all from Sigma–Aldrich) at 60 °C and 10 rpm for 18 h. DNA content was quantified using a Quant-iT™ PicoGreen™ dsDNA Assay Kit (Invitrogen) as per the manufacturer's instructions. Sulphated glycosaminoglycans (sGAGs) were quantified using a 1,9-Dimethyl-Methylene Blue (DMMB) assay. Briefly, digested samples were mixed with a DMMB staining solution and absorbance was measured at 530nm and 590nm. sGAG levels were interpolated from a standard curve of 530/590nm absorbance ratio using a chondroitin sulfate standard.

4.2.4 LiveDead Viability

Cell viability was assessed after µwell culture using a LIVE/DEAD™ viability/cytotoxicity assay kit (Invitrogen, Bioscience, Ireland). µDBOs were washed with phosphate buffered saline (PBS) followed by incubation with PBS containing 2 µM calcein AM (green fluorescence of membrane for live cells) and 4 µM ethidium homodimer-1 (red fluorescence of DNA for dead cells; both from Cambridge Bioscience, UK). µDBOs were again washed in PBS, imaged with a Leica SP8 scanning confocal excited at 494nm and 528nm, and read at 517nm and 617nm respectively.

4.2.5 Microphysiological Chip Fabrication

Microfluidic Devices were fabricated using replica moulding. Master moulds were fabricated by laser cutting the channel geometries from 1mm thick PMMA sheets and adhering to 30mm diameter PMMA plates using acrylic glue (Scigrip 4SC, USA). Master moulds were then glued to the bottom of 100mm diameter petri dishes. To create microfluidic chips, sylgard 184 polydimethylsiloxane (Dowsil, USA), was mixed at 10:1 (polymer:catalyst), degassed under 40 mbar vacuum for 10 minutes and poured on master moulds. PDMS was allowed to cure overnight at 80˚C. Once cured, PDMS replicas were removed by cutting around the circumference of the mould and removing with a spatula. PDMS replicas were then trimmed and cleaned using adhesive tape. To form the microfluidic devices, PDMS replicas and 1.5 thickness glass coverslips were plasma treated with corona plasma (Corona SB, BlackHole Labs, Paris) for 1 minute each and pressed together. Devices were then placed in an oven overnight at 60˚C for hydrophobic recovery. Finally, devices were sterilised using ethylene oxide and allowed to air for 2 days before culture.

4.2.6 Microfluidic Device culture

Microfluidic devices were seeded with a co-culture of µDBOs and HUVECs. Each device holds 100 µL of hydrogel. µDBOs and HUVECs were harvested and resuspended in medium containing with 4U/ml thrombin (Sigma Aldrich, Ireland). 50 µL of cell / µDBO suspension was then mixed with an equal volume of 6mg/ml bovine fibrinogen (Sigma Aldrich, Ireland), mixed and quickly pipetted into the microfluidic devices to minimise µDBO settling. Fibrin was allowed to clot for 40 mins in a humidified incubator, after which EGM-2MV is added to each device. Media was exchanged daily. Final concentrations were 2000 µDBOs/ml (200/device) and $4x10^6$ HUVECs/ml (400,000 / device).

4.2.7 Histology

µwell culture µDBOs were fixed overnight at 4˚C in 4% paraformaldehyde (PFA), washed with PBS and allowed to settle at the bottom of a well of a flat bottom 96 well plate. Once settled, PBS was removed, and a 4% molten agarose solution was pipetted on to the settled µDBOs and allowed to cool to hold them in place. For MPS culture, devices were washed with PBS, fixed with 4% paraformaldehyde at 4˚C overnight, and again washed with PBS. To remove tissues from the MPS devices, coverslips were covered with tape to avoid cracking and a scalpel was used to separate the PDMS device from the coverslip. Both µwell culture and MPS samples were then dehydrated in a graded series of ethanol, embedded in paraffin wax, sectioned at 5µm and affixed to microscope slides. Samples were stained with H+E to assess cell and tissue morphology, picrosirius red to assess collagen deposition, alizarin red to assess mineralisation, and alcian blue to assess glycosaminoglycan (GAG) deposition.

4.2.8 Vascular Network Morphology Analysis

Entire MPS devices were imaged after 7 days to analyse vascular formation. Images were analysed using a custom macro to automate processing in FIJI [236] (Appendix 1). Images were cropped into user defined regions of interest (ROIs), despeckled, and contrast adjusted to increase signal to noise ratio. Images were then gaussian blurred and thresholded. Finally the resulting binary image was skeletonised and analysed using FIJI's analyse skeleton function [237]. Automated thresholding was checked against the original image. Two regions of interest were analysed: regions containing a single µDBO, and regions without µDBOs. To compare vascularisation in these two regions, a 1.37µm^2 area was analysed. For regions without µDBOs, this region is a simple square of area 1.37µm^2. For regions with a µDBO, this region is a square with the area of the µDBO removed from the analysis, but also of area 1.37µm^2 (Figure 4.1).

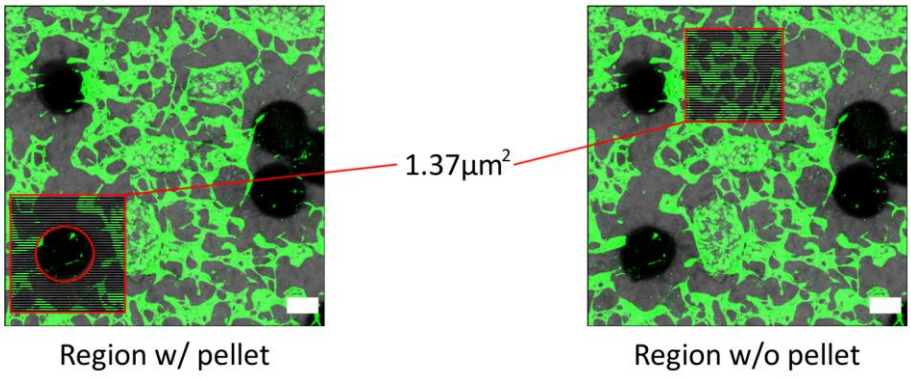

Figure 4.1: Method for analysing vascular formation in µDBO / HUVEC co-cultures. Vascular morphology was analysed in 1.37µm^2 ROIs. Areas containing µDBOs has the µDBO removed from the area for analysis, while maintaining the same area.

4.2.9 Perfusion

Vascular network perfusion was evaluated at day 7 by perfusion of fluorescent dextran. 70kDa rhodamine conjugated dextran (Sigma Aldrich, Ireland) was diluted in PBS to 2mg/ml, vortexed and stored at 4˚C protected from light. Media was removed

from both channels and device placed on a Leica SP8 scanning confocal microscope stage. Once positioned for imaging, dextran was introduced to one channel and filled to the top of the feeding port of each device to create a hydrostatic pressure gradient across the vascularised hydrogel. Images were taken immediately to avoid excessive diffusion of dye across the bulk hydrogel.

4.2.10 Gene Expression Analysis

Sample Handling

At termination of µDBO µwell culture, µDBOs were washed in PBS and snap frozen in liquid nitrogen before RNA isolation. Upon termination of in MPS culture, fibrin gels containing the µDBO / HUVEC co-culture was removed as per section 4.2.3. The exposed hydrogel was then transferred to 1.5 ml Eppendorf and 1 ml of a fibrinolytic solution; prepared by dissolving 50 FU/mL (fibrin degradation units) of nattokinase (NSK-SD; Japan Bio Science Laboratory Co. Ltd), was added and rotated at 37 degrees for 40 minutes. The resulting µDBO / HUVEC suspension was passed through a 100µm cell strainer and washed with 10 mls of PBS to separate µDBOs from individual HUVECs. The µDBOs were then retrieved from the filter, placed in a 1.5ml Eppendorf, spun down to remove excess PBS and frozen in liquid nitrogen. Samples were stored at -80˚C until RNA isolation.

RNA Isolation and CDNA Transcription

µDBOs frozen at -80˚C were thawed on ice. Once thawed, 500µL of TRIzol (Invitrogen, LifeTechnologies, Carlsbad, CA) was added and µDBOs were mechanically disrupted with a pestle (treated with diethyl pyrocarbonate) for 10 seconds and centrifugation to pull insoluble material to the bottom of the Eppendorf. This process of disruption and centrifugation was repeated until no insoluble material remained in the Eppendorf (~2

times). The pestle was then rinsed with another 500µL of TRIzol into the sample for a total volume of 1ml. The sample was then left to stand at room temperature for 7 minutes. 200µL Chloroform (Sigma, Ireland), was then added to each sample, vortexed and incubated for 5 minutes at 4˚C. Samples were then centrifuged at 12000g for 15 mins at 4˚C. 500 µL of the top aqueous, RNA containing phase of the sample was removed and transferred into an RNAse free Eppendorf. 500µL of 2-Propanol (Sigma, Ireland) and 2µL of GlycoBlue co-precipitant (Invitrogen) were mixed to precipitate the RNA and left to stand at room temperature for 10 minutes. Samples were the centrifuged at 14000g for 15 mins at 4˚C. Supernatants were removed and each RNA pellet was washed with 1ml of 75% ethanol and incubated at -20 for 1 day. Samples were then centrifuged at 7000g for 5 mins at 4˚C. All ethanol was then removed and the RNA pellet was resuspended in 20µL of RNAse free water. RNA quantity and quality was checked with a spectrophotometer.

RNA samples were immediately transcribed into CDNA following isolation. Reverse transcription was carried using a CDNA RT kit (Applied Biosystems, USA) according to the manufacturer's instructions using a thermocycler. Following reverse transcription, cDNA was measured using a Qubit™ ssDNA assay kit (Invitrogen, USA) as per the manufacturer's instructions using a Qubit™ fluorometer (Invitrogen, USA). Samples were stored at a concentration of 2ng/µL at -20˚C.

PCR

Levels of gene expression were measured with real-time PCR (ABI 7500-fast, Applied Biosystems) using SYBR green master mix (Applied Biosystems) and human specific primers (Table 2). The quantity of gene transcripts was normalised to that of a stable housekeeping gene, in this case GAPDH. Efficiency of all primer pairs were calculated by 10-fold serial dilutions of cDNA starting at 50ng per reaction.

Table 4-1: List of primer pairs used for PCR reactions

Gene Name	Gene Full Name	Forward / Reverse	Tm (˚C) in use	Tm (˚C) predicted
GAPDH	Glyceraldehyde-3-Phosphate Dehydrogenase	F: 5' ACAGTTGCCATGTAGACC 3' R: 5' TTGAGCACAGGGTACTTTA 3'	60	59.0 58.3
RUNX2	Runt-Related Transcription Factor 2	F: 5' GCAGTATTTACAACAGAGGG 3' R: 5' TCCCAAAAGAAGTTTTGCTG 3'	60	58.1 59.3
MMP-13	Matrix Metallopeptidase 13	F: 5' AGGCTACAACTTGTTTCTTG 3' R: 5' AGGTGTAGATAGGAAACAT 3'	60	58.4 55.1
COL10a1	Collagen Type X Alpha 1 Chain	F: 5' GCTAGTATCCTTGAACTTGG 3' R: 5' CCTTTACTCTTTATGGTGTA 3'	60	50.2 54.5
SOX2	SRY-Box Transcription Factor 2	F: 5' ATAATAACAATCATCGGCGG 3' R: 5' AAAAAGAGAGAGGCAAACT 3'	60	57.1 58.1
POU5F1 (OCT4)	POU Class 5 Homeobox 1	F: 5' GATCACCCTGGGATATACAC 3' R: 5' GCTTTGCATATCTCCTGAAG 3'	60	58.1 59.1
NANOG	Nanog Homeobox	F: 5' CCAGAACCAGAGAATGAAATC 3' R: 5' TGGTGGTAGGAAGAGTAAAG 3'	60	60.1 55.9
THBS1	Thrombospondin 1	F: 5' GTGACTGAAGAGAACAAAGAG 3' R: 5' CAGCTATCAACAGTCCATTC 3'	60	55.6 57.3
SPARC	Secreted Protein Acidic and Cysteine Rich	F: 5' AGTATGTGTAACAGGAGGAC 3' R: 5' AATGTTGCTAGTGTGATTGG 3'	60	52.9 57.6
COL18a1	Collagen Type XVIII Alpha 1 Chain	F: 5' TTACGACAGCAATGTGTTTG 3' R: 5' AGAAAGTCAAACGGAAACTG 3'	60	59.8 58.4

4.2.11 Statistical Analysis

GraphPad Prism (GraphPad, USA) was used for all statistical analysis. comparisons made between 2 groups, or multiple groups were conducted using student's t-test or one-way analysis of variance (ANOVA) respectively. Two-way ANOVA was used to compare multiple groups at multiple levels. Non-parametric tests were used where

assumptions of normality could not be justified. Graph notation for deemed significance is as follows: * $p<0.05$, ** $p<0.01$, *** $p<0.001$, **** $p<0.0001$.

4.3 Results

4.3.1 Fabrication of µDBOs for modelling EO within MPS systems

To investigate the changing cross-talk between vasculature and developing bone as it matures, anaolgues of developing bone suitable for MPS applications are required. To this end, microscale developing bone organoids (µDBOs) were developed. hBMSCs were aggregated in a µwell culture system prior to seeding in vascularised MPS devices. Figure 4.2A illustrates the µwell culture system; fabricated by imprinting a master mould (Figure 4.2A(i)) into molten agarose (Figure 4.2A(ii)) and allowing it to cool before seeding of a single cell suspension, which is evenly distributed amongst the wells (Figure 4.2A(iii)). µDBOs can be maintained in culture until they progress towards a hypertrophic cartilage phenotype and accumulate a mineralised cartilageneous matrix, or removed from culture at earlier timepoints for DBOs representative of earlier stages of maturation (Figure 4.2B and C). GAG deposition normalised to DNA increases as DBOs mature, with no further increase as they progress to hypertrophy (Figure 4.2D). To ensure µDBO viability after µwell culture, viable cell distribution was analysed using LIVE/DEAD, with no evidence of cytotoxiticy observed within the µDBOs. Finally, gene expression analysis revealed a maturity depenedent expression of genes associated with hypertropy and osteogenesis; with the relative expression of *RUNX2*, *MMP13* and *COL10a1* increasing in the DBOs as they mature from early cartilage (EC), to mature cartilage (MC) and finally to hypertrophic cartilage (HC).

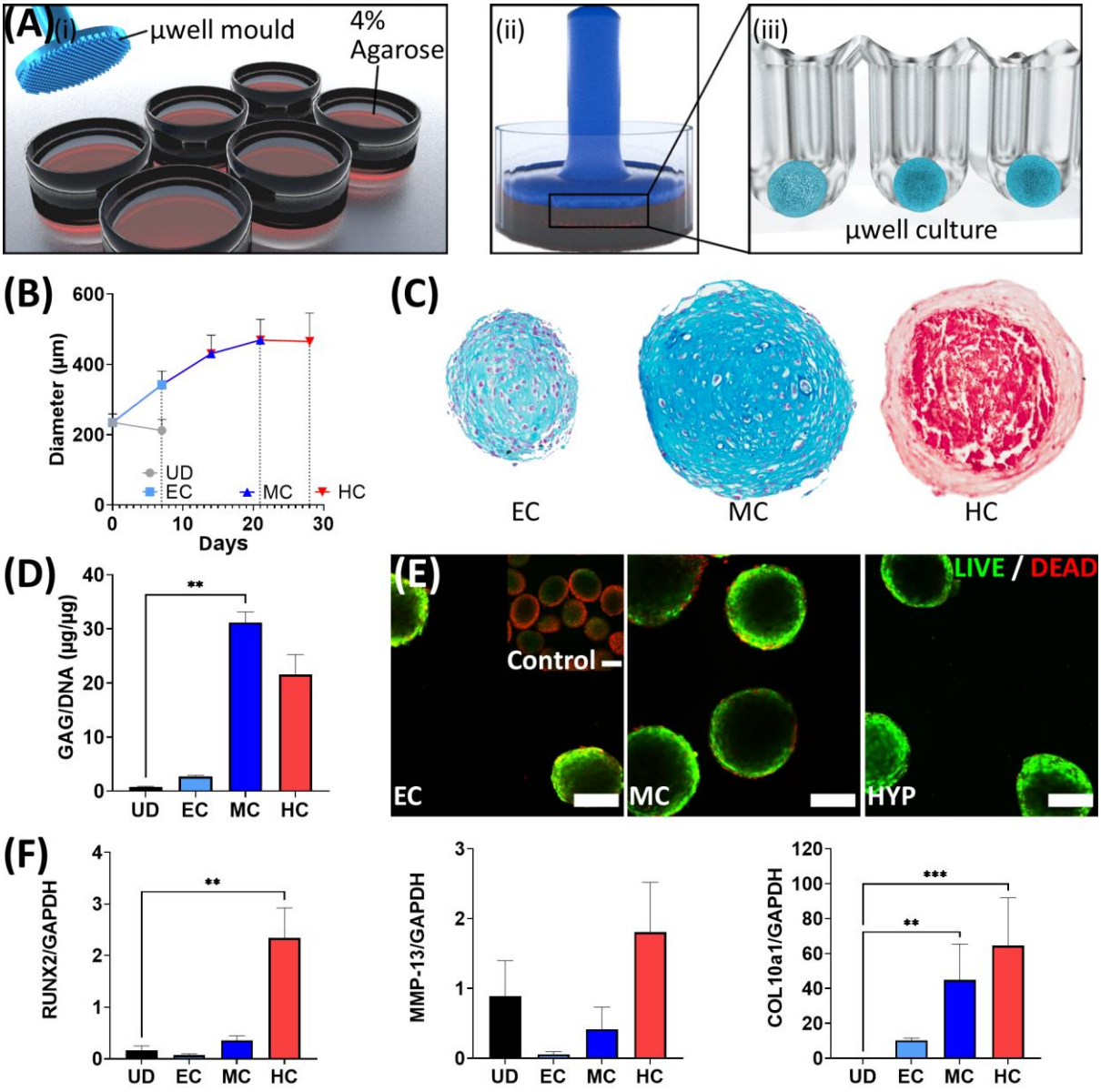

Figure 4.2: Fabrication of DBOs for modelling EO within MPS systems. (A) Schematic of µwell culture system fabrication. **(B)** Scatter plot showing increase in µDBO diameter as µDBOs synthesize matrix over 28 days **(C)** Representative histological sections of early cartilage (EC), mature cartilage (MC) and hypertrophic cartilage organoids. **(D)** sGAG deposition normalised to DNA for each stage of DBO maturity. **(E)** LIVE/DEAD staining at each stage of DBO maturity indicates no evidence of cytotoxicity. Scale bar = 200µm. **(F)** Hypertrophic genes *RUNX2, MMP13,* and *Col10a1* increase in expression as µDBOs mature to hypertrophy.

4.3.2 Optimisation of µDBO vascularisation in a MPS device

Having developed µDBOs to model developing endochondral bone tissue, the µDBOs were then vascularised within a MPS device. The schematic Figure 4.3A illustrates the arrangement of vasculature and µDBOs within the MPS device. HUVECs and µDBOs

were seeded into MPS devices within a fibrin hydrogel, resulting in the development of vascular networks around the µDBOs over 7 days in culture. In order to optimise resource requirements for the model, two µDBOs cell densities, 4000 cells / µDBO (as per previous figure) and 1000 cells/µDBO were evaluated. Additionally, to potentially mimic the physioxic/hypoxic environment in a fracture callus, and given the sensitivity of key cells, such as immune cells [257] and osteoprogenitors [258] to oxygen tension, 20% O_2 and 5% O_2 were also investigated. 4000 cell µDBOs cells are viable (Figure 4.3B), whereas in 1000 cell µDBOs some cell death is observed on the outside of the spheroid, and disconnected vasculature forms with evidence of cell debris, which is confirmed semi quantitatively (Figure 4.3D(i)). µDBOs were confirmed to be viable before MPS culture (data not shown). Furthermore, 4000 cell µDBOs also supported the development of perfusable vasculature within the MPS devices, as evident by the transport of 70kDa rhodamine conjugated dextran through the vascular networks at 20% O_2. (Figure 4.3C, Figure 4.3D(ii)). Additionally, the µDBO viability and network formation proceeds at physiologically relevant levels of oxygen (5%).

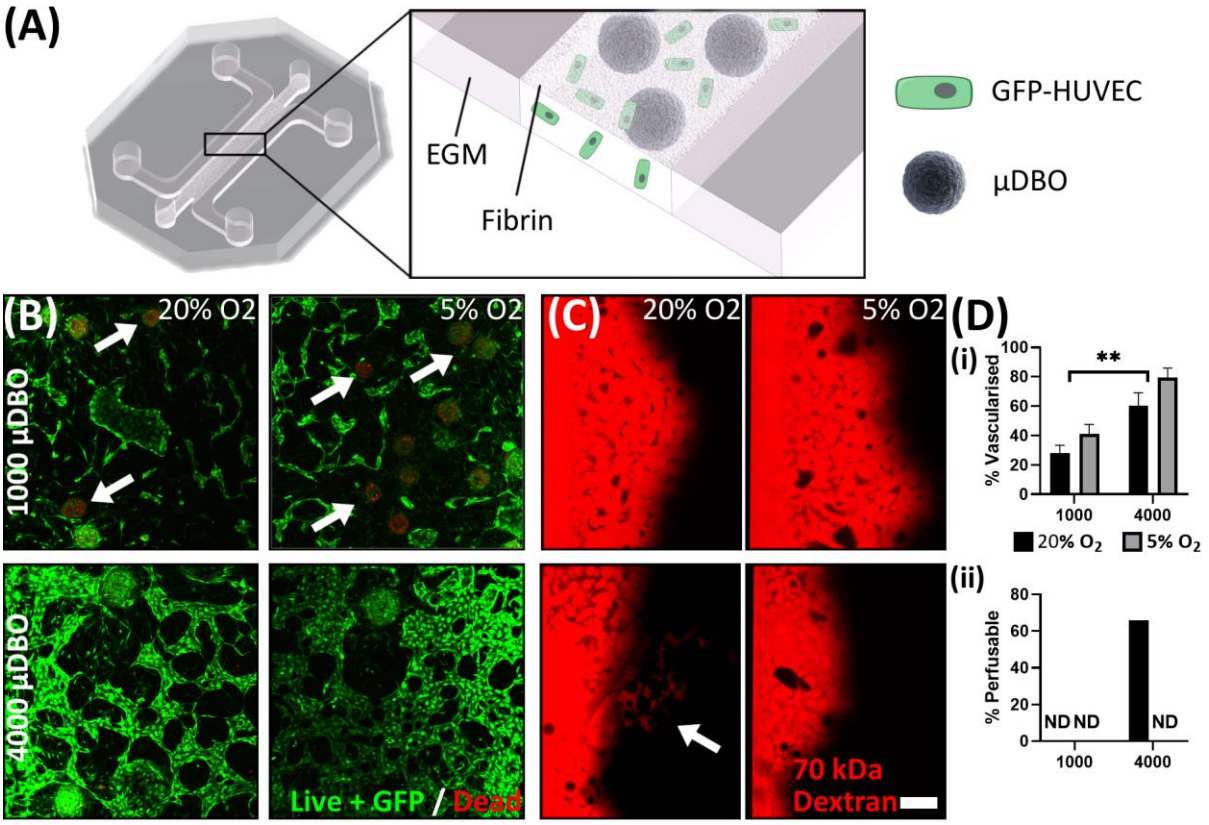

Figure 4.3: Optimisation of vascularised µDBO culture. (A) Schematic illustrating the vascularised µDBO culture, GFP labelled HUVECs and µDBOs are seeded in a fibrin gel and cultured in EGM. **(B)** LIVE/DEAD staining of vascularised µDBOs. Cytotoxicity was observed in µDBOs with lower cell numbers (white arrows) **(C)** Vascularised µDBO perfusion with Rhodamine conjugated dextran identifies perfusable vasculature in 4000 cell µDBOs. Scale bar = 200µm **(D)** Observed **(i)** % area vascularised and (ii) % devices perfusable confirmed using image analysis.

4.3.3 Vascular network development is dependent on the phenotype of the developing bone organoids

Having identified conditions to vascularise the µDBOs within the MPS device, the next step was to characterise µDBO-vascular cross talk and assess whether the phenotype of the µDBOs (early cartilage, mature cartilage, hypertrophic cartilage) influenced the development of the vascular network. At day 3, no discernible differences were observable between groups, as vascular structures have not formed and cross talk between the two tissue niches have yet to have an appreciable influence (Appendix 2). However, by day 7, a striking disparity in vascular morphogenesis with µDBO

maturity was observed (Figure 4.4A(i)); early cartilage (EC) µDBOs exhibited a pro angiogenic phenotype that drives the invasion of small diameter vessels towards the µDBOs. In contrast, the more differentiated mature cartilage µDBOs (MC) exhibit an anti-angiogenic phenotype that inhibits vascular invasion in the area surrounding the µDBO. Additionally, the vessels around MC µDBOs were of larger diameter than with EC µDBOs. As the µDBOs mature to hypertrophy (HC), a morphologically different vasculature again surrounds the µDBOs, with higher vascular coverage in the bulk gel. In an attempt to determine if paracrine factors secreted by the µDBOs were responsible for changes in vascular formation, HUVEC only MPS devices were cultured in µDBO conditioned media for 7 days. Interestingly, similar vascular morphologies were observed in HUVEC only MPS devices fed with µDBOs conditioned media (Appendix 2), thus the observed differences in vascular morphology are at least partially attributable to paracrine mechanisms. Perfusion of the formed vasculature shows that chondrogenic differentiation of the µDBO can impact network developments, as the vasculature surrounding these µDBOs was unperfusable (Figure 4.4A(ii)). However further µDBO maturation to hypertrophy correlates with a switch to a more pro-angiogenic phenotype, as evident by the development of patent and perfusable vasculature.

Quantification of developing vascular networks confirmed the suppression of vascularisation around MC µDBOs (Figure 4.4B). Area vascularised, branch density, and junction density were significantly reduced in the area directly around the MC µDBOs compared to vasculature in other regions of the same hydrogel. Even in regions of the gel distant to the µDBO, the vasculature morphology was strongly dependent on the phenotypic maturation; producing a markedly different morphology

depending on the µDBO maturity. Less branched, thicker vessels were observed in the presence of µDBOs at the latter stages of hypertrophic maturation.

To investigate the mechanism by which µDBOs exert their changing pro or anti-angiogenic effects, the expression of 3 anti-angiogenic genes was assessed; thrombospondin-1 (*THBS1*), Collagen type 18 (*COL18a1*), and Secreted Protein Acidic and Cysteine Rich (SPARC)/OSTEONECTIN (*SPARC*) (Figure 4.4C). These genes were quantified before MPS culture (µwell culture), and after 3 days of MPS culture in the absence (-EC) and presence (+EC) of HUVECs. The expression of *THBS1* and *COL18a1* were both significantly upregulated in MC µDBOs in the presence of ECs; correlating with the inhibited morphology observed morphologically. In contrast, SPARC was downregulated in all differentiated spheroids in both vascularised and unvascularised conditions.

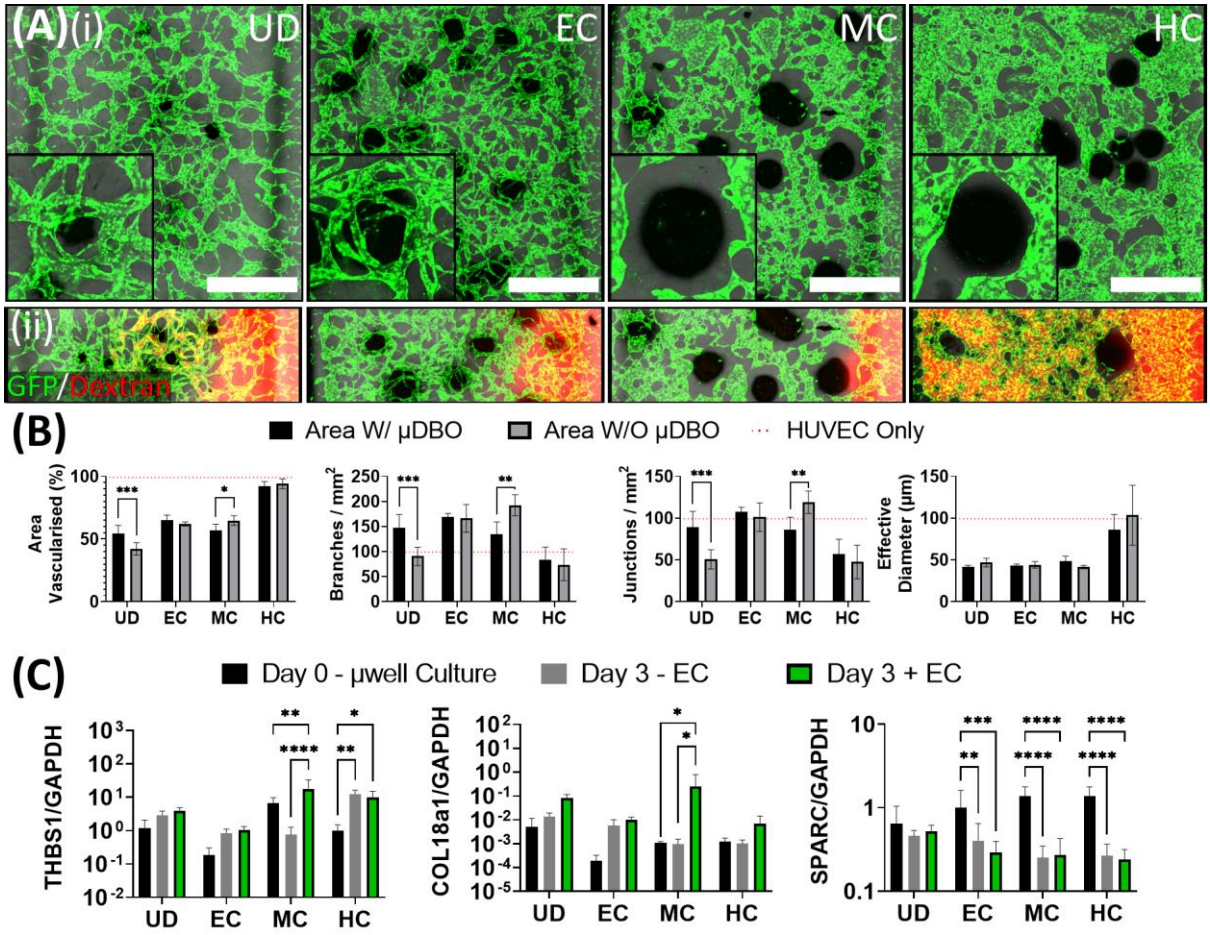

Figure 4.4: Vascularised µDBOs mimic in vivo maturity-dependent vascular response. (A) (i) Wide microscopic images of vascularised µDBOs show a range of vascular morphologies form and are sensitive to µDBO maturity. Inset - higher magnification image of single representative µDBO. Scale bar wide image = 1mm. (ii) Perfusion of the formed vascular networks with Rhodamine-conjugated dextran. Representative images shown. UD, EC, MC and HC had 2/2, 0/2, 0/2, and 2/2 devices perfusable respectively. **(B)** Semi-quantification of vascular morphology in vascularised µDBOs indicates inhibited vascularisation around mature cartilage. n=6 **(C)** Expression of anti-angiogenic genes THBS1, COL18a1 and SPARC by vascularised µDBOs. n=6**.**

4.3.4 The composition of developing bone organoids in the presence of vasculature

To further characterise the µDBO-vasculature cross talk, changes in µDBO ECM compositions after 7 days of vascularised MPS culture were evaluated. The changes in general cell and tissue structure were assessed with (H&E), collagen deposition (picrosirius red), GAG deposition (alcian blue), and mineralisation (alizarin red), after one week of MPS culture in the presence (+EC) and absence (-EC) of vascularisation

for μDBOs at increasing stages of differentiation (Figure 4.5). Gross ECM composition was unaffected by vascularised culture.

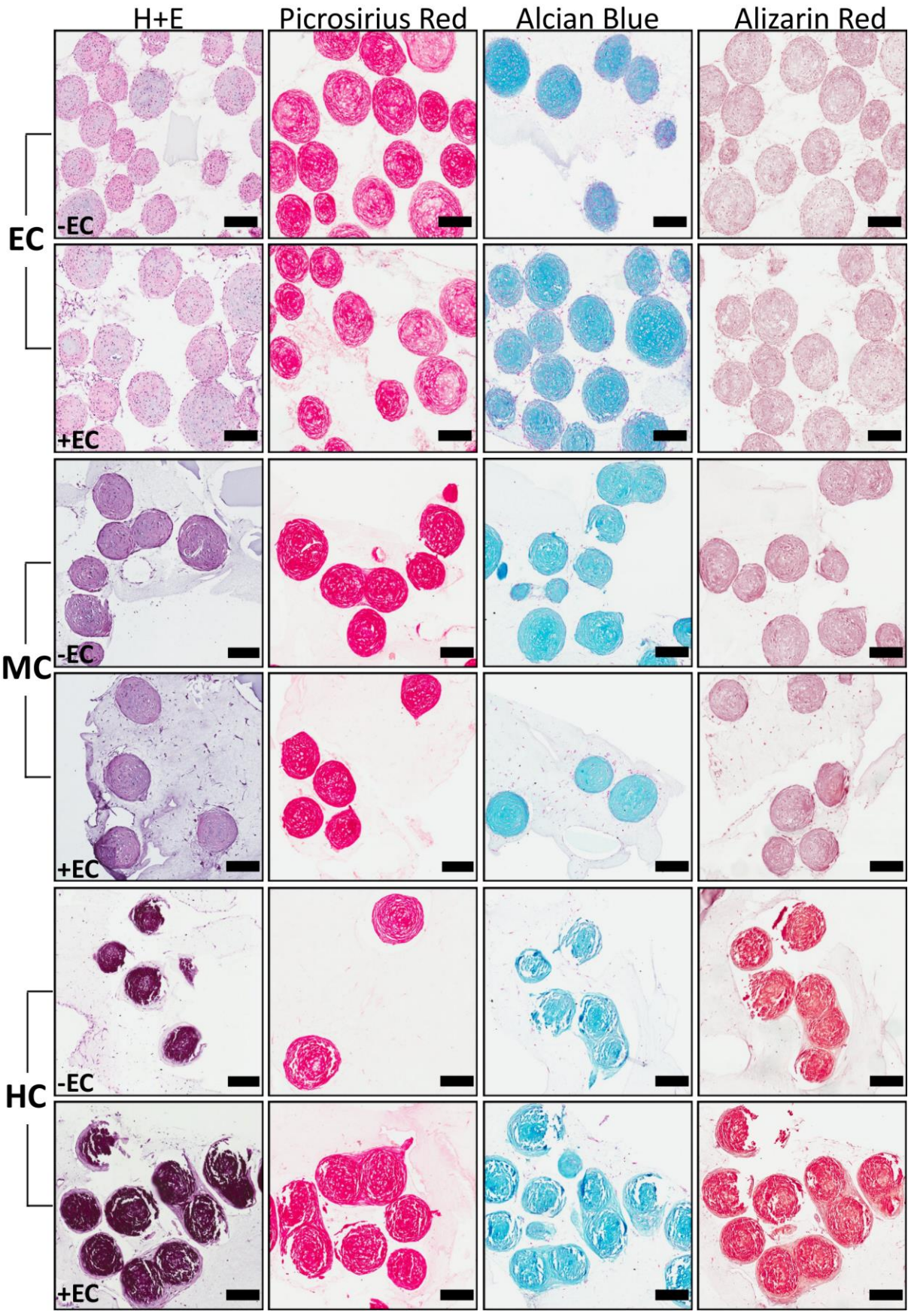

Figure 4.5: Characterisation of gross ECM changes in vascularised μDBOs. Changes in general cell and tissue structure (H&E), collagen deposition (picrosirius red), GAG deposition (alcian blue), and mineralisation

(alizarin red), after one week of MPS culture in the presence (+EC) and absence (-EC) of vascularisation for µDBOs at increasing stages of differentiation. Scale bar = 200µm.

4.3.5 MPS incorporating vascularised µDBOs mimic key events observed during EO

Finally, this thesis next sought to examine whether this MPS could capture some of the key events observed during EO *in vivo*; the induction of pluripotency genes in chondrocytes with vascular invasion, and their subsequent transdifferentiation into osteoblasts. For this, gene expression in unvascularised µDBOs (-ECs), vascularised (+EC), and µDBOs before MPS seeding (Day 0 - µwell Culture) were quantified using qRT-PCR. Interestingly, MPS culture (Day 3 ± EC) generally increased the expression, though non-significantly, of pluripotency genes in all µDBOs compared to day 0 µwell culture (Figure 4.6A), indicating a possible effect of the angiogenic factors in the medium. However, the specific presence of vasculature significantly increased the expression of the pluripotency associated genes *SOX2*, and *OCT4* in MC DBOs, having no effect on the expression of these genes in UC, EC or HC µDBOs. This indicates specific endothelial cell driven induction of pluripotency in the MC µDBOs.

Next, the extent to which µDBO vascularisation accelerated hypertrophy and progression towards an osteogenic phenotype was examined. Hypertrophic/osteogenic genes *RUNX2*, *MMP13*, and *COL10a1* were quantified after 3 and 7 days in unvascularised and vascularised µDBOs (Figure 4.6B). At day 3, the presence of vasculature alone lead to a reduction in *RUNX2* expression in HC DBOs, but otherwise had little effect on hypertrophic/osteogenic gene expression. After 7 days, the presence of the vasculature enhanced the expression of *MMP-13* in the EC DBOs, but had no effect on *RUNX2* or *COL10a1* expression. Gene expression was largely unaffected by vascularisation in MC µDBOs. Finally, in HC µDBOs, the presence of vasculature again reduced the expression of RUNX2, but has no effect

on MMP-13 or *COL10a1* expression. Taken together, these results suggest vascularisation induces upregulation of hypertrophic genes, specifically MMP-13, in EC µDBOs, but not in MC or HC µDBOs by 3 or 7 days.

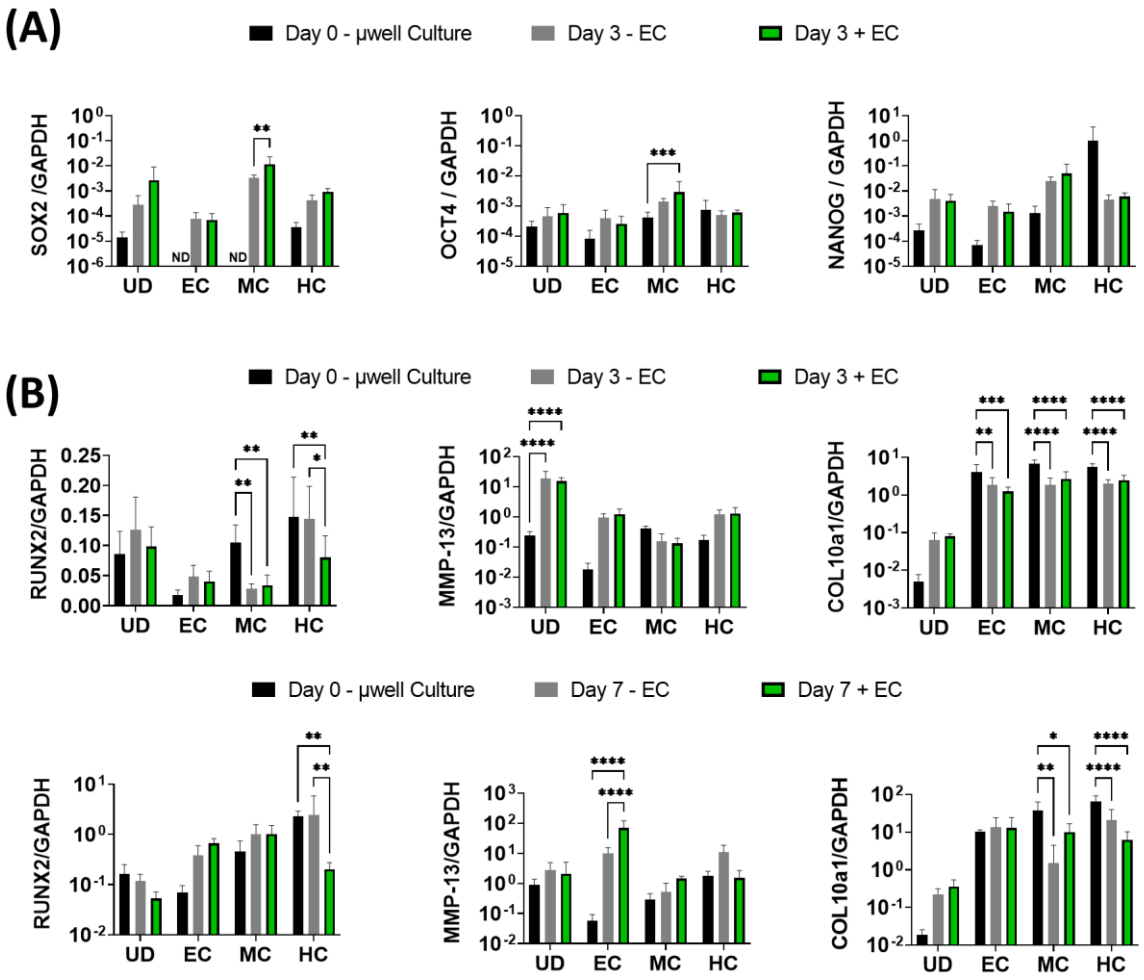

Figure 4.6: Vascularised µDBOs mimic key events in endochondral bone development. (A) Expression of pluripotency genes in µDBOs prior to MPS culture (µwell culture), after 3 days culture unvascularised (– EC) and after 3 days vascularised culture (+EC). **(B)** Expression of hypertrophic genes in µDBOs prior to MPS culture, after 3 and 7 days culture unvascularised, and after 3 and 7 days vascularised culture. n =6

4.4 Discussion

Transition of a cartilage template to bone during endochondral ossification is essential in bone development and regeneration, yet it is still poorly understood. The cartilage template matures over time during EO, initially supressing but later promoting vascularization of the developing bone template [259-261]. The change in cross-talk

between these two tissues niches ensures proper bone development, and, in a therapeutic context, also dictates its potential to effectively develop into bone tissue [155]. Currently, *in vitro* model systems to model and further understand this process are lacking [9]. Until advanced *in vitro* bone substitutes have been developed and validated, the bone research community will continue to rely on *in vivo* models that are under ethical scrutiny [262], can be prohibitively expensive, and do not adequately predict efficacy when translating bone therapies to humans [263]. In light of this problem, this study describes the design and development of an in vitro model of human EO consisting of developing bone organoids and their interaction with invading vasculature. This MPS system is validated by demonstrating its potential to recapitulate key events observed during EO.

Angiogenesis of the developing bone rudiment occurs as the cartilage template matures towards hypertrophy. Thus, to further understand the crosstalk between vasculature and developing bone as it matures, a range of DBO representative of the stages of early bone development (early cartilage, mature cartilage, hypertrophic cartilage) was required. To achieve this, a µwell culture system to generate microscale cartilage µDBOs for seeding within an MPS platform was used. Consistent with the literature[264], it was demonstrated that these microscale DBOs accumulate a cartilaginous matrix, mineralise, and exhibit an upregulation of genes associated with hypertrophy. By simply terminating µwell culture at specific stages, microscale developing bone organoids (µDBOs) with unique phenotypes representative of the different stages in early endochondral bone development can be fabricated. Once primed in µwell culture, µDBOs can be vascularised by seeding with endothelial cells in a matrix that permits vascular formation. The advantage of this approach is the vasculogenesis can proceed in the presence of the µDBOs, and the two tissues can

be subsequently separated and analysed. This approach was further motivated by the inability of HUVECs to vascularise a chondrogenically primed bulk cartilage matrix (Appendix 4).

This model was able to recreate key biological phenomena that have been observed *in vivo*. Firstly, stable cartilage is avascular, and inhibits angiogenesis through the expression of anti-angiogenic factors [265] such as thrombospondin-1 [266], collagen type 18 [267], and SPARC [268], among others (Appendix 5). In the model, inhibition of vascular invasion was observed around mature cartilage organoids, which correlated with an upregulation of THBS1. THBS1 exerts its antiangiogenic properties by three different mechanisms: ligation of CD36 on ECs to induce apoptosis [269], binding with the VLDL receptor to induce cell cycle arrest [270], and direct binding and inhibition of VEGF via the low density lipoprotein receptor-related protein-1 (LRP-1) [271]. Morphologically, no cellular debris indicative of apoptosis was observed in the model, thus cell cycle arrest or VEGF inhibition would be more likely candidate antiangiogenic mechanisms, which could be deciphered by probing for downstream effectors of both mechanisms with Ki67 or an LRP-1 antagonist. COL18a1 was also upregulated in MC µDBOs in the presence of vasculature. Endostatin is a cleaved fragment of collagen XVIII (gene product of COL18a1) that has well documented anti-angiogenic properties and is being trialled for treatment of solid tumours [272]. COL18a1 was found to be upregulated in both unvascularised and vascularised µDBOs, with vascularised µDBOs having significantly upregulated expression, which corresponded with decreased vascularisation. Collagen XVIII is strongly expressed in cartilage and fibrocartilage [267] but not much else known about its biogenesis, or induction of its expression. Finally, a downregulation of SPARC was observed in all µDBO groups, irrespective of the presence of vasculature. Downregulation of SPARC

coincided with both increased vascularisation around EC µDBOs and decreased vascularisation around MC µDBOs. The results cannot definitively explain the range of these observations, however, the effects of SPARC are complex, as it has been demonstrated to have both angiogenic and antiangiogenic effects [273]. In this case, SPARC could potentially be regulated by another protein that modulates its activity post-transcriptionally, such as TGF-β activation [274], where it is the variance in this factor that induces the variance in vascular phenotypes. Further studies would be required to test such hypotheses. In addition, the difference in size of the spheroids would indicate a difference in oxygen tension in cells at the centre of the spheroids, suggesting a potential role for HIF-1α in the observed vascular morphologies.

The EO model was also able to recapitulate the vasculature-induced induction of pluripotency associated genes in hypertrophic chondrocytes, a phenomena observed during EO in fracture healing [14, 15, 64]. SOX2 and was upregulated in all µDBOs when cultured in both vascularised and unvascularised devices. However, a significant increase in SOX2 expression was evident in MC µDBOs in the presence of vasculature. This correlates with vasculature induced SOX2 expression observed in EO bone formation [14]. Thus, the model recreates vasculature induced expression of pluripotency genes *in vitro*, and warrants exploration of canonical angiogenic growth factors as possible mediators of this induction. OCT4 was also upregulated in vascularised and unvascularised devices, and again, significantly so in MC µDBOs within the onset of vascularization. This also correlates with increased OCT4 expression observed in chondrocytes undergoing EO mediated bone formation [14].

At day 3 post seeding in MPS devices, the presence of vasculature had little effect on the expression of hypertrophic/osteogenic genes across all µDBOs. The exception to this was in HC, where vasculature actually downregulated RUNX2 expression. IGF-

1, which is an essential component of the medium used in these experiments, has been used to promote stable cartilage formation, and inhibits hypertrophic gene expression; inhibiting the expression of RUNX2 and MMP-13 [275], which may partially account for this particular observation. At day 7, vasculature again generally had little effect on osteogenic/hypertrophic gene expression, with MMP-13 upregulation in early cartilage µDBOs the notable exception. This observation was amongst a general increasing trend in hypertrophic gene expression observed from day 3 to day 7 in all µDBOs. It has been shown that angiogenic factors, such as VEGF, direct MSCs toward an osteoblastic phenotype, possibly accounting for the upregulation of these bone related genes [38].

It is clear from the data that ECs contribute to induction of pluripotency and hypertrophy in µDBOs, particularly in MC µDBOs. However, it is also clear that µDBOs are perhaps more sensitive to the angiogenic milieu of the EGM-2MV media that contains a number of angiogenic growth factors. While the model still substantiates the canonical actions of endothelial cells in EO driven bone formation, it also suggests that secreted angiogenic factors may have a significant role to play. Optimising the vascularised media formulation to decouple the EC-µDBO interaction from the effects of growth factors is a prudent future step, as subtle cell interactions may be lost in growth factor laden medium at supraphysiological doses.

Additional steps are required to facilitate further development and translatability of this EO MPS. Firstly, HUVECs were used as they are a practical and well characterised primary human ECs type for MPS applications. However ECs are a heterogeneous population that vary depending on their origin [276], and ECs specifically from bone have been shown to be sensitive to key signalling molecules involved in EO, such as PTHrP, while those from other tissues have not [183]. Also, as noted previously,

optimising media formulations to decouple the stimulatory nature of EGM-2MV from other factors would better allow subtle interactions between the μDBOs and vasculature to be probed. Nonetheless, the results described here indicate that the introduction of vasculature, and/or the angiogenic milieu, regulates the phenotype of human developing bone organoids with MPS, enabling the developing of *in vitro* models of EO that mimic key phenomena observed *in vivo*.

4.5 Conclusion

This study details the development of an advanced *in vitro* model of endochondral ossification. Specifically, we model the critical cross talk between developing bone and vasculature in EO that underpins the cartilage to bone transition. Our model mimics key events in endochondral bone development: the changing angiogenic profile of cartilage as hypertrophy proceeds as well as the vasculature induced expression of pluripotency associated genes. Further development of these advanced *in vitro* systems could bring about a more complete understanding of EO, and has the potential to expedite the development of therapeutics for a range of skeletal conditions

Normal progression of EO results in formation of the bones of the adult skeleton. Mature adult bone has a vast array of functions in homeostasis, such as self-regulation of bone metabolism, and endocrine regulation of biological processes in distant organs. Furthermore, mature bone is the target of a number of the most prominent skeletal diseases and off-target effects of common drugs. However, models of mature bone, the key cells that make up mature bone tissue are lacking. This situation manifests as model human *in vitro* systems for mature bone cells have proven difficult to engineer. Thus, the next chapter, will focus specifically on the cell-biomaterial

component of a mature bone MPS, and specifically detail an *in vitro* hydrogel system that can produce functional human bone cells as a model of mature human bone for use in MPSs.

Chapter 5: Developing an Engineered Bone Tissue that Recreates Mature Bone Function for MPS Applications

5.1 Introduction

The traditional function of mature bone is to maintain a protective framework, facilitate locomotion, and act as a mineral reserve to balance serum ion levels. Critical to all of these is the process of bone remodelling; the coordinated actions of osteoblasts, osteoclasts and osteocytes to balance bone formation and resorption [277]. Bone cells, specifically osteocytes, regulate this process by secreting regulatory factors that alter the balance of remodelling [85]. Indeed, targeting these osteocyte derived factors has become one of the key therapeutic approaches for treating metabolic bone disease [1]. Additionally, osteoblasts that line the bone surfaces have been shown to be a hormone source that mediates glucose handling in the pancreas [16], and may have a critical role to play in conditions such as diabetes [115]. Thus, osteoblast and osteocyte secretions have essential roles in maintaining bone homeostasis, and mediating bone's endocrine function through secretion of regulatory factors. It is clear from this that developing new bone tissue analogues for pre-clinical evaluation of mature bone function will require recapitulation of this regulatory function, however a suitable engineered bone tissue analogue for such applications has yet to be realised.

Osteoblasts secrete a number of bone specific proteins, of which osteocalcin (OCN) is the mediator of bone's regulatory role in glucose metabolism. OCN stimulates β-cell proliferation and insulin secretion, and furthermore increases insulin sensitivity in muscle and adipose tissue [16, 106, 150]. Once matured, osteoblasts begin a continuum of differentiation into osteocytes [94], where they become orchestrators of bone remodelling by secretion of factors such as sclerostin [278]. Romosozumab, an

anti-sclerostin antibody, blocks sclerostin's inhibitory effects osteoblasts, improving bone formation, and has been recently approved for treating osteoporosis [279]. However, as a result of the lack of predictivity of pre-clinical models [280], romosozumab was shown to have off-target effects once it reached the clinic; with patients taking romosozumab having increased risk of cardiac incidents [1]. Thus, while these factors hold great promise for treatment of disease, their development requires improved preclinical models, as current pre-clinical models are evidently inadequate, and are leading to higher risk products.

From this, it is clear improved models of human bone that overcome the limitations of current pre-clinical models are needed, and MPSs are an ideal platform on which to build these systems. MPS systems have been used to model some aspects of bone biology, such as metastatic invasion of bone tissue in breast cancer [33]. However, an MPS to model mature bone, and particularly its regulatory secretome, has yet to be realised. Primary bone cells and cell lines exist that could be applied in this context, however primary cells are difficult to isolate, dedifferentiate in culture, while cell lines are typically of murine origin and often don't produce the necessary clinically relevant regulatory factors, such as sclerostin [171]. Despite MPS technology showing high potential as a platform on which to model bone, pre-requisite components, such as the cell type and biomaterial that can differentiate the required cells of mature bone have yet to be developed.

In light of this, this chapter details the development of an engineered human bone tissue containing osteoblast / early osteocytes expressing known regulatory factors for use in MPSs. This tissue is engineered by encapsulating human bone marrow stromal cells (hBMSCs) into collagen based hydrogels functionalised with nHA. A sequential screening and optimisation experimental approach is applied to identify and optimise

the key factors involved in hBMSC maturation to late osteoblasts / early osteocytes. This approach leads to an engineered tissue that mimics key features of bone and exhibits excretion of endocrine and bone remodelling factors. This engineered human bone tissue is a key development towards the integration of functional bone into multi-organ pre-clinical models for drug discovery and basic research.

5.2 Methods

5.2.1 Experimental flow and design

Experimental Design

The goal of this series of experiments is to deduce the important factors regulating hBMSC to mature osteoblasts / osteocytes and optimise these factors. To do this, factorial experimental designs was used [229] [238]; a statistical method that uses reduced experimental size to study a large number of factors, designed to sort the key factors influencing a process from the less significant effects. Experiments like these are termed screening experiments, as they are typically employed to screen a number of potential factors influencing a process. Optimisation of the process is then carried out by further exploring the key factors identified during the screening experiment.

In the screening experiment, hBMSCs were seeded in cylindrical collagen gels and cultured over 14 days. Matrix stiffness, cell density, media type, retinoic acid concentration, nano-hydroxyapatite (nHA) concentration, and oxygen tension were varied between two levels, high and low, to establish their relative effects on hBMSC differentiation towards a late osteoblast / osteocyte phenotype (Table 5-1). A 2^{6-1} experimental design, which includes half of the groups used to study these 6 factors at two levels, was used. This design produces 32 experimental groups which were

evaluated in triplicate. The experimental groups generated using this method are shown in Appendix 3.

Table 5-1: Factors investigated to drive late osteoblast / osteocyte differentiation of hBMSCs. OSM – osteogenically supplemented medium

Factor	Low	High	Unit
Collagen Stiffness [281]	4	8	kPa
Cell Density [282]	0.1	0.5	$x10^6$ cell/ml
Media	XPAN	OSM	N/A
Retinoic Acid Concentration [283, 284]	5	10	µM
Nano-Hydroxyapatite [285]	0.27	2.7	mg/ml
Oxygen Tension [286-288]	5	20	%

Results of the 2^{6-1} fractional factorial DOE were analysed using Minitab (Minitab, USA). The response variables, or measured outputs, used to assess osteogenesis were extracellular alkaline phosphatase (ALP) expression, sclerostin expression, and cell shape. These quantified responses were mathematically best fit to the input factor levels to create a mathematical model of the experimental system. This mathematical model is in the form:

$$y\,(response) = \bar{x} + \alpha_1 A + \alpha_2 B + \alpha_3 C \ldots + \alpha_7 AB + \alpha_8 AC + \alpha_9 AD \ldots + \alpha_n ABCDEFG$$

Where $\bar{x}$ is the mean response, A,B,C..F are levels of the factors, (-1 for low, +1 for high), and $\alpha_{1\text{-}n}$ are the coefficients for each term. The results are displayed on a pareto chart, sorting the coefficient α for each term of the equation in ascending order, placing the factors with the largest effects on the top. The main effects plot is also displayed, which simply shows the overall difference in means for each factor set at their high and low levels. Additionally, interaction plots, that detail interactions between factors are displayed. Interaction effects show large coefficients when two or more factors act synergistically or destructively. For each model, the R^2 value, indicating how well the model fits the experimental data is calculated.

5.2.2 Cell culture

Human bone marrow (Lonza, USA) was purchased and hBMSCs were isolated. Whole bone marrow was plated at 2000 cells/cm^2 and expanded in high-glucose Dulbecco's modified Eagle's medium supplemented with 10% v/v fetal bovine serum (FBS), 100 U/ml penicillin, 100mg/ml streptomycin (all Gibco Biosciences, Dublin, Ireland) and 5ng/ml FGF-2 (Peprotech, UK), herein referred to expansion media (XPAN), for one week at 37°C, 5% O_2 and 5% CO_2. Once colonies had formed, cells were trypsinised and subcultured until sufficient cell numbers were achieved, cells were then frozen down and stored in LN_2 before use. The donor used was evaluated for osteogenic capacity. For experimental expansion, hBMSCs were plated at 5000 cells/cm^2, expanded in XPAN+FGF in 5% O_2 until confluent and passaged at 80% confluence. hBMSCs at P4 were used for all experiments.

5.2.3 Nano hydroxyapatite synthesis

Nano-hydroxyapatite (nHA) particles were synthesised according to previously described protocol [289]. Briefly, a phosphate solution (12mM), containing 0.017% (V/V) Darvan 821A dispersant reagent (RT Vandervilt), was added dropwise to an equal volume of calcium chloride solution (20mM) under agitation. The resulting nHA suspension was centrifuged at 5000 rpm for 60 minutes. The supernatant was decanted and the resulting nHA pellet was re-suspended in DI water and sonicated for 2 minutes at 20 kHz and 80% amplitude. The resulting nHA is in the form of nanosized rod-like particles whose length and width range from approximately 50 to 100 nm and from 15 to 25 nm, respectively.

5.2.4 3D Collagen – nHA gel Culture

Rat tail type 1 Collagen (Corning, UK) was used to make Coll-nHA hydrogels as per the manufacturer's protocol with the following modifications. 10X PBS was replaced with 10X PBS with 0.159 mg/ml phenol red (Sigma, Ireland) to visualise gel pH. DI Water was substituted with concentrated nHA and cell suspensions to bring final cell ($0.1x10^6$ and $05x10^6$ cells/ml), nHA (0.27 and 2.7 mg/ml) and collagen (4 and 8 mg/ml) concentrations to those required for each experimental group (Appendix 3). Cell seeded collagen-nHA gels were pipetted into cylindrical (Ø6.25 x 2mm) silicone moulds and allowed to crosslink for 30 mins at 37°C. Gels were removed from moulds and placed in coverslip bottom 24 well plates. Constructs were then cultured in the appropriate media and oxygen conditions as per Appendix 3. Media was exchanged twice per week and cultured media was collected and stored at -20°C for analysis.

5.2.5 Cell morphology quantification

hBMSCs were labelled with PKH26 cell membrane label (Sigma Aldrich, Ireland) before seeding in constructs for live cell imaging and morphology quantification. Cell labelling was carried out as per the manufacturers protocol with one exception; 2µM dye per 10^6 cells was used instead of 0.1µM per 10^6.

PKH67 labelled MSCs were imaged at specified time points using a Leica SP8 scanning confocal microscope (Leica, Germany). For each sample, a 50µm Z stack was acquired and collapsed to one 2D image. Images were processed as follows: first, cell outlines were selected by thresholding fluorescence images. For each group, 3 representative cells were selected from 5 samples. Cell morphology was quantified using a normalised shape factor index (Equation 1). First, shape factor, the ratio of cell area (A) to cell perimeter (P) was calculated (Equation 2); shape factor varies from 0

(highly dendritic or elongated cells) to 1 (round cells). Dendritic cells and elongated cells have similarly low shape factors. To account for this, the number of processes were counted on each cell, and shape factor index was calculated by dividing the shape factor by the number of cell processes:

$$Shape\ factor\ Index = \frac{Shape\ factor}{Number\ of\ Cell\ Processes} \qquad (1)$$

$$Shape\ Factor = \frac{4\pi A}{P^2} \qquad (2)$$

5.2.6 Alkaline Phosphatase (ALP) activity quantification

Extracellular ALP production was determined using a colorimetric assay of the ALP enzyme activity, which uses p-nitrophenyl phosphate (pNPP) as a phosphatase substrate with ALP enzyme (Sigma Aldrich) as a standard. Solutions of 2-Amino-2 Methyl-1-Propanol (AMP) (1.5 M with a pH 10.25), pNPP (20 mM), and Magnesium Chloride (MgCl2) (10 mM) were prepared. Each of these solutions was combined in a ratio of 1:1:1 to make the substrate working solution (AMP-pNPP-MgCl2). Next, 50 µL of culture media was added to a 96-well plate in triplicate with 50 µL of substrate working solution. The samples were shielded from direct light at 37°C for one hour. After this, 100 µL of Stop Solution (1M NaOH) was added to the wells and the plate was read at 405 nm in a micro-plate reader.

5.2.7 DNA analysis

Constructs were thawed from -80°C and digested with papain (125 µg mL−1) in 0.1 M sodium acetate, 5 mM L-cysteine HCl, 0.05 M EDTA, pH 6.0 (all from Sigma-Aldrich)

at 60 °C and 10 rpm for 18 h. dsDNA was quantified using a Quant-iT™ PicoGreen® dsDNA Assay Kit (Biosciences, Ireland) as per the manufacturers' instructions.

5.2.8 Sclerostin ELISA

600 µL of media supernatants from bi-weekly media changes were stored in Eppendorf tubes and frozen down to -20°C before analysis. Media samples were thawed and concentrated 7x using a 10 kDa amicon filters (Merck, USA) (Sclerostin M_w = 21 kDa). Concentrated samples were assayed using a human Sclerostin ELISA kit (R&D Systems, USA) as per the manufacturer's instructions.

5.2.9 Collagen-Alginate-nHA IPN fabrication

In order to increase the stiffness of collagen-nHA constructs in latter experiments, low viscosity (197 mPa.s) alginate (NovaMatrix, Norway) was added to the Collagen-nHA solution to create a Collagen-Alginate-nHA IPN. 30mg/ml collagen solution with 1.22M calcium sulfate was added to a 1ml syringe (BD Biosciences) and coupled to another 1ml syringe containing 40mg/ml alginate and 5.35mg/ml nanohydroxyapatite suspension and mixed on ice for 10 seconds before depositing into silicone moulds. This IPN pre-polymer was incubated at 37°C for 90 mins to allow both IPN components to gel. IPN gels were then removed and placed in media for culture.

5.2.10 Mechanical Testing

Unconfined compression was performed using a compression testing rig (Zwick-Roell, Germany). Acellular gels were fabricated as per section 5.2.4 and section 5.2.9 and kept in DMEM overnight at 4°C. Constructs were subjected to 30% strain at a displacement rate of 1mm/min once a pre-load of 0.1 N was reached. Compressive modulus was calculated at the first linear portion of the graph, typically 10-15%.

5.2.11 Gene Expression Analysis

Sample Handling

Upon termination of culture, all gels were rinsed with PBS and immediately snap frozen in liquid nitrogen and stored at -80˚C.

RNA Isolation and CDNA Transcription

RNA isolation and CDNA transcription was carried out as previously described in Section 4.2.10. Primer pairs used for PCR reactions are detailed in Table 5-2.

Table 5-2: Primer pairs used for PCR reactions

Gene Name	Gene Full Name	Forward / Reverse	Tm (˚C) in use	Tm (˚C) predicted
MEPE	Matrix Extracellular Phosphoglycoprotein	F: 5' GGTGAAAGATACCAGAGATTC 3' R: 5' CTCAGTCTGTGGTTGAAATG 3'	60	56.7 58.3
SOST	Sclerostin	F: 5' GAACAACAAGACCATGAACC 3' R: 5' TACTCGGACACGTCTTTG 3'	60	59.4 57.2

5.2.12 Histology

For histological analysis, samples were washed with PBS, fixed with 4% paraformaldehyde at 4˚C overnight, and again washed with PBS. Samples were then immersed in 30% sucrose overnight, followed by immersion in 15% sucrose 50% optimal cutting temperature (OCT) compound overnight. Samples were then frozen in isopentane (Sigma Aldrich, Ireland) cooled in liquid nitrogen, and stored at -80˚C. Samples were warmed to -22˚C in a cryostat (Leica, UK) and sliced at a thickness of 50 µm.

For tissue morphology, slices were stained with alizarin red to assess mineralisation.

Osteocyte marker E11/Podoplanin was assessed using immunofluorescence. Sliced samples were warmed to room temperature, outlined with a pap-pen and hydrated with PBS for 5 minutes. Samples were then treated with 0.5% Triton X-100 (Sigma Aldrich, Ireland) washed and blocked for 1 hour at room temperature with 10% goat serum (host species of the secondary antibody) in PBS. Primary antibody for E11/Podoplanin (Origene, DM3500P, stock 0.2 mg/ml, 1:100) was diluted in blocking buffer (10% goat serum + 1% BSA) and incubated on samples overnight at room temperature. Samples were then washed copiously with PBS and Goat α-Mouse Alexa Fluor® 488 (Life Technologies, A11001, 1:500) was added and incubated for 4 hours at room temperature. Samples were then washed and incubated in 1µg/ml 4′,6-diamidino-2-phenylindole (DAPI), washed and mounted in prolong gold antifade mounting medium (Invitrogen).

F-Actin staining was carried out using Alexa Flour 660 Phalloidin (Thermofisher) at 165nM in PBS.

5.2.13 Statistical Analysis

Fractional factorial experimental set up and analysis was performed using Minitab statistics package (Minitab, USA). For analysis, main effects plots and pareto charts were generated. The standardised effect of each factor was considered significant at $\alpha=0.05$.

Elsewhere, comparisons made between 2 independent groups, or multiple independent groups were analysed using GraphPad Prism (GraphPad, USA) using student's t-test or one-way ANOVA respectively. Comparisons made between groups split into multiple factors were analysed using two-way ANOVA. Statistical comparisons were carried out using non-parametric tests unless normality and

homoscedasticity could be evaluated and proven [290]. Graph notation for deemed significance is as follows: * $p<0.05$, ** $p<0.01$, *** $p<0.001$, **** $p<0.0001$.

5.3 Results

5.3.1 Matrix stiffness and nanohydroxyapatite concentration are important mediators driving hBMSC osteogenic lineage commitment.

To identify factors that support the differentiation of hBMSCs into mature osteoblasts / osteocytes, 6 different experimental parameters were varied (cell density, media type, nanohydroxyapatite concentration, collagen stiffness, oxygen tension, and retinoic acid concentration; see Table 5-1) using a fractional factorial DOE [229]. The first output monitored in the screening experiment was extracellular ALP activity, with culture supernatants being analysed on day 3,7,10 and 14. On day 14, cell density and media type were the two most influential factors on overall ALP activity (normalised to DNA; see Figure 5.1A), with a lower cell density and osteogenic media supporting increased ALP activity (Figure 5.1B). However, the intent of this assay was to assess whether ALP activity decreased over time in culture, which was not observed but is expected to occur as osteoblast begin to differentiate into osteocytes [94]. Nonethelss, the most influential factors that governed ALP activity over this 14 day culture period were cell density (Figure 5.1C(i)) and media type (Figure 5.1C(ii)).

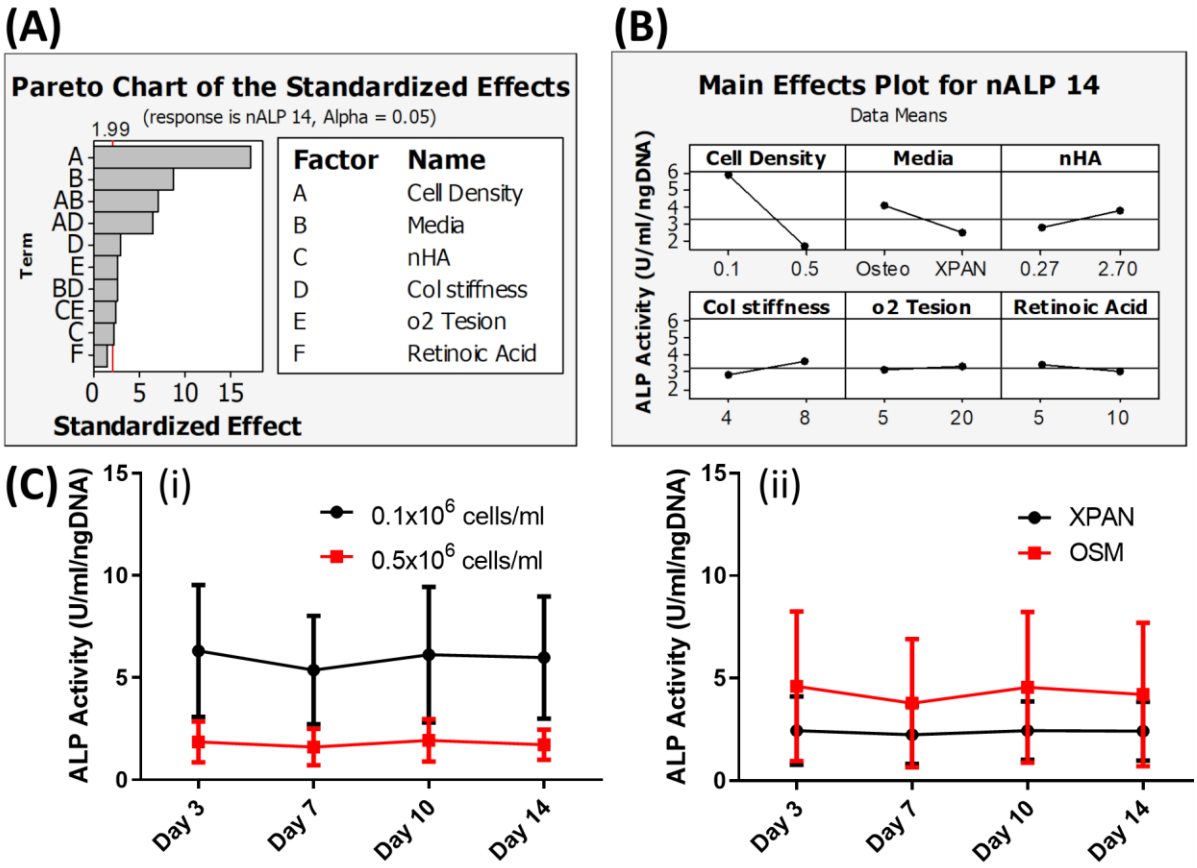

Figure 5.1: Cell density and media type influence overall ALP activity, with no change in ALP activity observed over time in culture. (A) Pareto chart showing the factors contributing to ALP activity, in order of their effect size. (B) Main effects plot showing the effects of the 6 studied factors on ALP activity. (C) ALP activity over 14 days in culture grouped by main effects cell density (i) and media type (ii). No change in ALP activity was observed over the 14 day culture period. Model shown is reduced to the 10 most influential factors. R^2 for the model is 84%.

Sclerostin secretion was also measured by ELISA at day 14. Collagen matrix stiffness and nHA concentration were found to be the most influential factors (Figure 5.2A). More specifically, sclerostin expression was shown to be increased in groups with stiffer 8 kPa matrices, and groups with lower nHA concentration (0.27mg/ml) (Figure 5.2B). Media type was also a significantly influential factor but had the lowest effect of the significant factors. Overall, these chosen factors could predict 70% of the variation in sclerostin values (R^2=70%). Critically, Figure 5.2A shows a significant interaction term; nHA and matrix stiffness (CD),indicating there is a synergistic effect of stiffer collagen matrices (8kPa) at low nHA concentrations (0.27mg/ml) (Figure 5.2C).

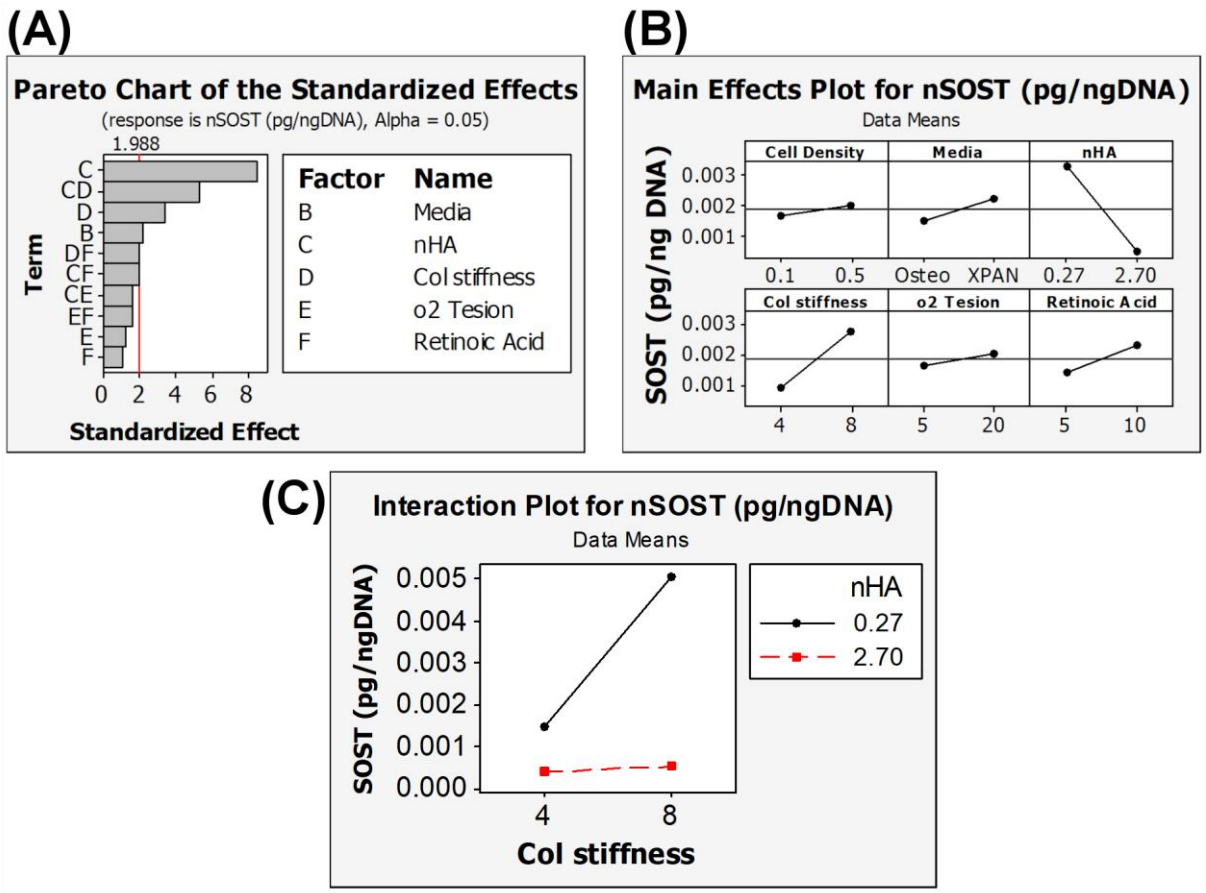

Figure 5.2: Pareto chart, main effects plot, and interaction plot of extracellular sclerostin expression at day 14. (A) Pareto chart showing the factors contributing to sclerostin production, in order of their effect size. (B) Main effects plot showing the effects of the 6 studied factors on sclerostin production. Model shown is reduced to the 10 most influential factors. R^2 for the model is 70%

Finally, cell shape was quantified to identify factors that produced dendritic cell morphologies; indicative of differentiation towards a late osoteblastic / early osteocytic phenotype. The 32 different experimental permutations produced a range of cell morphologies (Figure 5.3A); a ‘dendritic’ low shape factor (Figure 5.3A(i)), an ‘elongated’ medium shape factor (Figure 5.3A(ii), and a ‘rounded’ high shape factor (Figure 5.3A(iii)). The factors that most influence cell shape factor are shown in descending order in Figure 5.3 (B). Of these, media type (A) and cell density (B) were key main effects. A lower shape factor (i.e. more dendritic cells) was evident in expansion media and at a higher cell density (Figure 5.3C). While such factors could

account for some variance in cell shape, the entire model could only account for 46% of the total variance (R^2=46%), indicating these factors alone are not good predictors of cell shape, or cell shape is too variable a measure on which to build a predictive model.

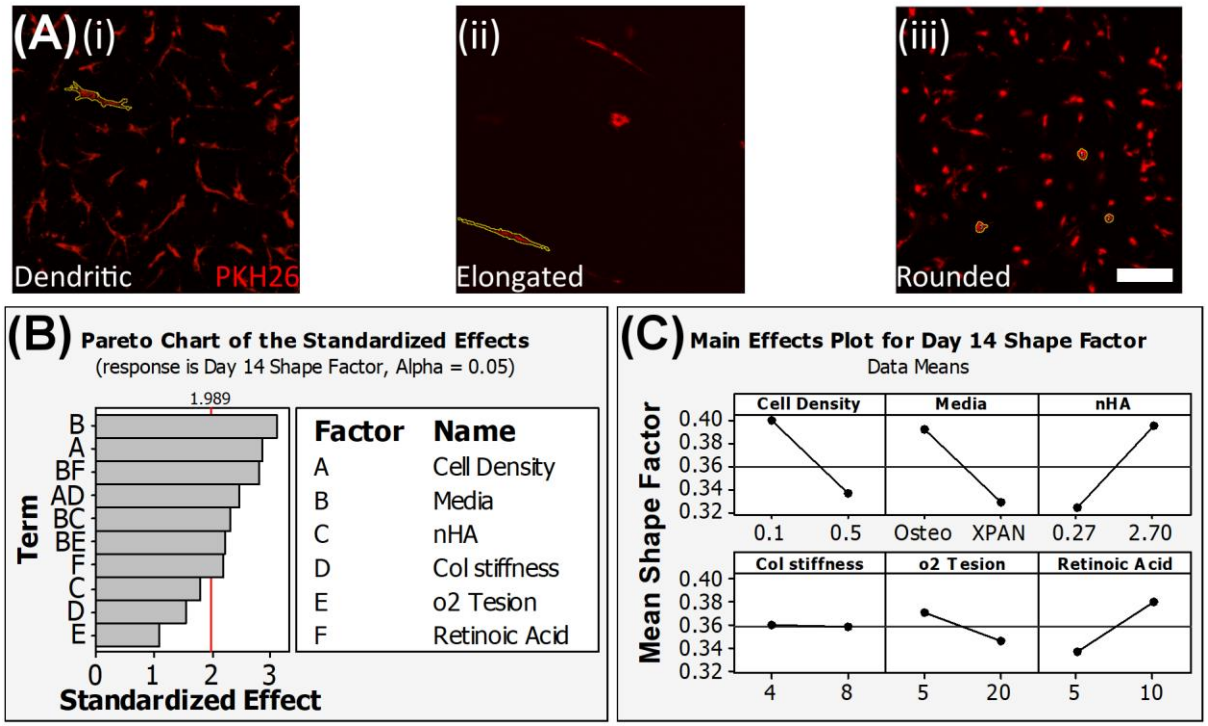

Figure 5.3: Cell morphology analysis at Day 14. (A) Experimental groups presented variation in observed cell morphology. (B) Pareto distribution of standardised effects of each factor on shape factor index. (C) Main effects plot for each of the 6 studied factors. Note: lower shape factor index values correspond with more dendritic morphology. Model shown is reduced to the 10 most influential factors. R^2 for the model is 46%

The intent of this screening experiment was to inform further experiments to optimise hBMSC differentiation into mature bone cells. The different analysis methods pointed to a number of influential factors that mediate this process. However, this information must be distilled into the choice of a subset of main factors to bring forward for subsequent experimentation. For this, collagen matrix stiffness and nHA concentration were chosen as the two factors to optimise. The approach was most heavily weighted

on the analysis of sclerostin secretion, as it is a key marker of osteocyte differentiation and is an important secreted regulatory factor. Moreover, the model could account for an acceptable amount of the observed variance, suggesting the factors chosen are indeed influential. For cell shape, the model could not sufficiently account for the variance in the results (R^2=46%), and cell shape is influenced by a multitude of factors that may be unrelated to differentiation. While the ALP model could account for 84% of the variance in results, ALP is a marker of early osteoblast differentiation, and its utility in screening was as a temporal measure of osteoblast maturity and early osteocyte differentiation when ALP expression drops, which was not observed in this model system.

Based on these results, medium, oxygen tension, retinoic acid, and cell density were not explored further, and were maintained at osteogenic medium, 20% O_2, 10µM and $2x10^6$ cells/ml respectively for subsequent experimentation. Cell density was increased from the screening experiment given its negligible effects on SOST expression and to increase detectable signals in subsequent assays. The effects of further increasing collagen matrix stiffness and decreasing nHA concentration, from 8kPa and 0.27mg/ml respectively, on hBMSC differentiation into mature osteoblasts / osteocytes was explored in subsequent experiments.

5.3.2 Optimal nHA concentration enhances mineralisation and sclerostin expression by hBMSCs in collagen hydrogels

Following the screening experiment, the osteogenic effect of further decreasing the amount of nHA in the 8kPa collagen hydrogel was first assessed. At day 21, maximum mineralisation was again observed in the 0.27mg/ml nHA collagen hydrogel, as

assessed by alizarin red staining (Figure 5.4A), with no staining observed at day 0 (data not shown). Additionally, hBMSCs expressed E11, a marker of late osteoblasts/early osteocytes, at all concentrations of nHA (Figure 5.4B). Finally, similarly to the mineralisation data, maximum sclerostin expression was observed in the 0.27mg/ml nHA collagen hydrogels, with sclerostin decreasing with decreasing concentrations of nHA (Figure 5.4C). Based on these results, 0.27mg/ml was the concentration of nHA that best promoted hBMSC differentiation and was therefore used for subsequent experiments.

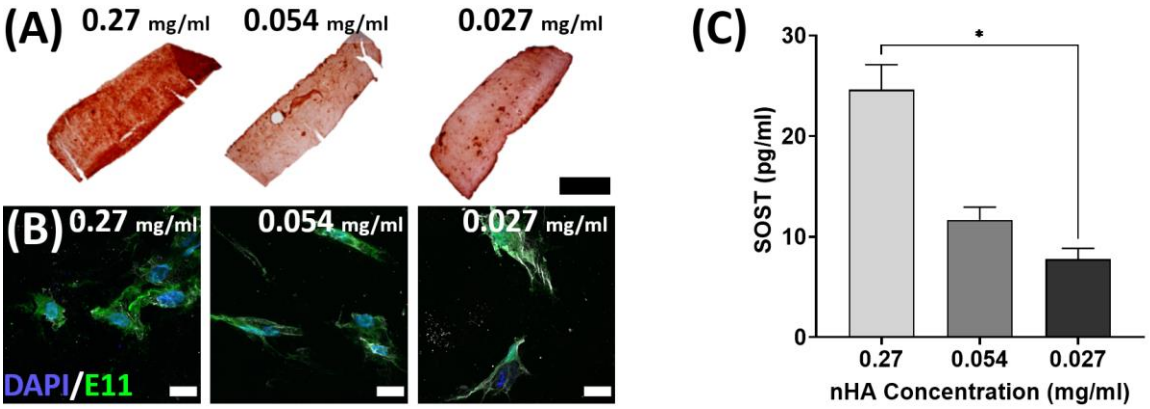

Figure 5.4: Optimal nHA concentration maximises mineralisation and sclerostin expression. (A) Alizarin red staining showing maximum mineralisation is observed in 0.27mg/ml nHA collagen gels at 21 days. Scale bar = 2mm **(B)** Expression of E11 was consistent across all nHA concentrations. Scale bar = 20µm **(C)** At day 42**.** Maximum sclerostin expression was detected in supernatants of hBMSCs cultured in 0.27mg/ml nHA collagen gels.

5.3.3 Low stiffness collagen-nHA hydrogels drive a mature bone phenotype in hBMSCs

Having identified 0.27mg/ml as the nHA concentration that best promoted hBMSC differentiation into mature bone cells, the next step was to identify the optimal matrix stiffness. Screening experimentation suggested further increasing matrix stiffness of the 8kPa collagen-nHA hydrogel. To achieve this, ionically crosslinked alginate was introduced into the collagen-nHA matrix to create a collagen-nHA-alginate

interpenetrating network (IPN). This IPN configuration facilitated stiffening of the collagen-nHA matrix with an inert material that does not present any cell binding sites, while also allowing collagen concentration to remain constant. A number of calcium salts were evaluated to achieve homogeneous IPNs (Appendix 5), of which calcium sulfate dihydrate ($CaSO_4.2H_20$) produced homogenous hydrogels at 30mM (Figure 5.5A). Given their superior macroscopic appearance and homogeneity, these IPNs were taken forward for mechanical characterisation. 4mg/ml and 8mg/ml alginate (final concentration) were added to the 8mg/ml collagen – 0.27mg/ml nHA hydrogel. The three hydrogels were subjected to uniaxial unconfined compression to evaluate elastic modulus and viscoelastic properties (Figure 5.5B and C). Firstly, unconfined compression showed 8kPa collagen-nHA gels could be stiffened to 16kPa (IPN1) and 24kPa (IPN 2) respectively (Figure 5.5B). Following strain application, gels were tested for their viscoelastic response (Figure 5.5C). Collagen-nHA gels displayed quite viscoelastic properties; dissipating stored energy rapidly, while addition of alginate increases the amount of stored elastic energy response of the matrix.

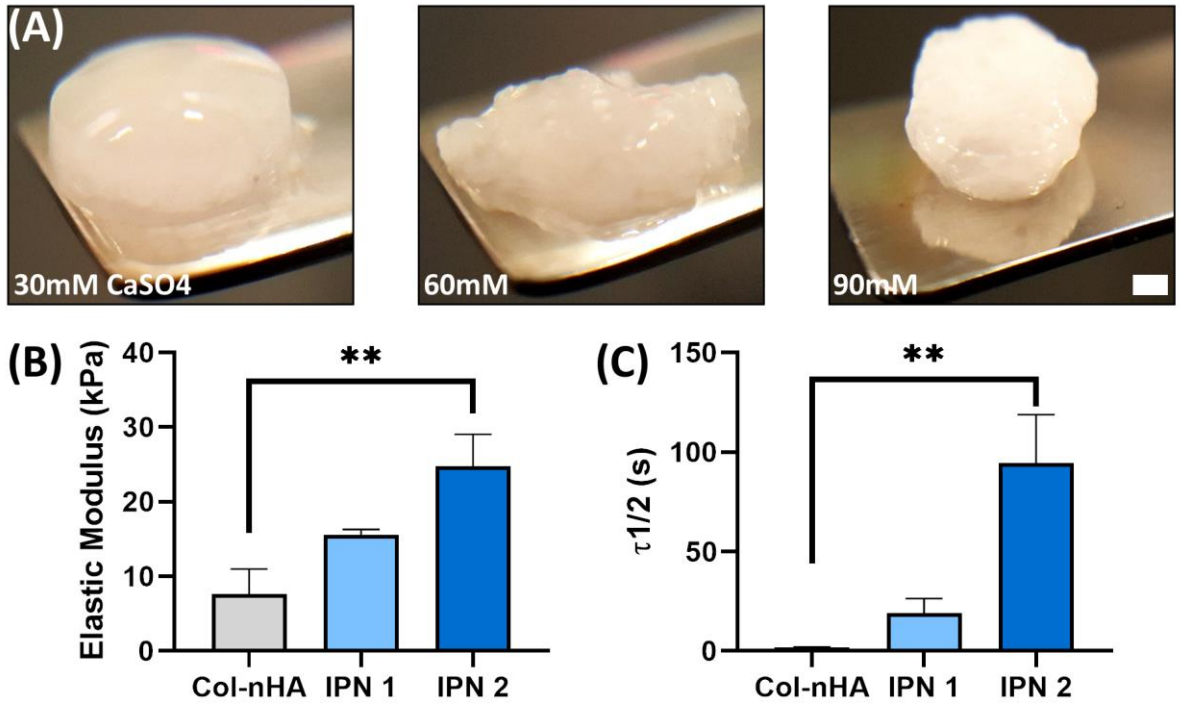

Figure 5.5: Incorporation of alginate into the collagen-nHA matrix to increase matrix stiffness. (A) Low concentration (30mM) calcium sulfate crosslinked IPNs were strong, homogeneous gels. Increasing calcium sulfate concentration resulted in less homogeneous gels with loosely connected alginate agglomerates. **(B)** Unconfined compression of hydrogels shows increasing elastic modulus when introducing alginate into the collagen matrix. **(C)** Stress relaxation time ($\tau_{1/2}$) shows collagen-nHA only hydrogels dissipate their stored elastin energy under strain, while IPNS exhibit more elastic behaviour.

Having mechanically characterised the collagen-nHA-alginate IPNs, their biological properties were next assessed. After 21 days of culture, DNA levels were highest in the lower stiffness collagen-nHA hydrogels, suggesting increased cell proliferation in these softer constructs (Figure 5.6A). Critically, hBMSCs in all materials secreted osteocalcin, however by week 3 higher levels were secreted by cells embedded in the collagen-nHA gels (Figure 5.6B). Osteocalcin secretion decreased over time in culture in the higher stiffness IPNs. hBMSCs in all hydrogels stained positive for E11 and produced a mineralised matrix (Figure 5.6C). Additionally, an osteocyte-like dendritic morphology was evident in all materials, with dendritic cell processes extending out into the matrix. However, hBMSCs in the collagen-nHA hydrogel adopt a more spread morphology, while hBMSCs in the stiffer IPNs exhibit less spreading, and shorter cell

processes in the case of the stiffest IPN (IPN2). Finally, gene expression showed that hBMSCs in the low stiffness collagen-nHA expressed detectable levels of SOST and MEPE transcripts, markers of osteocyte differentiation. Interestingly, SOST transcripts were not detectable in the higher stiffness IPNs (Figure 5.6D).

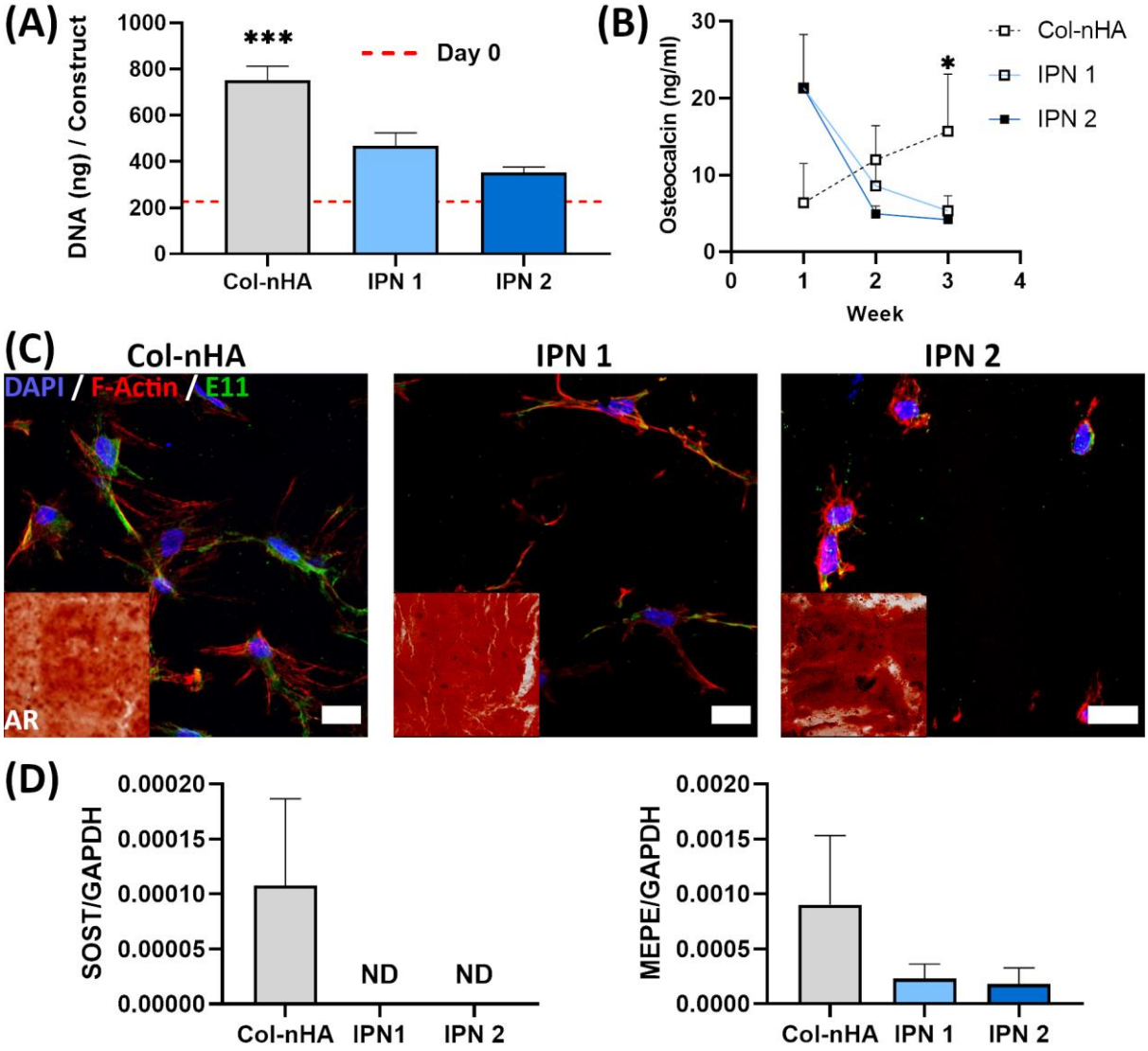

Figure 5.6: Low stiffness collagen-nHA hydrogels drive a mature bone phenotype in hBMSCs. (A) Addition of alginate into the collagen matrix cause a dose dependent decrease in cell viability. **(B)** hBMSCs secrete osteocalcin in all groups, however osteocalcin decreased over three weeks in IPNs, while increasing in collagen-nHA gels. **(C)** hBMSCs produce a mineralised matrix and express osteocyte marker E11 in all groups. A lower cell volume and more dendritic cell shape evident in IPNs compared to collagen-nHA gels. Scale bar = 20µm **(D)** Gene expression at day 21 shows signs of commitment to an osteocytic phenotype, with detectable transcripts of SOST and MEPE in collagen-nHA gels.

Over 42 days in culture, hBMSCs encapsulated in all hydrogels continuously mineralised their local matrix; with all hydrogels accumulating calcium over the 42 day culture period (Figure 5.7A). However, the medium stiffness IPN 1 appeared to accumulate matrix at a slower rate compared to the collagen-nHA and IPN2 gel, which was evident at day 42. Interestingly, after SOST gene expression was detected in collagen-nHA at day 21, analysis of the cell culture media at day 42 indicated that only cells in this material secreted sclerostin, a key regulator of bone remodelling, indicative of osteocytic differentiation and regulatory function of the *in vitro* model (Figure 5.7B).

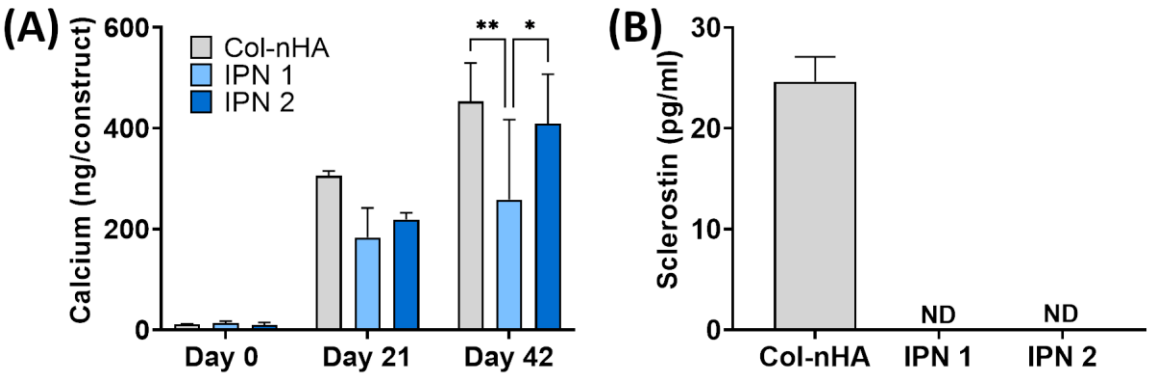

Figure 5.7: hBMSCs in Collagen-nHA gels exhibit markers of mature bone at 6 weeks. (A) All hydrogels accumulate calcium over the 42 day culture period, with collagen-nHA and IPN2 containing more calcium at day 42. **(B)** hBMSCs express sclerostin at day 42, with incorporation of an IPN into the matrix decreasing sclerostin expression to undetectable levels.

5.4 Discussion

Functional, human derived osteoblasts and osteocytes are critical to engineer pre-clinical *in vitro* models of bone organ function. *In vitro* models that accurately predict human bone physiology are evidently lacking as bone therapies can have serious off target effects [1], and other medicines have off target effects on bone [23]. In response to this, MPSs can be a platform for developing more physiologically relevant models of bone physiology that may improve this clinical predictivity through integration of multiple organ systems, for example. However, primary bone cells are difficult to

isolate in significant numbers and dedifferentiate in culture [171], thus their application is limited. In addition, current osteocyte analogues are murine derived, and typically do not produce the therapeutically targeted factors in bone formation [171]. Thus, the aim of this chapter was to use human adult stem cells to develop *in vitro* models of bone capable of recreating the cellular function of mature bone cells. This chapter demonstrates that collagen based hydrogels functionalised with nHA can support the differentiation of hBMSCs into functional mature osteoblasts and osteocytes. Such a system can form the basis of a model of mature bone function for incorporation into MPS devices.

This chapter first sought to identify key factors that would drive hBMSC differentiation to a mature bone cell phenotype. A design of experiments (DOE) method, specifically a fractional factorial design [229, 238], was employed to identify the main *in vitro* environmental factors supportive of osteocytic differentiation. Collagen matrix stiffness and nHA concentration were the most influential factors in modulating sclerostin expression in hBMSCs. Specifically, hBMSCs in 8kPa matrices produced higher amounts of sclerostin compared to 4 kPa matrices. Contrary to these findings, lower substrate stiffness in 2D has been shown to improve osteocytic differentiation of an osteoblast cell line [282]. However, in the specific context of 3D matrices, the literature largely suggests increased stiffness is associated with enhanced osteogenic differentiation [291-293]. Importantly, ALP, cell shape and sclerostin responses observed in this experiment were attributed to the increased matrix stiffness of the higher concentration collagen gel, as the relationship between stiffness and osteogenesis is well documented [294]. However, the effects could possibly be attributed to other parameters that change with collagen concertation, such as increased ligand availability. To confirm that improved osteogenesis was not

attributable to lurking variables in increased collagen concentration, an additional higher concentration gel was subsequently analysed, which showed no improvement in biological properties (Appendix 6).

In addition to matrix stiffness, nHA was also found to be an influential factor. It was found that groups with 0.27mg/ml nHA better supported osteocytic differentiation, as evident by increases in sclerostin expression, compared to groups with 2.7mg/ml nHA. Mineralisation has been shown to trigger osteocytic differentiation of osteoblasts [295, 296], but it is unclear how this result can be extrapolated to directing the differentiation of hBMSCs. HA has been shown to support osteogenic differentiation of hBMSCs in multiple studies [285, 297, 298], however it has also been shown to be cytotoxic at higher concentrations, which may explain the reduced bioactivity observed at high nHA concentrations [299]. Thus, the results of our factorial screening experiment were generally consistent with findings in the literature and motivated further exploration of the role of nHA concentration and collagen matrix stiffness in promoting an osteocytic phenotype.

To further probe the role of matrix stiffness in regulating the development of a mature bone cell phenotype, the collagen matrix was stiffened by the inclusion of an alginate network. Stiffness was increased to 16kPa and 24kPa for IPN1 and IPN 2 respectively, which is similar to osteoid [281] and within the osteogenic range for dynamic gels such as alginate [300]. However, it was found that increasing matrix stiffness was detrimental to hBMSC progression towards an osteocytic phenotype, with decreased proliferation, osteocytic gene expression and protein secretion. The cause of this is unclear, but may be related to decreased nutrient diffusion in the denser collagen-alginate IPNs [301], which may also explain the decreased proliferation. Additionally, the stiffer IPNs also possessed longer stress relaxation times, which has also been

associated with decreased osteogenesis [302]. Furthermore, the reduced cell spreading observed in IPNs, may be indicative of inhibited remodelling of the alginate matrix, resulting in reduced traction generated at the hBMSCs-matrix interface; driving hBMSCs more towards adipogenesis than osteogenesis [303]. Thus, though the IPN proved inferior biomaterials for driving osteocyte differentiation, the cause for this may be multifactorial, and not just attributed to the increased stiffness of these gels.

While hBMSCs have been shown in numerous reports to differentiate into osteoblast-like cells [304], reports of MSC differentiation into osteocytes are much less prevalent. One report has shown that the mineralised nodules that form in murine bone marrow cultures eventually express DMP-1, a marker for osteocytic differentiation [305]. Results demonstrating mineralisation and OCN expression at 21 days are consistent with differentiation into a mature osteoblast phenotype [306]. However, to the best of my knowledge, sclerostin gene expression at this late osteoblast stage, followed by sclerostin protein expression has not been shown in hBMSCs. Thus, the developed collagen-nHA based engineered bone tissue can drive not only a mature osteoblast phenotype, but also an osteocyte-like cell phenotype in extended culture using an accessible human cell source.

These results suggest a promising role for tissue engineered models of mature osteoblasts and osteocytes from readily available human derived stem cells in MPS applications. Some limitations will need to be addressed before such an approach can be integrated into a MPS of bone. Firstly, standardisation is key for *in vitro* models, repeatability and reproducibility of results is critical for any pre-clinical *in vitro* system, thus establishing quality control for the influence of cell, culture medium and biomaterial variability on model outputs is crucial [307]. Secondly, one of the main advantages of an *in vitro* system over *in vivo* models is time; short experiment time

frames are important in increasing experimental throughput. The most clinically relevant result is secretion of sclerostin by hBMSCs, which is targeted clinically [279], but requires 6 weeks of culture. Finally, the intent of this study was to engineer a biomaterial system to drive hBMSC differentiation into mature bone cells for MPS applications. While this was achieved, the hBMSC-biomaterial system has yet to be incorporated into an MPS device. The primary concern with collagen based materials in MPS systems is contraction [308], however a number of surface treatment processes can be applied to PDMS to abrogate this issue [309, 310].

Finally, future work on this model will seek to provide a more complete characterisation of the biomaterial and the encapsulated hBMSCs. For example, osteocytes are a source of Receptor activator of nuclear factor kappa-B ligand (RANKL) [311], an inducer of osteoclast differentiation and activity, that is also targeted clinically for metabolic bone disease [312]. It is unknown whether the differentiated hBMSCs in the collagen-nHA hydrogel are secreting this factor. Additionally, integration of this system, producing osteocalcin from bone derived cells, with a human islets as a model of the crosstalk between bone and pancreas would facilitate the study of this poorly understood but evidently critical relationship [16]. Such a system could test this cellular relationship through disrupting the signalling pathway between the two cell types through neutralising antibodies or blocking receptors on the islet cells. In the same context, integrating this model with models of other organ systems would allow researchers to assess drug efficacy in target tissues while simultaneously probing for off-target effects [1].

5.5 Conclusion

This study describes the development of an engineered human mature bone tissue for *in vitro* evaluation of human bone regulatory function. Specifically, the secretions and activity of mature osteoblasts and osteocytes in mature bone are both clinically relevant in the most prominent bone diseases. Thus, this chapter sought to engineer a mature bone system that recreates the function of these cells using hBMSCs. The mature bone tissue consists of mature osteoblast-like cells, as evidenced by mineralisation of the matrix and osteocalcin secretion that can be used to evaluate changes in bone formation, or the effects of osteocalcin on distant cells. Additionally, further culture facilitates further differentiation into sclerostin secreting osteocyte-like cells that could facilitate further study into this key remodelling regulator. This system represents a promising platform and steppingstone towards a clinically predictive model to accelerate effective therapeutic development.

Chapter 6: Overall Discussion

6.1 Summary

The objective of this thesis was to apply MPS technology to modelling key aspects of bone physiology. MPS technology will be a key contributor to bone research as an additional research platform and the ability rapidly iterate *in vitro* and to complement *in vivo* research. The specific aims were to build an *in vitro* MPS of endochondral ossification as a model of bone development/regeneration, and a second MPS that recreates clinically relevant cellular functions of adult bone. Chapter 3 first established methods by which hBMSCs, the canonical bone progenitor cell, could be incorporated in MPS devices and support the formation of perfusable vascular networks as a foundational template for engineering these bone models. Two methods, direct and indirect vascularisation were developed that could produce vascular networks; forming templates on which to build vascularised bone models in the ensuing chapters. Chapter 4 focussed on developing a MPS model of EO as it is the primary mechanism through which long bones develop and regenerate. The EO model was developed by combining human cartilage organoids with HUVECs in an approach analogous to the direct vascularisation approach from chapter 3. The EO model could recreate critical EO functions such as the change in cartilage angiogenic properties as it matures and vascular induced expression of pluripotent genes. Finally, Chapter 4 describes the development of an engineered mature bone tissue for incorporation into a MPS device. To achieve this, mature osteoblast and osteocyte-like cells were differentiated from hBMSC progenitors in a hydrogel system designed to drive osteogenesis. These differentiated mature bone cells could secrete clinically relevant proteins, making them an applicable analogue of human bone for MPS applications.

The third chapter of this thesis describes methods by which hBMSCs could be incorporated with HUVECs into MPS devices to produce perfusable vascularised tissues. hBMSCs give rise to osteoblasts and osteocytes, whose functions and secretions are implicated in key clinically relevant processes, making hBMSCs an essential cell to incorporate into a MPS device to build a physiologically relevant model of bone tissue. hBMSCs were incorporated with HUVECs into MPS devices in two configurations; direct and indirect, that both produced perfusable interconnected vasculature. The direct method incorporates hBMSCs and HUVECs in one hydrogel channel and requires low numbers of hBMSCs to generate perfusable vascular structures. In contrast, the indirect vascularisation method separates the hBMSCs and HUVECs into separate hydrogel channels, which facilitates the formation of perfusable interconnected vasculature with much higher amounts of hBMSCs. These two methods produce vascularised MPS devices with hBMSC laden tissues for bone research applications, and allow for flexibility depending on the application.

In chapter 4 the direct vascularisation approach was applied to engineering a model of endochondral ossification, as direct contact between cartilage and vasculature is critical in EO, and was deemed an essential feature of the prospective model. The EO model consisted of chondrogenically differentiated hBMSC organoids that mimicked the transient stages of cartilage maturity within a developing bone, or a healing fracture callus. These organoids were combined with HUVECs to mimic the invading vasculature that initiates cartilage to bone transformation. In line with *in vivo* observations, matured cartilage had an anti-angiogenic phenotype; inhibiting vascular invasion around the mature cartilage organoids. This anti-angiogenic phenotype was reversed when the cartilage organoids had matured to hypertrophy, again analogous

to the *in vivo* condition. Interestingly, anti-angiogenic factors that exist naturally in cartilage were found to be up regulated at the genetic level in mature cartilage organoids, which correlates with their anti-angiogenic phenotype. A new paradigm in EO has been postulated that chondrocytes assume a pluripotent state before transdifferentiation into osteoblasts; initiating bone formation [78]. Mature chondrocytes in the EO model increased expression of two key pluripotency factors, SOX2 and OCT4; recreating what has been shown *in vivo* supporting this hypothesis. Together the results from this chapter describe an MPS model of EO that recreates key biological processes and represents a platform building more physiologically relevant models of human bone development and regeneration.

The final chapter of this thesis aimed to recreate the clinically relevant cellular functions of mature bone for use in MPSs. Specifically, the secretome of mature bone cells that governs bone remodelling and mediates bone's endocrine effects. Currently, no human bone tissue analogues exist that can recreate these functions. To realise an engineered bone tissue that can recreate this regulatory function, the differentiation of hBMSCs was optimised through development of a bone-mimetic 3D collagen-nHA hydrogel. Specifically, a statistical experimental approach was used to identify critical factors in the collagen-nHA system that drove osteogenic differentiation toward a phenotype indicative of osteocytes. The stiffness of the matrix, and the concentration of nHA were the identified critical factors, and the influence of these factors on mature osteogenic differentiation was explored. This sequential experimentation identified an optimal collagen-nHA hydrogel that could differentiate hBMSCs into functional mature osteoblast/osteocyte-like cells; exhibiting a mineralised matrix, gene and protein expression indictive of osteocyte differentiation, and critically, secretion of osteocalcin and sclerostin, key proteins in bone's endocrine function and regulation of remodelling.

6.2 Limitations

The specific limitations of each individual chapter has been detailed in the corresponding discussion section. However, this section intends to address the limitations that apply more broadly to the work described in this thesis.

Firstly, any *in vitro* model of physiology or pathophysiology must be reproducible. Due to the nascency of the field, the works described in this thesis, and in the published literature, use a plethora of cells and biomaterials from a number of biological sources; resulting in a lack of standardisation. hBMSCs were used to model bone tissue in both its developing and mature form in this thesis. hBMSCs have natural donor variation [313-316] and this variation is compounded by numerous isolation methods. The same is the case for HUVECs, which are typically obtained commercially from pooled donors. The solution to this may come in the development of iPSCs that can account for this donor variability and could also represent disease states at the cellular level. iPSCs derived MSCs have been reported [317], but are currently mostly used for implant applications. In the case of HUVECs, ECs derived from iPSCs (iPSC-ECs) have the ability to form vascular networks *in vitro* and *in vivo*, and display the molecular signature of mature vessels [318, 319]. However iPSCs-ECs have been reported to grow much slower, and undergo sprouting less than primary cells [320], potentially hindering their adoption in the absence of standards. Furthermore, the endpoint of iPSC-EC differentiation has yet to be standardised, thus reported iPSC-ECs function in literature likely represent the function of a range of iPSC-EC phenotypes.

The work described in the first two chapters used fibrin as an ECM analogue, given its ability to support vascular network formation. However, an ideal ECM analogue would

not have the natural compositional variation inherent in these biologically derived materials. There are current efforts to synthetically recreate a synthetic analogue of fibrin by engineering the cell matrix interface [321, 322], however these systems have yet to be translated into MPS applications. Additionally, the fibrinogen and thrombin used are bovine derived, which is current standard practice for vascular applications in the field [323]. However, human fibrinogen has structural [324] cell adhesion [325] differences to bovine fibrinogen, which would need to be considered for the translation of any MPS.

The models presented in this thesis demonstrate the potential of MPS technology for bone applications. However, a number of economic limitations would need to be overcome to best facilitate commercial translation. Firstly, the models can require extensive culture periods, up to 8 weeks in total, before endpoints can be analysed. These long lead times to results naturally increase costs and resource use associated with cell culture such as reagent use and labour hours. Additionally, shorter culture periods are more favourable to increase scientific throughput. Given that these models are at early stages of development, traditional destructive analysis methods, such as histology and RT-qPCR were used. While these destructive methods are necessary in early development, reliance on such analysis methods will limit translatability as they can be expensive and resource intensive. Development of non-destructive analysis methods allows for real time analysis and reduction of sample sizes; allowing greater return for a given resource input. An example of such a method could be in analysis of mineralisation; mineralisation of aortic valves can be imaged non-destructively through multiphoton microscopy [326]. If such a method could be applied a bone MPS system, it would be invaluable as mineralisation is essential to bone

physiology. Thus, support of the scientific promise these systems have shown with favourable economics would improve their potential commercial translatability.

Finally, the MPS systems described in this thesis follow the ubiquitous design of a PDMS replica bound to a glass coverslip. More specific to this particular device is its size; requiring hydrogel volumes of approximately 100µL, with typical devices requiring approximately 10-20µL. The MPS fabrication process used in this thesis does produce larger MPS devices, which may require more raw materials, but also negates the need for expensive resources needed for photolithography. However, the size of the device and the organ systems engineered therein may have to be adjusted to match the more common scale of MPS devices should they be fluidically linked to investigate inter-organ communication. Additionally, as discussed in chapter 2, a number of approaches are being pursued to retrofit MPS technology on to common lab apparatus such as 96 and 384 well plates to improve translatability. For the models described in this thesis to be amenable to such applications, the scale would need to be reduced. Finally, one drawback of PDMS is it lipophilicity, and hence tendency to absorb small lipophilic proteins [327, 328]. In a bone context, oestrogen falls into this category, and given oestrogen's role in bone remodelling, may limit its application.

In summary, the models presented in this thesis demonstrate the potential of MPS technology for bone development and mature bone function applications. However, until addressed, the points discussed above should be considered going forward in order to maximise adoption and translation of the technology.

6.3 Conclusions

- This thesis demonstrates the potential for bone development and mature function to be captured in MPS devices.

- hBMSCs can be incorporated into MPS devices and support perfusable vascular network formation. This was achieved in two different MPS devices, which can be used as templates for vascularised bone model development.
- A model of EO was developed that can recreate some of the key events in endochondral ossification
- A bone mimetic collagen-nanohydroxyapatite hydrogel was developed that can recreate clinically relevant mature bone function for use in MPS devices.
- The models developed in this thesis demonstrate the potential to recreate bone physiology within an MPS device . Further development of these MPS models, such as integration of mechanical stimulation or multi organ fluidic coupling, holds great promise to improve health outcomes for many bone related diseases.

6.4 Future Work

Future work should aim to address some of the limitations outlined in the individual chapters of this thesis and the overall limitations outlined above. Naturally, the future work can be short or long term depending on complexity or the development work required to achieve a given body of work. Thus, both long- and short-term future work will be discussed for each thesis chapter in the ensuing paragraphs.

To provide vascularised bone tissue for general use in MPS devices, concurrent EC vasculogenesis and hBMSC osteogenesis is a prudent next step for chapter 3. While osteo-MSCs have been pre-differentiated before use in MPS systems [33], however this process is not analogous to the concurrent osteoblast-endothelial cell cross-talk that occurs in angiogenic-osteogenic coupling (AOC) in bone remodelling and intramembranous ossification [329]. Realisation of such system would require iterative

optimisation of ECM materials, cell culture medium, and osteogenic cues. A model that could recreate AOC in an MPS device would facilitate advanced probing of how these two biological processes progress in tandem, providing insights into how to improve bone healing strategies, for example. More long term, such a model could be incorporated into a multi-organ system to asses adverse effects on the AOC process, which may be affected in the numerous therapies that inadvertently lower bone quality [23-25, 142].

Optimising the media formulation used in the EO model will be critical to facilitate further exploration of EO *in vitro*. EGM-2MV contains a number of pro-angiogenic factors that could potentially be masking subtle interactions between ECs and chondro-differentiated/hypertrophic hBMSCs. This would involve systematically defining an angio-chondro medium, or a medium change regime that facilitates concurrent vasculogenesis and chondrogenesis/hypertrophy. Additionally, further demonstrating biological mechanisms that mimic *in vivo* EO is another next experimental step for the model. For example, IHH/PTH signalling is critical in the regulation of endochondral ossification and controls the progression of chondrocyte hypertrophy, and administration of recombinant PTHrP should downregulate hypertrophy in the cartilage organoids. Finally, a simple disease state could be recreated by substitution of healthy hBMSCs with those from patients with non-unions or poor bone healing.

The mature bone function model in this thesis secreted factors that regulate bone's endocrine and remodelling processes. Thus, future work should aim to demonstrate this mature bone function model can regulate these systems *in vitro*. For example, pancreatic islets could be included in a 5 channel device with the mature bone tissue and assess the presence of the tissue on β-cell proliferation and insulin secretion.

Additionally, given then mechanosensitivity of bone, mechanical stimulation could be applied to see if sclerostin secretion is mechanosensitive, as it is *in vivo*. Lastly, a more long-term focus would aim to build in a more complete model of bone remodelling; integrating human-derived osteoblasts, osteocytes, and monocyte-derived human osteoclasts. The integration of osteoclasts is critical as the molecular players involved in osteoclast proliferation and function are the primary target of many current and proposed therapeutics.

Finally, a method of assessing bone formation non-destructively would be a significant analytical development for the field. As noted previously, two photon excited fluorescence can identify calcified nodule formation in aortic valves [326]. Applying this method to *in vitro* bone formation would allow bone formation to be monitored non-destructively in real time. Moreover, in the context of this thesis, the coupling of vascularisation and bone formation in chapter 4 would then be could have two distinct readouts of bone formation and vascularisation in real time.

References

1. Lv, F., et al., *Denosumab or romosozumab therapy and risk of cardiovascular events in patients with primary osteoporosis: Systematic review and meta-analysis.* Bone, 2020. **130**: p. 115121.
2. Chen, J., et al., *Bone vasculature and bone marrow vascular niches in health and disease.* Journal of Bone and Mineral Research, 2020. **35**(11): p. 2103-2120.
3. Filipowska, J., et al., *The role of vasculature in bone development, regeneration and proper systemic functioning.* Angiogenesis, 2017: p. 1-12.
4. Hernlund, E., et al., *Osteoporosis in the European Union: medical management, epidemiology and economic burden.* Archives of osteoporosis, 2013. **8**(1-2): p. 136.
5. Kelly, M.A., et al., *Emerging trends in hospitalisation for fragility fractures in Ireland.* Irish journal of medical science, 2018. **187**(3): p. 601-608.
6. Kim, D.D. and A. Basu, *Estimating the medical care costs of obesity in the United States: systematic review, meta-analysis, and empirical analysis.* Value in Health, 2016. **19**(5): p. 602-613.
7. Association, A.D., *Economic costs of diabetes in the US in 2017.* Diabetes care, 2018. **41**(5): p. 917-928.
8. Brent, M.B., A. Brüel, and J.S. Thomsen, *A Systematic Review of Animal Models of Disuse-Induced Bone Loss.* Calcified Tissue International, 2021: p. 1-15.
9. Schafrum Macedo, A., et al., *Animal modeling in bone research—Should we follow the White Rabbit?* Animal models and experimental medicine, 2019. **2**(3): p. 162-168.
10. Kimmel, D.B., *Animal models in bone research*, in *Bone Toxicology*. 2017, Springer. p. 129-171.
11. Komori, T., *Animal models for osteoporosis.* European Journal of Pharmacology, 2015. **759**: p. 287-294.
12. Simmons, J., et al., *Animal models of bone metastasis.* Veterinary pathology, 2015. **52**(5): p. 827-841.
13. A., M.L. and S.A.H.R. W., *In vivo models of bone repair.* The Journal of Bone and Joint Surgery. British volume, 2012. **94-B**(7): p. 865-874.
14. Hu, D.P., et al., *Cartilage to bone transformation during fracture healing is coordinated by the invading vasculature and induction of the core pluripotency genes.* Development, 2017. **144**(2): p. 221-234.
15. Wong, S.A., et al., *Trans differentiation of Chondrocytes to Osteoblasts during Endochondral Ossification in the Healing Mandible.* The FASEB Journal, 2016. **30**(1 Supplement): p. 1039.11-1039.11.
16. Liu, J.-M., et al., *Regulation of glucose handling by the skeleton: insights from mouse and human studies.* Diabetes, 2016. **65**(11): p. 3225-3232.
17. Ferron, M., et al., *Intermittent injections of osteocalcin improve glucose metabolism and prevent type 2 diabetes in mice.* Bone, 2012. **50**(2): p. 568-575.
18. Lee, N.K., et al., *Endocrine Regulation of Energy Metabolism by the Skeleton.* Cell, 2007. **130**(3): p. 456-469.

19. Franco, R. and A. Cedazo-Minguez, *Successful therapies for Alzheimer's disease: why so many in animal models and none in humans?* Frontiers in pharmacology, 2014. **5**: p. 146.
20. FDA;. *Overview of the Animal Model Qualification Program*. 2020 [cited 2020 10/01/2020]; Overview of the Animal Model Qualification Program on the FDA official website]. Available from: https://www.fda.gov/drugs/animal-model-qualification-program-amqp/overview-animal-model-qualification-program.
21. Paul, S.M., et al., *How to improve R&D productivity: the pharmaceutical industry's grand challenge.* Nature reviews Drug discovery, 2010. **9**(3): p. 203-214.
22. McClung, M., *Cancel the denosumab holiday*. 2016, Springer.
23. Taylor, S.I., J.E. Blau, and K.I. Rother, *Possible adverse effects of SGLT2 inhibitors on bone.* The lancet Diabetes & endocrinology, 2015. **3**(1): p. 8-10.
24. Perucca, P. and F.G. Gilliam, *Adverse effects of antiepileptic drugs.* The Lancet Neurology, 2012. **11**(9): p. 792-802.
25. Abraham, N.S., *Proton pump inhibitors: potential adverse effects.* Current opinion in gastroenterology, 2012. **28**(6): p. 615-620.
26. Ghouri, A. and P.G. Conaghan, *Update on novel pharmacological therapies for osteoarthritis.* Therapeutic advances in musculoskeletal disease, 2019. **11**: p. 1759720X19864492.
27. Huh, D., G.A. Hamilton, and D.E. Ingber, *From 3D cell culture to organs-on-chips.* Trends in cell biology, 2011. **21**(12): p. 745-754.
28. Stokes, C.L., M. Cirit, and D.A. Lauffenburger, *Physiome-on-a-chip: The challenge of "scaling" in design, operation, and translation of microphysiological systems.* CPT: pharmacometrics & systems pharmacology, 2015. **4**(10): p. 559-562.
29. Chou, D.B., et al., *On-chip recapitulation of clinical bone marrow toxicities and patient-specific pathophysiology.* Nature biomedical engineering, 2020: p. 1-13.
30. Chen, M.B., et al., *On-chip human microvasculature assay for visualization and quantitation of tumor cell extravasation dynamics.* Nature protocols, 2017. **12**(5): p. 865.
31. Occhetta, P., et al., *Hyperphysiological compression of articular cartilage induces an osteoarthritic phenotype in a cartilage-on-a-chip model.* Nature biomedical engineering, 2019. **3**(7): p. 545.
32. Herland, A., et al., *Quantitative prediction of human pharmacokinetic responses to drugs via fluidically coupled vascularized organ chips.* Nature Biomedical Engineering, 2020: p. 1-16.
33. Bersini, S., et al., *A microfluidic 3D in vitro model for specificity of breast cancer metastasis to bone.* Biomaterials, 2014. **35**(8): p. 2454-2461.
34. Novicky, A., et al., *Chapter 2 - The Mechanics of Skeletal Development*, in *Developmental Biology and Musculoskeletal Tissue Engineering*, M.J. Stoddart, et al., Editors. 2018, Academic Press: Boston. p. 25-51.
35. Verbruggen, S.W. and L.M. McNamara, *Bone mechanobiology in health and disease*, in *Mechanobiology in Health and Disease*. 2018, Elsevier. p. 157-214.
36. Florencio-Silva, R., et al., *Biology of bone tissue: structure, function, and factors that influence bone cells.* BioMed research international, 2015. **2015**.
37. Oury, F., et al., *Endocrine regulation of male fertility by the skeleton.* Cell, 2011. **144**(5): p. 796-809.
38. Berendsen, A.D. and B.R. Olsen, *Bone development.* Bone, 2015. **80**: p. 14-18.

39. Du, X., et al., *Role of FGFs/FGFRs in skeletal development and bone regeneration.* Journal of cellular physiology, 2012. **227**(12): p. 3731-3743.
40. Takada, I., et al., *A histone lysine methyltransferase activated by non-canonical Wnt signalling suppresses PPAR-γ transactivation.* Nature cell biology, 2007. **9**(11): p. 1273-1285.
41. Ornitz, D.M. and P.J. Marie, *FGF signaling pathways in endochondral and intramembranous bone development and human genetic disease.* Genes & development, 2002. **16**(12): p. 1446-1465.
42. Roscioli, T., et al., *Clinical findings in a patient with FGFR1 P252R mutation and comparison with the literature.* American journal of medical genetics, 2000. **93**(1): p. 22-28.
43. Kawaguchi, H., *Bone fracture and the healing mechanisms. Fibroblast growth factor-2 and fracture healing.* Clinical calcium, 2009. **19**(5): p. 653-659.
44. Kawaguchi, H., et al., *Local application of recombinant human fibroblast growth factor-2 on bone repair: A dose–escalation prospective trial on patients with osteotomy.* Journal of orthopaedic research, 2007. **25**(4): p. 480-487.
45. Kawaguchi, H., et al., *A local application of recombinant human fibroblast growth factor 2 for tibial shaft fractures: A randomized, placebo-controlled trial.* Journal of Bone and Mineral Research, 2010. **25**(12): p. 2735-2743.
46. Bialek, P., et al., *A twist code determines the onset of osteoblast differentiation.* Developmental cell, 2004. **6**(3): p. 423-435.
47. Carver, E.A., K.F. Oram, and T. Gridley, *Craniosynostosis in Twist heterozygous mice: A model for Saethre-Chotzen syndrome.* The Anatomical Record: An Official Publication of the American Association of Anatomists, 2002. **268**(2): p. 90-92.
48. Firulli, B.A., et al., *Altered Twist1 and Hand2 dimerization is associated with Saethre-Chotzen syndrome and limb abnormalities.* Nature genetics, 2005. **37**(4): p. 373-381.
49. Seo, H.-S. and R. Serra, *Tgfbr2 is required for development of the skull vault.* Developmental biology, 2009. **334**(2): p. 481-490.
50. Iwata, J.-i., et al., *Transforming growth factor-β regulates basal transcriptional regulatory machinery to control cell proliferation and differentiation in cranial neural crest-derived osteoprogenitor cells.* Journal of Biological Chemistry, 2010. **285**(7): p. 4975-4982.
51. Nyary, T. and B.E. Scammell, *Principles of bone and joint injuries and their healing.* Surgery (Oxford), 2018. **36**(1): p. 7-14.
52. Marsell, R. and T.A. Einhorn, *The biology of fracture healing.* Injury, 2011. **42**(6): p. 551-555.
53. Gerstenfeld, L.C., et al., *Three-dimensional reconstruction of fracture callus morphogenesis.* Journal of Histochemistry & Cytochemistry, 2006. **54**(11): p. 1215-1228.
54. Phillips, A., *Overview of the fracture healing cascade.* Injury, 2005. **36**(3): p. S5-S7.
55. Lefebvre, V. and P. Bhattaram, *Vertebrate skeletogenesis.* Current topics in developmental biology, 2010. **90**: p. 291-317.
56. Hall, B.K. and T. Miyake, *The membranous skeleton: the role of cell condensations in vertebrate skeletogenesis.* Anatomy and embryology, 1992. **186**(2): p. 107-124.
57. Einhorn, T.A. and L.C. Gerstenfeld, *Fracture healing: mechanisms and interventions.* Nature Reviews Rheumatology, 2015. **11**(1): p. 45.

58. Hall, B.K. and T. Miyake, *All for one and one for all: condensations and the initiation of skeletal development.* Bioessays, 2000. **22**(2): p. 138-147.
59. Feng, X.-H. and R. Derynck, *Specificity and versatility in TGF-β signaling through Smads.* Annu. Rev. Cell Dev. Biol., 2005. **21**: p. 659-693.
60. Long, F. and D.M. Ornitz, *Development of the endochondral skeleton.* Cold Spring Harbor perspectives in biology, 2013. **5**(1): p. a008334.
61. Retting, K.N., et al., *BMP canonical Smad signaling through Smad1 and Smad5 is required for endochondral bone formation.* Development, 2009. **136**(7): p. 1093-1104.
62. Hill, T.P., et al., *Canonical Wnt/β-catenin signaling prevents osteoblasts from differentiating into chondrocytes.* Developmental cell, 2005. **8**(5): p. 727-738.
63. Dong, Y., et al., *RBPjκ-dependent Notch signaling regulates mesenchymal progenitor cell proliferation and differentiation during skeletal development.* Development, 2010. **137**(9): p. 1461-1471.
64. Aghajanian, P. and S. Mohan, *The art of building bone: emerging role of chondrocyte-to-osteoblast transdifferentiation in endochondral ossification.* Bone research, 2018. **6**(1): p. 1-9.
65. Aghajanian, P., et al., *Epiphyseal bone formation occurs via thyroid hormone regulation of chondrocyte to osteoblast transdifferentiation.* Scientific reports, 2017. **7**(1): p. 1-12.
66. Kronenberg, H.M., *PTHrP and skeletal development.* Annals of the New York Academy of Sciences, 2006. **1068**(1): p. 1-13.
67. Lanske, B., et al., *PTH/PTHrP receptor in early development and Indian hedgehog--regulated bone growth.* Science, 1996. **273**(5275): p. 663-666.
68. Colnot, C., *Skeletal cell fate decisions within periosteum and bone marrow during bone regeneration.* Journal of Bone and Mineral Research, 2009. **24**(2): p. 274-282.
69. Chen, H., et al., *Runx2 regulates endochondral ossification through control of chondrocyte proliferation and differentiation.* Journal of Bone and Mineral Research, 2014. **29**(12): p. 2653-2665.
70. Ding, M., et al., *Targeting Runx2 expression in hypertrophic chondrocytes impairs endochondral ossification during early skeletal development.* Journal of cellular physiology, 2012. **227**(10): p. 3446-3456.
71. Soung, D.Y., et al., *Runx3/AML2/Cbfa3 regulates early and late chondrocyte differentiation.* Journal of Bone and Mineral Research, 2007. **22**(8): p. 1260-1270.
72. Paglia, D.N., et al., *Deletion of Runx1 in osteoclasts impairs murine fracture healing through progressive woven bone loss and delayed cartilage remodeling.* Journal of Orthopaedic Research®, 2020. **38**(5): p. 1007-1015.
73. Lin, H.N. and J.P. O'Connor, *Osteoclast depletion with clodronate liposomes delays fracture healing in mice.* Journal of Orthopaedic Research, 2017. **35**(8): p. 1699-1706.
74. Gerstenfeld, L.C., et al., *Impaired fracture healing in the absence of TNF-α signaling: The role of TNF-α in endochondral cartilage resorption.* Journal of Bone and Mineral Research, 2003. **18**(9): p. 1584-1592.
75. Adams, C.S. and I.M. Shapiro, *The fate of the terminally differentiated chondrocyte: evidence for microenvironmental regulation of chondrocyte apoptosis.* Critical Reviews in Oral Biology & Medicine, 2002. **13**(6): p. 465-473.

76. Shapiro, I.M., et al., *Fate of the hypertrophic chondrocyte: microenvironmental perspectives on apoptosis and survival in the epiphyseal growth plate.* Birth Defects Research Part C: Embryo Today: Reviews, 2005. **75**(4): p. 330-339.
77. Mackie, E., et al., *Endochondral ossification: how cartilage is converted into bone in the developing skeleton.* The international journal of biochemistry & cell biology, 2008. **40**(1): p. 46-62.
78. Zhou, X., et al., *Chondrocytes transdifferentiate into osteoblasts in endochondral bone during development, postnatal growth and fracture healing in mice.* PLoS Genet, 2014. **10**(12): p. e1004820.
79. Reznikov, N., R. Shahar, and S. Weiner, *Bone hierarchical structure in three dimensions.* Acta biomaterialia, 2014. **10**(9): p. 3815-3826.
80. Young, M.F., *Bone matrix proteins: their function, regulation, and relationship to osteoporosis.* Osteoporosis International, 2003. **14**(3): p. 35-42.
81. George, A. and A. Veis, *Phosphorylated proteins and control over apatite nucleation, crystal growth, and inhibition.* Chemical reviews, 2008. **108**(11): p. 4670-4693.
82. Boskey, A.L. and P.G. Robey, *The regulatory role of matrix proteins in mineralization of bone*, in *Osteoporosis*. 2013, Elsevier. p. 235-255.
83. Boskey, A., et al., *Fourier transform infrared microspectroscopic analysis of bones of osteocalcin-deficient mice provides insight into the function of osteocalcin.* Bone, 1998. **23**(3): p. 187-196.
84. Schaffler, M.B. and O.D. Kennedy, *Osteocyte signaling in bone.* Current osteoporosis reports, 2012. **10**(2): p. 118-125.
85. Klein-Nulend, J. and L.F. Bonewald, *Chapter 6 - The osteocyte*, in *Principles of Bone Biology (Fourth Edition)*, J.P. Bilezikian, et al., Editors. 2020, Academic Press. p. 133-162.
86. Klein-Nulend, J., et al., *Mechanosensation and transduction in osteocytes.* Bone, 2013. **54**(2): p. 182-190.
87. Zou, W. and S.L. Teitelbaum, *Integrins, growth factors, and the osteoclast cytoskeleton.* Annals of the New York Academy of Sciences, 2010. **1192**(1): p. 27-31.
88. Teitelbaum, S.L., *Bone resorption by osteoclasts.* Science, 2000. **289**(5484): p. 1504-1508.
89. Drake, F.H., et al., *Cathepsin K, but not cathepsins B, L, or S, is abundantly expressed in human osteoclasts.* Journal of Biological Chemistry, 1996. **271**(21): p. 12511-12516.
90. Tang, Y., et al., *TGF-β1–induced migration of bone mesenchymal stem cells couples bone resorption with formation.* Nature medicine, 2009. **15**(7): p. 757-765.
91. Xian, L., et al., *Matrix IGF-1 maintains bone mass by activation of mTOR in mesenchymal stem cells.* Nature medicine, 2012. **18**(7): p. 1095.
92. Su, P., et al., *Mesenchymal stem cell migration during bone formation and bone diseases therapy.* International journal of molecular sciences, 2018. **19**(8): p. 2343.
93. Li, Y., et al., *Biomechanical stimulation of osteoblast gene expression requires phosphorylation of the RUNX2 transcription factor.* Journal of Bone and Mineral Research, 2012. **27**(6): p. 1263-1274.
94. Franz-Odendaal, T.A., B.K. Hall, and P.E. Witten, *Buried alive: how osteoblasts become osteocytes.* Developmental Dynamics, 2006. **235**(1): p. 176-190.

95. Holmbeck, K., et al., *The metalloproteinase MT1-MMP is required for normal development and maintenance of osteocyte processes in bone.* Journal of cell science, 2005. **118**(1): p. 147-156.
96. Robling, A.G. and L.F. Bonewald, *The Osteocyte: New Insights.* Annual Review of Physiology, 2020. **82**: p. 485-506.
97. Putnam, A.J., *The instructive role of the vasculature in stem cell niches.* Biomaterials science, 2014. **2**(11): p. 1562-1573.
98. Kusumbe, A.P., S.K. Ramasamy, and R.H. Adams, *Coupling of angiogenesis and osteogenesis by a specific vessel subtype in bone.* Nature, 2014. **507**(7492): p. 323-328.
99. Sato, T., et al., *A FAK/HDAC5 signaling axis controls osteocyte mechanotransduction.* Nature communications, 2020. **11**(1): p. 1-18.
100. Sasaki, F., et al., *Mechanotransduction via the Piezo1-Akt pathway underlies Sost suppression in osteocytes.* Biochemical and biophysical research communications, 2020. **521**(3): p. 806-813.
101. Silva, I. and J. Branco, *Rank/Rankl/opg: literature review.* Acta reumatologica portuguesa, 2011. **36**(3): p. 209-218.
102. Boyce, B.F. and L. Xing, *Biology of RANK, RANKL, and osteoprotegerin.* Arthritis research & therapy, 2007. **9**(1): p. 1-7.
103. Theoleyre, S., et al., *The molecular triad OPG/RANK/RANKL: involvement in the orchestration of pathophysiological bone remodeling.* Cytokine & growth factor reviews, 2004. **15**(6): p. 457-475.
104. O'Brien, C.A., T. Nakashima, and H. Takayanagi, *Osteocyte control of osteoclastogenesis.* Bone, 2013. **54**(2): p. 258-263.
105. Kamiya, N., et al., *BMP signaling negatively regulates bone mass through sclerostin by inhibiting the canonical Wnt pathway.* Development, 2008. **135**(22): p. 3801-3811.
106. Ferron, M., et al., *Insulin signaling in osteoblasts integrates bone remodeling and energy metabolism.* Cell, 2010. **142**(2): p. 296-308.
107. Hauschka, P.V., et al., *Osteocalcin and matrix Gla protein: vitamin K-dependent proteins in bone.* Physiological reviews, 1989. **69**(3): p. 990-1047.
108. Cipriani, C., et al., *The interplay between bone and glucose metabolism.* Frontiers in endocrinology, 2020. **11**: p. 122.
109. Ducy, P., T. Schinke, and G. Karsenty, *The osteoblast: a sophisticated fibroblast under central surveillance.* Science, 2000. **289**(5484): p. 1501-1504.
110. Khosla, S., et al., *Relationship of serum sex steroid levels to longitudinal changes in bone density in young versus elderly men.* The Journal of Clinical Endocrinology & Metabolism, 2001. **86**(8): p. 3555-3561.
111. Pi, M., et al., *GPRC6A null mice exhibit osteopenia, feminization and metabolic syndrome.* PloS one, 2008. **3**(12).
112. Sabek, O.M., et al., *Osteocalcin effect on human β-cells mass and function.* Endocrinology, 2015. **156**(9): p. 3137-3146.
113. Liu, D.-M., et al., *Association between osteocalcin and glucose metabolism: a meta-analysis.* Osteoporosis International, 2015. **26**(12): p. 2823-2833.
114. Liu, J.-m., et al., *An independent positive relationship between the serum total osteocalcin level and fat-free mass in healthy premenopausal women.* The Journal of Clinical Endocrinology & Metabolism, 2013. **98**(5): p. 2146-2152.
115. Yeap, B.B., et al., *Higher serum undercarboxylated osteocalcin and other bone turnover markers are associated with reduced diabetes risk and lower estradiol*

concentrations in older men. The Journal of Clinical Endocrinology & Metabolism, 2015. **100**(1): p. 63-71.
116. Pittas, A.G., et al., *Association between serum osteocalcin and markers of metabolic phenotype.* The Journal of Clinical Endocrinology & Metabolism, 2009. **94**(3): p. 827-832.
117. Hwang, Y.-C., et al., *Circulating osteocalcin level is not associated with incident type 2 diabetes in middle-aged male subjects: mean 8.4-year retrospective follow-up study.* Diabetes care, 2012. **35**(9): p. 1919-1924.
118. Schafer, A.L., et al., *Change in undercarboxylated osteocalcin is associated with changes in body weight, fat mass, and adiponectin: parathyroid hormone (1-84) or alendronate therapy in postmenopausal women with osteoporosis (the PaTH study).* The Journal of Clinical Endocrinology & Metabolism, 2011. **96**(12): p. E1982-E1989.
119. Toulis, K.A., et al., *Bisphosphonates and glucose homeostasis: a population-based, retrospective cohort study.* The Journal of Clinical Endocrinology & Metabolism, 2015. **100**(5): p. 1933-1940.
120. Adler, C.-P., *Disorders of Skeletal Development*, in *Bone Diseases: Macroscopic, Histological, and Radiological Diagnosis of Structural Changes in the Skeleton*. 2000, Springer Berlin Heidelberg: Berlin, Heidelberg. p. 31-63.
121. Kornak, U. and S. Mundlos, *Genetic disorders of the skeleton: a developmental approach.* The American Journal of Human Genetics, 2003. **73**(3): p. 447-474.
122. Martini, L., *Encyclopedia of endocrine diseases*. 2004: Elsevier acad. press.
123. Nandra, R., L. Grover, and K. Porter, *Fracture non-union epidemiology and treatment.* Trauma, 2016. **18**(1): p. 3-11.
124. Mills, L.A., S.A. Aitken, and A.H.R. Simpson, *The risk of non-union per fracture: current myths and revised figures from a population of over 4 million adults.* Acta orthopaedica, 2017. **88**(4): p. 434-439.
125. Kanakaris, N. and P.V. Giannoudis, *The health economics of the treatment of long-bone non-unions.* Injury, 2007. **38**: p. S77-S84.
126. Santolini, E., R. West, and P.V. Giannoudis, *Risk factors for long bone fracture non-union: a stratification approach based on the level of the existing scientific evidence.* Injury, 2015. **46**: p. S8-S19.
127. Aleem, I.S., et al., *Efficacy of electrical stimulators for bone healing: a meta-analysis of randomized sham-controlled trials.* Scientific reports, 2016. **6**(1): p. 1-10.
128. Koester, M.C. and K.P. Spindler, *Pharmacologic agents in fracture healing.* Clinics in sports medicine, 2006. **25**(1): p. 63-73.
129. Ytrehus, B., C.S. Carlson, and S. Ekman, *Etiology and pathogenesis of osteochondrosis.* Veterinary pathology, 2007. **44**(4): p. 429-448.
130. Olstad, K., et al., *Juvenile osteochondritis dissecans of the knee is a result of failure of the blood supply to growth cartilage and osteochondrosis.* Osteoarthritis and cartilage, 2018. **26**(12): p. 1691-1698.
131. Gómez-Alonso, C., *Paediatric Metabolic Bone Disease: A Lifetime Ahead.* Advances in therapy, 2020. **37**(2): p. 38-46.
132. Cundy, T., I.R. Reid, and A. Grey, *CHAPTER 31 - Metabolic bone disease*, in *Clinical Biochemistry: Metabolic and Clinical Aspects (Third Edition)*, W.J. Marshall, et al., Editors. 2014, Churchill Livingstone. p. 604-635.
133. Gallagher, J.C. and A. Sai, *Molecular biology of bone remodeling: implications for new therapeutic targets for osteoporosis.* Maturitas, 2010. **65**(4): p. 301-307.

134. Waziri, B., R. Duarte, and S. Naicker, *Chronic kidney disease–mineral and bone disorder (CKD-MBD): current perspectives.* International journal of nephrology and renovascular disease, 2019. **12**: p. 263.
135. Van Staa, T., et al., *Incidence and natural history of Paget's disease of bone in England and Wales.* Journal of Bone and Mineral Research, 2002. **17**(3): p. 465-471.
136. Laurin, N., et al., *Recurrent mutation of the gene encoding sequestosome 1 (SQSTM1/p62) in Paget disease of bone.* The American Journal of Human Genetics, 2002. **70**(6): p. 1582-1588.
137. Salminen, A., et al., *Activation of innate immunity system during aging: NF-kB signaling is the molecular culprit of inflamm-aging.* Ageing research reviews, 2008. **7**(2): p. 83-105.
138. Ralston, S.H., A.L. Langston, and I.R. Reid, *Pathogenesis and management of Paget's disease of bone.* The Lancet, 2008. **372**(9633): p. 155-163.
139. Manson, J.E., et al., *Menopausal hormone therapy and health outcomes during the intervention and extended poststopping phases of the Women's Health Initiative randomized trials.* Jama, 2013. **310**(13): p. 1353-1368.
140. Ettinger, B., et al., *Reduction of vertebral fracture risk in postmenopausal women with osteoporosis treated with raloxifene: results from a 3-year randomized clinical trial.* Jama, 1999. **282**(7): p. 637-645.
141. Chen, L.-R., N.-Y. Ko, and K.-H. Chen, *Medical treatment for osteoporosis: From molecular to clinical opinions.* International journal of molecular sciences, 2019. **20**(9): p. 2213.
142. Greenspan, S.L., et al., *Bone loss after initiation of androgen deprivation therapy in patients with prostate cancer.* The Journal of Clinical Endocrinology & Metabolism, 2005. **90**(12): p. 6410-6417.
143. Martin, A., V. David, and L.D. Quarles, *Regulation and function of the FGF23/klotho endocrine pathways.* Physiological reviews, 2012.
144. Delanaye, P., et al., *Can we use circulating biomarkers to monitor bone turnover in CKD haemodialysis patients? Hypotheses and facts.* Nephrology Dialysis Transplantation, 2014. **29**(5): p. 997-1004.
145. Blau, J.E. and M.T. Collins, *The PTH-Vitamin D-FGF23 axis.* Reviews in Endocrine and Metabolic Disorders, 2015. **16**(2): p. 165-174.
146. Carpenter, T.O., et al., *Burosumab therapy in children with X-linked hypophosphatemia.* New england journal of medicine, 2018. **378**(21): p. 1987-1998.
147. Faul, C., et al., *FGF23 induces left ventricular hypertrophy.* The Journal of clinical investigation, 2011. **121**(11).
148. Lin, X., et al., *Undercarboxylated osteocalcin: experimental and human evidence for a role in glucose homeostasis and muscle regulation of insulin sensitivity.* Nutrients, 2018. **10**(7): p. 847.
149. Lambert, L.J., et al., *Increased trabecular bone and improved biomechanics in an osteocalcin-null rat model created by CRISPR/Cas9 technology.* Disease models & mechanisms, 2016. **9**(10): p. 1169-1179.
150. Moser, S.C. and B.C. van der Eerden, *Osteocalcin—A versatile bone-derived hormone.* Frontiers in endocrinology, 2019. **9**: p. 794.
151. Atsumi, T., et al., *A chondrogenic cell line derived from a differentiating culture of AT805 teratocarcinoma cells.* Cell Differentiation and Development, 1990. **30**(2): p. 109-116.

152. Newton, P., et al., *Chondrogenic ATDC5 cells: An optimised model for rapid and physiological matrix mineralisation.* International journal of molecular medicine, 2012. **30**(5): p. 1187-1193.
153. Yao, Y. and Y. Wang, *ATDC5: an excellent in vitro model cell line for skeletal development.* Journal of cellular biochemistry, 2013. **114**(6): p. 1223-1229.
154. Gelse, K., et al., *Molecular differentiation between osteophytic and articular cartilage–clues for a transient and permanent chondrocyte phenotype.* Osteoarthritis and cartilage, 2012. **20**(2): p. 162-171.
155. Scotti, C., et al., *Recapitulation of endochondral bone formation using human adult mesenchymal stem cells as a paradigm for developmental engineering.* Proceedings of the National Academy of Sciences, 2010. **107**(16): p. 7251-7256.
156. Hess, R., et al., *High affinity leptin receptors are present in human mesenchymal stem cells (MSCs) derived from control and osteoporotic donors.* Journal of cellular biochemistry, 2005. **94**(1): p. 50-57.
157. Sawa, N., et al., *Alternating Differentiation and Dedifferentiation between Mature Osteoblasts and Osteocytes.* Scientific reports, 2019. **9**(1): p. 1-9.
158. Klein-Nulend, J., et al., *Donor age and mechanosensitivity of human bone cells.* Osteoporosis International, 2002. **13**(2): p. 137-146.
159. Sacchetti, B., et al., *Self-renewing osteoprogenitors in bone marrow sinusoids can organize a hematopoietic microenvironment.* Cell, 2007. **131**(2): p. 324-336.
160. Langenbach, F. and J. Handschel, *Effects of dexamethasone, ascorbic acid and β-glycerophosphate on the osteogenic differentiation of stem cells in vitro.* Stem cell research & therapy, 2013. **4**(5): p. 117.
161. Mohamed-Ahmed, S., et al., *Adipose-derived and bone marrow mesenchymal stem cells: a donor-matched comparison.* Stem cell research & therapy, 2018. **9**(1): p. 168.
162. Wang, L., et al., *Dynamic expression profiles of marker genes in osteogenic differentiation of human bone marrow-derived mesenchymal stem cells.* Chinese Medical Sciences Journal, 2015. **30**(2): p. 108-113.
163. Isenmann, S., et al., *TWIST family of basic helix-loop-helix transcription factors mediate human mesenchymal stem cell growth and commitment.* Stem cells, 2009. **27**(10): p. 2457-2468.
164. Rutkovskiy, A., K.-O. Stensløkken, and I.J. Vaage, *Osteoblast differentiation at a glance.* Medical science monitor basic research, 2016. **22**: p. 95.
165. Thompson, W.R., et al., *Osteocyte specific responses to soluble and mechanical stimuli in a stem cell derived culture model.* Scientific reports, 2015. **5**: p. 11049.
166. Elabd, C., et al., *Human adipose tissue-derived multipotent stem cells differentiate in vitro and in vivo into osteocyte-like cells.* Biochemical and biophysical research communications, 2007. **361**(2): p. 342-348.
167. Thrivikraman, G., et al., *Rapid fabrication of vascularized and innervated cell-laden bone models with biomimetic intrafibrillar collagen mineralization.* Nature communications, 2019. **10**(1): p. 1-14.
168. Czekanska, E.M., et al., *Differentiating MSCs towards an early osteocyte-like phenotype in vitro*, in *ORS*. 2017: San Diego, California.
169. Kato, Y., et al., *Establishment of an osteoid preosteocyte-like cell MLO-A5 that spontaneously mineralizes in culture.* Journal of Bone and Mineral Research, 2001. **16**(9): p. 1622-1633.

170. Barragan-Adjemian, C., et al., *Mechanism by which MLO-A5 late osteoblasts/early osteocytes mineralize in culture: similarities with mineralization of lamellar bone.* Calcified tissue international, 2006. **79**(5): p. 340-353.
171. Kalajzic, I., et al., *In vitro and in vivo approaches to study osteocyte biology.* Bone, 2013. **54**(2): p. 296-306.
172. Woo, S.M., et al., *Cell line IDG-SW3 replicates osteoblast-to-late-osteocyte differentiation in vitro and accelerates bone formation in vivo.* Journal of bone and mineral research, 2011. **26**(11): p. 2634-2646.
173. Prideaux, M., et al., *Parathyroid hormone induces bone cell motility and loss of mature osteocyte phenotype through L-calcium channel dependent and independent mechanisms.* PloS one, 2015. **10**(5).
174. Xu, H., et al., *Impact of flow shear stress on morphology of osteoblast-like IDG-SW3 cells.* Journal of bone and mineral metabolism, 2018. **36**(5): p. 529-536.
175. Ito, N., et al., *Regulation of FGF23 expression in IDG-SW3 osteocytes and human bone by pro-inflammatory stimuli.* Molecular and cellular endocrinology, 2015. **399**: p. 208-218.
176. Ito, N., et al., *Extracellular phosphate modulates the effect of 1α, 25-dihydroxy vitamin D3 (1, 25D) on osteocyte like cells.* The Journal of steroid biochemistry and molecular biology, 2013. **136**: p. 183-186.
177. Yamamoto, H., et al., *Posttranslational processing of FGF23 in osteocytes during the osteoblast to osteocyte transition.* Bone, 2016. **84**: p. 120-130.
178. Spatz, J.M., et al., *The Wnt inhibitor sclerostin is up-regulated by mechanical unloading in osteocytes in vitro.* Journal of Biological Chemistry, 2015. **290**(27): p. 16744-16758.
179. Xu, L.H., et al., *OCY454 osteocytes as an in vitro cell model for bone remodeling under mechanical loading.* Journal of Orthopaedic Research®, 2019. **37**(8): p. 1681-1689.
180. Qin, Y., et al., *Myostatin inhibits osteoblastic differentiation by suppressing osteocyte-derived exosomal microRNA-218: A novel mechanism in muscle-bone communication.* Journal of Biological Chemistry, 2017. **292**(26): p. 11021-11033.
181. Wood, C.L., P.D. Pajevic, and J.H. Gooi, *Osteocyte secreted factors inhibit skeletal muscle differentiation.* Bone reports, 2017. **6**: p. 74-80.
182. Wang, K., et al., *A novel osteogenic cell line that differentiates into GFP-tagged osteocytes and forms mineral with a bone-like lacunocanalicular structure.* Journal of Bone and Mineral Research, 2019. **34**(6): p. 979-995.
183. Streeten, E.A., et al., *Cloned endothelial cells from fetal bovine bone.* Proceedings of the National Academy of Sciences, 1989. **86**(3): p. 916-920.
184. Brandi, M.L., et al., *Bone endothelial cells as estrogen targets.* Calcified tissue international, 1993. **53**(5): p. 312-317.
185. LiáJeon, N., *Microfluidic vascularized bone tissue model with hydroxyapatite-incorporated extracellular matrix.* Lab on a Chip, 2015. **15**(20): p. 3984-3988.
186. Li, X., et al., *Targeted deletion of the sclerostin gene in mice results in increased bone formation and bone strength.* Journal of Bone and Mineral Research, 2008. **23**(6): p. 860-869.
187. Seok, J., et al., *Genomic responses in mouse models poorly mimic human inflammatory diseases.* Proceedings of the National Academy of Sciences, 2013. **110**(9): p. 3507-3512.

188. Simpson, A.H. and I.R. Murray, *Osteoporotic fracture models.* Current osteoporosis reports, 2015. **13**(1): p. 9-15.
189. Aerssens, J., et al., *Interspecies Differences in Bone Composition, Density, and Quality: Potential Implications for in Vivo Bone Research*.* Endocrinology, 1998. **139**(2): p. 663-670.
190. Caplin, J.D., et al., *Microfluidic Organ-on-a-Chip Technology for Advancement of Drug Development and Toxicology.* Advanced healthcare materials, 2015. **4**(10): p. 1426-1450.
191. Low, L.A., et al., *Organs-on-chips: Into the next decade.* Nature Reviews Drug Discovery, 2020: p. 1-17.
192. Whitesides, G.M., et al., *Soft lithography in biology and biochemistry.* Annual review of biomedical engineering, 2001. **3**(1): p. 335-373.
193. Faustino, V., et al., *Biomedical microfluidic devices by using low-cost fabrication techniques: A review.* Journal of biomechanics, 2016. **49**(11): p. 2280-2292.
194. Benam, K., et al., *Matched-comparative modeling of normal and diseased human airway responses using a micro-engineered breathing lung chip. Cell Syst 3 (5): 456–466*. 2016.
195. Si, L., et al., *Human organ chip-enabled pipeline to rapidly repurpose therapeutics during viral pandemics.* bioRxiv, 2020: p. 2020.04.13.039917.
196. Si, L., et al., *Discovery of influenza drug resistance mutations and host therapeutic targets using a human airway chip.* bioRxiv, 2019: p. 685552.
197. Weber, E.J., et al., *Human kidney on a chip assessment of polymyxin antibiotic nephrotoxicity.* JCI Insight, 2018. **3**(24).
198. Huh, D., et al., *Reconstituting organ-level lung functions on a chip.* Science, 2010. **328**(5986): p. 1662-1668.
199. Mastrangeli, M., S. Millet, and J. van den Eijnden-van Raaij, *Organ-on-chip in development: towards a roadmap for organs-on-chip.* 2019.
200. Administration, T.F.a.D. *FDA Researchers Evaluate Organ Chips Technology*. 2017 01/02/2021]; Available from: https://www.fda.gov/food/cfsan-constituent-updates/fda-researchers-evaluate-organs-chips-technology.
201. Administration, T.F.a.D. *Organs-on-Chips for Radiation Countermeasures*. 2019 [cited 2021 01/02/2021]; Available from: https://www.fda.gov/emergency-preparedness-and-response/mcm-regulatory-science/organs-chips-radiation-countermeasures.
202. Gjorevski, N., et al., *Neutrophilic infiltration in organ-on-a-chip model of tissue inflammation.* Lab on a Chip, 2020. **20**(18): p. 3365-3374.
203. AstraZeneca. *Organs on Chips Enhancing our Ability to Translate Science into Innovative Medicines*. 2020 28/01/2020 [cited 2021 01/02/2021]; Available from: https://www.astrazeneca.com/what-science-can-do/labtalk-blog/collaboration/organs-on-chips-enhancing-our-ability-to-translate-science-into-innovative-medicines.html.
204. Piergiovanni, M., et al., *Standardisation needs for organ on chip devices.* Lab on a Chip, 2021. **21**(15): p. 2857-2868.
205. Compston, J., *Glucocorticoid-induced osteoporosis: an update.* Endocrine, 2018. **61**(1): p. 7-16.
206. Bussard, K.M., C.V. Gay, and A.M. Mastro, *The bone microenvironment in metastasis; what is special about bone?* Cancer and Metastasis Reviews, 2008. **27**(1): p. 41-55.

207. Jeon, J.S., et al., *Human 3D vascularized organotypic microfluidic assays to study breast cancer cell extravasation.* Proceedings of the National Academy of Sciences, 2015. **112**(1): p. 214-219.
208. Hao, S., et al., *A Spontaneous 3D Bone-On-a-Chip for Bone Metastasis Study of Breast Cancer Cells.* Small, 2018.
209. Marturano-Kruik, A., et al., *Human bone perivascular niche-on-a-chip for studying metastatic colonization.* Proceedings of the National Academy of Sciences, 2018: p. 201714282.
210. George, E.L., et al., *Lab-on-a-chip platforms for quantification of multicellular interactions in bone remodeling.* Experimental cell research, 2018. **365**(1): p. 106-118.
211. Wittkowske, C., et al., *In vitro bone cell models: impact of fluid shear stress on bone formation.* Frontiers in Bioengineering and Biotechnology, 2016. **4**: p. 87.
212. Owen, R. and G.C. Reilly, *In vitro models of bone remodelling and associated disorders.* Frontiers in bioengineering and biotechnology, 2018. **6**: p. 134.
213. Watson, E.C. and R.H. Adams, *Biology of Bone: The Vasculature of the Skeletal System.* Cold Spring Harbor Perspectives in Medicine, 2017: p. a031559.
214. Griffith, J.F., et al., *Compromised bone marrow perfusion in osteoporosis.* Journal of Bone and Mineral Research, 2008. **23**(7): p. 1068-1075.
215. Zhao, Q., et al., *Mice with increased angiogenesis and osteogenesis due to conditional activation of HIF pathway in osteoblasts are protected from ovariectomy induced bone loss.* Bone, 2012. **50**(3): p. 763-770.
216. Liu, X., et al., *Prolyl hydroxylase inhibitors protect from the bone loss in ovariectomy rats by increasing bone vascularity.* Cell biochemistry and biophysics, 2014. **69**(1): p. 141-149.
217. Peng, J., et al., *Low bone turnover and reduced angiogenesis in streptozotocin-induced osteoporotic mice.* Connective tissue research, 2016. **57**(4): p. 277-289.
218. Stabley, J.N., et al., *Type 2 diabetes alters bone and marrow blood flow and vascular control mechanisms in the ZDF rat.* The Journal of endocrinology, 2015. **225**(1): p. 47.
219. Napoli, N., et al., *Mechanisms of diabetes mellitus-induced bone fragility.* Nature Reviews Endocrinology, 2017. **13**(4): p. 208.
220. Guerado, E. and E. Caso, *The physiopathology of avascular necrosis of the femoral head: an update.* Injury, 2016. **47**: p. S16-S26.
221. Kim, S., et al., *Engineering of functional, perfusable 3D microvascular networks on a chip.* Lab on a Chip, 2013. **13**(8): p. 1489-1500.
222. Rubens, R.D., *Bone metastases: incidence and complications.* Cancer and the Skeleton. London: Martin Dunitz, 2000: p. 33-42.
223. Margolis, E.A., et al., *Stromal Cell Identity Modulates Vascular Morphogenesis in a Microvasculature-on-a-Chip Platform.* Lab on a Chip, 2021.
224. Oh, S., et al., *"Open-top" Microfluidic Device for In-vitro Three-Dimensional Capillary Bed.* Lab on a Chip, 2017.
225. Kehl, D., et al., *Proteomic analysis of human mesenchymal stromal cell secretomes: a systematic comparison of the angiogenic potential.* npj Regenerative Medicine, 2019. **4**(1): p. 8.
226. Joensuu, K., et al., *Angiogenic potential of human mesenchymal stromal cell and circulating mononuclear cell co-cultures is reflected in the expression profiles of proangiogenic factors leading to endothelial cell and pericyte*

differentiation. Journal of Tissue Engineering and Regenerative Medicine, 2017.
227. Mahmoudifar, N. and P.M. Doran, *Chondrogenesis and cartilage tissue engineering: the longer road to technology development.* Trends in biotechnology, 2012. **30**(3): p. 166-176.
228. Heino, T.J. and T.A. Hentunen, *Differentiation of osteoblasts and osteocytes from mesenchymal stem cells.* Current stem cell research & therapy, 2008. **3**(2): p. 131-145.
229. Box, G.E., W.G. Hunter, and J.S. Hunter, *Statistics for experimenters: an introduction to design, data analysis, and model building*. Vol. 1. 1978: JSTOR.
230. Jeon, J.S., et al., *Generation of 3D functional microvascular networks with human mesenchymal stem cells in microfluidic systems.* Integrative Biology, 2014. **6**(5): p. 555-563.
231. Shamloo, A., et al., *A comparative study of collagen matrix density effect on endothelial sprout formation using experimental and computational approaches.* Annals of biomedical engineering, 2016. **44**(4): p. 929-941.
232. Shamloo, A. and S.C. Heilshorn, *Matrix density mediates polarization and lumen formation of endothelial sprouts in VEGF gradients.* Lab on a Chip, 2010. **10**(22): p. 3061-3068.
233. Ghajar, C.M., et al., *The effect of matrix density on the regulation of 3-D capillary morphogenesis.* Biophysical journal, 2008. **94**(5): p. 1930-1941.
234. Whisler, J.A., M.B. Chen, and R.D. Kamm, *Control of perfusable microvascular network morphology using a multiculture microfluidic system.* Tissue Engineering Part C: Methods, 2012. **20**(7): p. 543-552.
235. Nauta, T.D., et al., *HIF-2α expression regulates sprout formation into 3D fibrin matrices in prolonged hypoxia in human microvascular endothelial cells.* PloS one, 2016. **11**(8): p. e0160700.
236. Schindelin, J., et al., *Fiji: an open-source platform for biological-image analysis.* Nature methods, 2012. **9**(7): p. 676-682.
237. Arganda-Carreras, I., et al., *3D reconstruction of histological sections: Application to mammary gland tissue.* Microscopy research and technique, 2010. **73**(11): p. 1019-1029.
238. Gunst, R.F. and R.L. Mason, *Fractional factorial design.* Wiley Interdisciplinary Reviews: Computational Statistics, 2009. **1**(2): p. 234-244.
239. Kim, H.J., et al., *Human gut-on-a-chip inhabited by microbial flora that experiences intestinal peristalsis-like motions and flow.* Lab on a Chip, 2012. **12**(12): p. 2165-2174.
240. Adriani, G., et al., *A 3D neurovascular microfluidic model consisting of neurons, astrocytes and cerebral endothelial cells as a blood–brain barrier.* Lab on a Chip, 2017. **17**(3): p. 448-459.
241. Kachgal, S., et al., *Bone marrow stromal cells stimulate an angiogenic program that requires endothelial MT1-MMP.* Journal of cellular physiology, 2012. **227**(11): p. 3546-3555.
242. Kachgal, S. and A.J. Putnam, *Mesenchymal stem cells from adipose and bone marrow promote angiogenesis via distinct cytokine and protease expression mechanisms.* Angiogenesis, 2011. **14**(1): p. 47-59.
243. Ghajar, C.M., et al., *Mesenchymal cells stimulate capillary morphogenesis via distinct proteolytic mechanisms.* Experimental cell research, 2010. **316**(5): p. 813-825.

244. Quade, M., et al., *The Secretome of Hypoxia Conditioned hMSC Loaded in a Central Depot Induces Chemotaxis and Angiogenesis in a Biomimetic Mineralized Collagen Bone Replacement Material.* Advanced Healthcare Materials, 2020. **9**(2): p. 1901426.
245. Rao, R.R., et al., *Matrix composition regulates three-dimensional network formation by endothelial cells and mesenchymal stem cells in collagen/fibrin materials.* Angiogenesis, 2012. **15**(2): p. 253-264.
246. Staines, K., et al., *Cartilage to bone transitions in health and disease.* The Journal of endocrinology, 2013. **219**(1): p. R1.
247. Betz, R.R., *Limitations of autograft and allograft: new synthetic solutions.* Orthopedics, 2002. **25**(5): p. S561-S570.
248. Sheehy, E.J., et al., *Tissue engineering whole bones through endochondral ossification: regenerating the distal phalanx.* BioResearch open access, 2015. **4**(1): p. 229-241.
249. Daly, A.C., et al., *3D printed microchannel networks to direct vascularisation during endochondral bone repair.* Biomaterials, 2018. **162**: p. 34-46.
250. Emons, J., et al., *Mechanisms of growth plate maturation and epiphyseal fusion.* Hormone research in paediatrics, 2011. **75**(6): p. 383-391.
251. Shukunami, C., et al., *Chondrogenic differentiation of clonal mouse embryonic cell line ATDC5 in vitro: differentiation-dependent gene expression of parathyroid hormone (PTH)/PTH-related peptide receptor.* The Journal of cell biology, 1996. **133**(2): p. 457-468.
252. Shukunami, C., et al., *Cellular hypertrophy and calcification of embryonal carcinoma-derived chondrogenic cell line ATDC5 in vitro.* Journal of Bone and Mineral Research, 1997. **12**(8): p. 1174-1188.
253. Mello, M.A. and R.S. Tuan, *High density micromass cultures of embryonic limb bud mesenchymal cells: an in vitro model of endochondral skeletal development.* In Vitro Cellular & Developmental Biology-Animal, 1999. **35**(5): p. 262-269.
254. Cheung, J., et al., *Apoptosis of terminal hypertrophic chondrocytes in an in vitro model of endochondral ossification.* The Journal of Pathology: A Journal of the Pathological Society of Great Britain and Ireland, 2003. **201**(3): p. 496-503.
255. Hirao, M., et al., *Oxygen tension regulates chondrocyte differentiation and function during endochondral ossification.* Journal of Biological Chemistry, 2006. **281**(41): p. 31079-31092.
256. Grass, G.M. and P.J. Sinko, *Physiologically-based pharmacokinetic simulation modelling.* Advanced Drug Delivery Reviews, 2002. **54**(3): p. 433-451.
257. Knighton, D.R., et al., *Oxygen tension regulates the expression of angiogenesis factor by macrophages.* Science, 1983. **221**(4617): p. 1283-1285.
258. Pfeiffenberger, M., et al., *Hypoxia and mesenchymal stromal cells as key drivers of initial fracture healing in an equine in vitro fracture hematoma model.* Plos one, 2019. **14**(4): p. e0214276.
259. Gerber, H.-P., et al., *VEGF couples hypertrophic cartilage remodeling, ossification and angiogenesis during endochondral bone formation.* Nature medicine, 1999. **5**(6): p. 623-628.
260. Harper, J. and M. Klagsbrun, *Cartilage to bone—angiogenesis leads the way.* Nature medicine, 1999. **5**(6): p. 617-618.
261. Pesesse, L., et al., *Consequences of chondrocyte hypertrophy on osteoarthritic cartilage: potential effect on angiogenesis.* Osteoarthritis and cartilage, 2013. **21**(12): p. 1913-1923.

262. National Centre for the Replacement, R., and Reduction of Animals in Research, *The 3Rs.*
263. Klar, R.M., *The induction of bone formation: the translation enigma.* Frontiers in Bioengineering and Biotechnology, 2018. **6**: p. 74.
264. Johnstone, B., et al., *In vitrochondrogenesis of bone marrow-derived mesenchymal progenitor cells.* Experimental cell research, 1998. **238**(1): p. 265-272.
265. Patra, D. and L.J. Sandell, *Antiangiogenic and anticancer molecules in cartilage.* 2012.
266. Bornstein, P., *Thrombospondins function as regulators of angiogenesis.* Journal of cell communication and signaling, 2009. **3**(3-4): p. 189-200.
267. Pufe, T., et al., *Endostatin/collagen XVIII—an inhibitor of angiogenesis—is expressed in cartilage and fibrocartilage.* Matrix Biology, 2004. **23**(5): p. 267-276.
268. Chandrasekhar, S., et al., *Osteonectin/SPARC is a product of articular chondrocytes/cartilage and is regulated by cytokines and growth factors.* Biochimica et Biophysica Acta (BBA)-Molecular Cell Research, 1994. **1221**(1): p. 7-14.
269. Volpert, O., *Modulation of endothelial cell survival by an inhibitor of angiogenesis thrombospondin-1: a dynamic balance.* Cancer and Metastasis Reviews, 2000. **19**(1-2): p. 87-92.
270. Yamauchi, M., S. Imajoh-Ohmi, and M. Shibuya, *Novel antiangiogenic pathway of thrombospondin-1 mediated by suppression of the cell cycle.* Cancer science, 2007. **98**(9): p. 1491-1497.
271. Greenaway, J., et al., *Thrombospondin-1 inhibits VEGF levels in the ovary directly by binding and internalization via the low density lipoprotein receptor-related protein-1 (LRP-1).* Journal of cellular physiology, 2007. **210**(3): p. 807-818.
272. Chen, J., et al., *A randomized Phase III trial of neoadjuvant recombinant human endostatin, docetaxel and epirubicin as first-line therapy for patients with breast cancer (CBCRT 01).* International Journal of Cancer, 2018. **142**(10): p. 2130-2138.
273. Rivera, L.B., A.D. Bradshaw, and R.A. Brekken, *The regulatory function of SPARC in vascular biology.* Cellular and Molecular Life Sciences, 2011. **68**(19): p. 3165.
274. WRANA, J.L., C.M. OVERALL, and J. SODEK, *Regulation of the expression of a secreted acidic protein rich in cysteine (SPARC) in human fibroblasts by transforming growth factor β: Comparison of transcriptional and post-transcriptional control with fibronectin and type I collagen.* European journal of biochemistry, 1991. **197**(2): p. 519-528.
275. Cucchiarini, M. and H. Madry, *Overexpression of human IGF-I via direct rAAV-mediated gene transfer improves the early repair of articular cartilage defects in vivo.* Gene therapy, 2014. **21**(9): p. 811-819.
276. Harvey, K., et al., *Comparative analysis of in vitro angiogenic activities of endothelial cells of heterogeneous origin.* Microvascular research, 2002. **63**(3): p. 316-326.
277. Crockett, J.C., et al., *Bone remodelling at a glance.* Journal of cell science, 2011. **124**(7): p. 991-998.

278. van Bezooijen, R.L., et al., *SOST/sclerostin, an osteocyte-derived negative regulator of bone formation.* Cytokine & growth factor reviews, 2005. **16**(3): p. 319-327.
279. Minisola, S., *Romosozumab: from basic to clinical aspects*. 2014, Taylor & Francis.
280. Denayer, T., T. Stöhr, and M. Van Roy, *Animal models in translational medicine: Validation and prediction.* New Horizons in Translational Medicine, 2014. **2**(1): p. 5-11.
281. Engler, A.J., et al., *Matrix elasticity directs stem cell lineage specification.* Cell, 2006. **126**(4): p. 677-689.
282. Mullen, C.A., et al., *Osteocyte differentiation is regulated by extracellular matrix stiffness and intercellular separation.* Journal of the mechanical behavior of biomedical materials, 2013. **28**: p. 183-194.
283. Goring, S., et al., *Retinoic acid and IGF1 stimulate the differentiation of human primary osteoblasts to osteocytes in 3D collagen gels.* 2013.
284. Mattinzoli, D., et al., *A novel model of in vitro osteocytogenesis induced by retinoic acid treatment.* Eur Cell Mater, 2012. **24**: p. 403-425.
285. Yang, X., et al., *In vitro uptake of hydroxyapatite nanoparticles and their effect on osteogenic differentiation of human mesenchymal stem cells.* Stem cells international, 2018. **2018**.
286. Sheehy, E.J., C.T. Buckley, and D.J. Kelly, *Oxygen tension regulates the osteogenic, chondrogenic and endochondral phenotype of bone marrow derived mesenchymal stem cells.* Biochemical and biophysical research communications, 2012. **417**(1): p. 305-310.
287. Zahm, A.M., et al., *Oxygen tension regulates preosteocyte maturation and mineralization.* Bone, 2008. **43**(1): p. 25-31.
288. Hirao, M., et al., *Oxygen tension is an important mediator of the transformation of osteoblasts to osteocytes.* Journal of bone and mineral metabolism, 2007. **25**(5): p. 266-276.
289. Cunniffe, G.M., et al., *The synthesis and characterization of nanophase hydroxyapatite using a novel dispersant-aided precipitation method.* Journal of Biomedical Materials Research Part A, 2010. **95**(4): p. 1142-1149.
290. Morgan, C.J., *Use of proper statistical techniques for research studies with small samples.* American Journal of Physiology-Lung Cellular and Molecular Physiology, 2017. **313**(5): p. L873-L877.
291. Lv, H., et al., *Mechanism of regulation of stem cell differentiation by matrix stiffness.* Stem cell research & therapy, 2015. **6**(1): p. 1-11.
292. Pek, Y.S., A.C. Wan, and J.Y. Ying, *The effect of matrix stiffness on mesenchymal stem cell differentiation in a 3D thixotropic gel.* Biomaterials, 2010. **31**(3): p. 385-391.
293. Hsieh, W.-T., et al., *Matrix dimensionality and stiffness cooperatively regulate osteogenesis of mesenchymal stromal cells.* Acta biomaterialia, 2016. **32**: p. 210-222.
294. Kelly, D.J. and C.R. Jacobs, *The role of mechanical signals in regulating chondrogenesis and osteogenesis of mesenchymal stem cells.* Birth Defects Research Part C: Embryo Today: Reviews, 2010. **90**(1): p. 75-85.
295. Prideaux, M., et al., *Extracellular matrix mineralization promotes E11/gp38 glycoprotein expression and drives osteocytic differentiation.* PLoS One, 2012. **7**(5): p. e36786.

296. Irie, K., et al., *Matrix mineralization as a trigger for osteocyte maturation.* Journal of Histochemistry & Cytochemistry, 2008. **56**(6): p. 561-567.
297. Lin, L., K.L. Chow, and Y. Leng, *Study of hydroxyapatite osteoinductivity with an osteogenic differentiation of mesenchymal stem cells.* Journal of Biomedical Materials Research Part A: An Official Journal of The Society for Biomaterials, The Japanese Society for Biomaterials, and The Australian Society for Biomaterials and the Korean Society for Biomaterials, 2009. **89**(2): p. 326-335.
298. Liu, Y., et al., *In vitro effects of nanophase hydroxyapatite particles on proliferation and osteogenic differentiation of bone marrow‐derived mesenchymal stem cells.* Journal of Biomedical Materials Research Part A: An Official Journal of The Society for Biomaterials, The Japanese Society for Biomaterials, and The Australian Society for Biomaterials and the Korean Society for Biomaterials, 2009. **90**(4): p. 1083-1091.
299. Motskin, M., et al., *Hydroxyapatite nano and microparticles: correlation of particle properties with cytotoxicity and biostability.* Biomaterials, 2009. **30**(19): p. 3307-3317.
300. Huebsch, N., et al., *Harnessing traction-mediated manipulation of the cell/matrix interface to control stem-cell fate.* Nature materials, 2010. **9**(6): p. 518.
301. da Cunha, C.B., et al., *Influence of the stiffness of three-dimensional alginate/collagen-I interpenetrating networks on fibroblast biology.* Biomaterials, 2014. **35**(32): p. 8927-8936.
302. Chaudhuri, O., et al., *Hydrogels with tunable stress relaxation regulate stem cell fate and activity.* Nature materials, 2016. **15**(3): p. 326-334.
303. Khetan, S., et al., *Degradation-mediated cellular traction directs stem cell fate in covalently crosslinked three-dimensional hydrogels.* Nature materials, 2013. **12**(5): p. 458-465.
304. Fakhry, M., et al., *Molecular mechanisms of mesenchymal stem cell differentiation towards osteoblasts.* World journal of stem cells, 2013. **5**(4): p. 136.
305. Kalajzic, I., et al., *Dentin matrix protein 1 expression during osteoblastic differentiation, generation of an osteocyte GFP-transgene.* Bone, 2004. **35**(1): p. 74-82.
306. Capulli, M., R. Paone, and N. Rucci, *Osteoblast and osteocyte: games without frontiers.* Archives of biochemistry and biophysics, 2014. **561**: p. 3-12.
307. Eskes, C., et al., *Good cell culture practices & in vitro toxicology.* Toxicology In Vitro, 2017. **45**: p. 272-277.
308. Park, Y.K., et al., *In vitro microvessel growth and remodeling within a three-dimensional microfluidic environment.* Cellular and molecular bioengineering, 2014. **7**(1): p. 15-25.
309. Tan, W. and T.A. Desai, *Layer-by-layer microfluidics for biomimetic three-dimensional structures.* Biomaterials, 2004. **25**(7): p. 1355-1364.
310. Chung, S., et al., *Surface‐treatment‐induced three‐dimensional capillary morphogenesis in a microfluidic platform.* Advanced materials, 2009. **21**(47): p. 4863-4867.
311. Nakashima, T., et al., *Evidence for osteocyte regulation of bone homeostasis through RANKL expression.* Nature medicine, 2011. **17**(10): p. 1231.
312. Cummings, S.R., et al., *Denosumab for prevention of fractures in postmenopausal women with osteoporosis.* New England Journal of Medicine, 2009. **361**(8): p. 756-765.

313. Pennings, I., et al., *Effect of donor variation on osteogenesis and vasculogenesis in hydrogel cocultures.* Journal of tissue engineering and regenerative medicine, 2019. **13**(3): p. 433-445.
314. Zhukareva, V., et al., *Secretion profile of human bone marrow stromal cells: donor variability and response to inflammatory stimuli.* Cytokine, 2010. **50**(3): p. 317-321.
315. Siddappa, R., et al., *Donor variation and loss of multipotency during in vitro expansion of human mesenchymal stem cells for bone tissue engineering.* Journal of orthopaedic research, 2007. **25**(8): p. 1029-1041.
316. Phinney, D.G., et al., *Donor variation in the growth properties and osteogenic potential of human marrow stromal cells.* Journal of cellular biochemistry, 1999. **75**(3): p. 424-436.
317. Wu, Q., et al., *Deriving osteogenic cells from induced pluripotent stem cells for bone tissue engineering.* Tissue Engineering Part B: Reviews, 2017. **23**(1): p. 1-8.
318. Kusuma, S., et al., *Self-organized vascular networks from human pluripotent stem cells in a synthetic matrix.* Proceedings of the National Academy of Sciences, 2013. **110**(31): p. 12601-12606.
319. Margariti, A., et al., *Direct reprogramming of fibroblasts into endothelial cells capable of angiogenesis and reendothelialization in tissue-engineered vessels.* Proceedings of the National Academy of Sciences, 2012. **109**(34): p. 13793-13798.
320. Osaki, T., V. Sivathanu, and R.D. Kamm, *Engineered 3D vascular and neuronal networks in a microfluidic platform.* Scientific reports, 2018. **8**(1): p. 5168.
321. Bayless, K.J., R. Salazar, and G.E. Davis, *RGD-dependent vacuolation and lumen formation observed during endothelial cell morphogenesis in three-dimensional fibrin matrices involves the αvβ3 and α5β1 integrins.* The American journal of pathology, 2000. **156**(5): p. 1673-1683.
322. Laurens, N., et al., *Single and combined effects of αvβ3-and α5β1-integrins on capillary tube formation in a human fibrinous matrix.* Angiogenesis, 2009. **12**(3): p. 275-285.
323. Haase, K. and R.D. Kamm, *Advances in on-chip vascularization.* Regenerative Medicine, 2017. **12**(3): p. 285-302.
324. Brown, J.H., et al., *The crystal structure of modified bovine fibrinogen.* Proceedings of the National Academy of Sciences, 2000. **97**(1): p. 85-90.
325. Thiagarajan, P., A.J. Rippon, and D.H. Farrell, *Alternative adhesion sites in human fibrinogen for vascular endothelial cells.* Biochemistry, 1996. **35**(13): p. 4169-4175.
326. Baugh, L.M., et al., *Non-destructive two-photon excited fluorescence imaging identifies early nodules in calcific aortic-valve disease.* Nature biomedical engineering, 2017. **1**(11): p. 914-924.
327. Mukhopadhyay, R., *When PDMS isn't the best*. 2007, ACS Publications.
328. Toepke, M.W. and D.J. Beebe, *PDMS absorption of small molecules and consequences in microfluidic applications.* Lab on a Chip, 2006. **6**(12): p. 1484-1486.
329. Grosso, A., et al., *It takes two to tango: coupling of angiogenesis and osteogenesis for bone regeneration.* Frontiers in bioengineering and biotechnology, 2017. **5**: p. 68.

List of Tables

List of Figures

Appendices

Appendix 1 FIJI macro for vascular network morphology analysis

```
// This macro is written to accept 2 channel Z stack images
imageTitle=getTitle();
imageRoot = File.directory;
getDimensions(width, height, channels, slices, frames)
getVoxelSize(Vwidth, Vheight, Vdepth, Vunit);

//This function creates a rectangular selection with specified width and height and an orign at the center
//of the image. This selection is then cropped out for analysis

function Trim(TrimWidth,TrimHeight)
{
ImageCenterX = width / 2;
RectXOrigin = ImageCenterX - (TrimWidth / 2);
ImageCenterY = height / 2;
RectYOrigin = ImageCenterY - (TrimHeight / 2);
makeRectangle(RectXOrigin, RectYOrigin, TrimWidth, TrimHeight);
waitForUser("choose area for analysis");
run("Crop");
}

Trimmed_Image_Size_um_X = 1170;
Trimmed_Image_Size_um_Y = 1170;
Trimmed_Image_Size_px_x = round(Trimmed_Image_Size_um_X/Vwidth);
Trimmed_Image_Size_px_y = round(Trimmed_Image_Size_um_Y/Vheight);

Trim(Trimmed_Image_Size_px_x,Trimmed_Image_Size_px_y)

getDimensions(width2, height2, channels2, slices2, frames2)
getVoxelSize(Vwidth2, Vheight2, Vdepth2, Vunit2);
TotalArea=(width2*Vwidth2)*(height2*Vheight2);

run("Split Channels");
selectWindow("C2-"+imageTitle);
close();
selectWindow("C1-"+imageTitle);

                Dialog.create("Slice Selection");
                Dialog.addNumber("Start Slice:",1);
                Dialog.addNumber("End Slice:",1);
                Dialog.show();
                Start_Slice = Dialog.getNumber();
                End_Slice = Dialog.getNumber();

run("Make Substack...", "channels=1 slices="+Start_Slice+"-"+End_Slice);

selectWindow("Substack ("+Start_Slice+"-"+End_Slice+")");
run("Despeckle", "stack");
run("Brightness/Contrast...");
waitForUser("Adjust Brightness / Contrast - Click Apply to Confim");
run("Gaussian Blur...", "sigma=4 stack");
run("Z Project...", "projection=[Max Intensity]");
run("Threshold...");
```

```
waitForUser("Set threshold - Press Apply to confirm - ensure vessel areas display max pixel intensity 255");
//setAutoThreshold("Li dark");
//setOption("BlackBackground", false);
//run("Convert to Mask");

getHistogram(values, counts, 2);
//Array.print(counts);
PercentVasc=100*(counts[1]/(counts[0]+counts[1]));
AreaVasc= (PercentVasc/100)*TotalArea;
run("Skeletonize (2D/3D)");
run("Analyze Skeleton (2D/3D)", "prune=none show display");
//Table.sort("# Branches");
selectWindow("MAX_Substack ("+Start_Slice+"-"+End_Slice+")");
run("Create Selection");
roiManager("Add");
selectWindow("Substack ("+Start_Slice+"-"+End_Slice+")");
run("Z Project...", "projection=[Max Intensity]");
//selectWindow("MAX_Substack ("+Start_Slice+"-"+End_Slice+")-1");
roiManager("Show All");
print("Total area = "+TotalArea+" micron^2 \nArea analysed is "+PercentVasc+"% Vascularised\nArea Vascularised = "+AreaVasc+" micron^2")
```

Appendix 2 Vascular formation with µDBOs

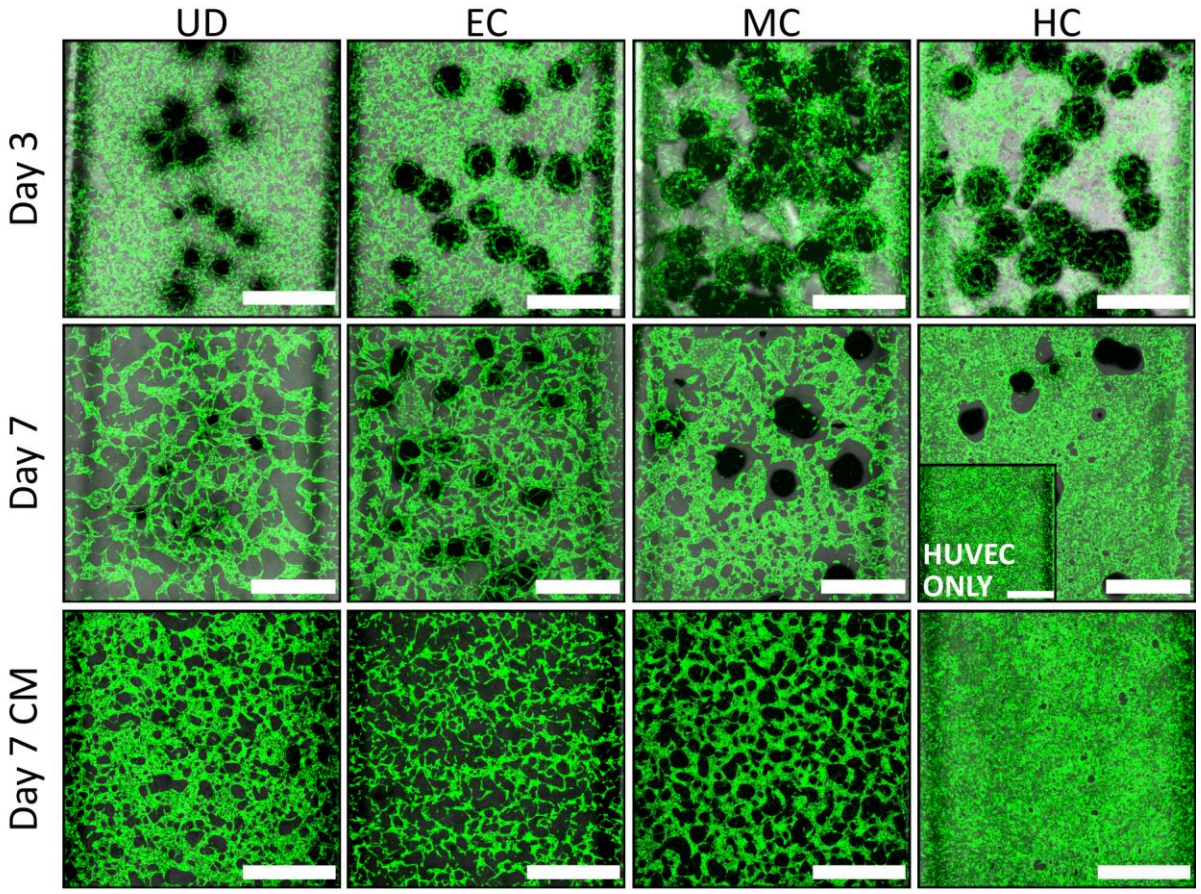

Figure Appendix 2: Vasculature formation with µDBOs in MPS devices. At day 3, no discernible differences between formed vasculature is observable between µDBOs. At day 7, stark differences between groups is observable. When HUVEC only cultures in MPS devices were fed with conditioned media from each of the µDBO groups at day 7, in HUVEC only MPS devices cultured in µDBO conditioned medium, similar observations are observed in vascular morphology with differentiated (EC,MC,HC) µDBO conditioned medium. Scale bar = 1mm.

Appendix 3 Screening experimental groups

Table Appendix 3: Screening experimental groups.

Sample		Cell Density (x10^6 / ml)	Media	nHA (mg/ml)	Collagen Concentration (mg/ml)	Oxygen Tesion (%)	Retinoic Acid (µM)
1		0.5	Osteo Media	0.27	4	5	5
2		0.5	Osteo Media	0.27	4	5	10
3		0.5	XPAN	0.27	4	5	10
4		0.5	XPAN	0.27	4	5	5
5		0.1	Osteo Media	2.7	4	5	10
6		0.5	Osteo Media	2.7	4	5	5
7		0.1	XPAN	2.7	4	5	5
8		0.5	XPAN	2.7	4	5	10
9		0.1	Osteo Media	0.27	8	5	10
10		0.5	Osteo Media	0.27	8	5	5
11		0.1	XPAN	0.27	8	5	5
12		0.5	XPAN	0.27	8	5	10
13		0.1	Osteo Media	2.7	8	5	5
14		0.5	Osteo Media	2.7	8	5	10
15		0.1	XPAN	2.7	8	5	10
16		0.5	XPAN	2.7	8	5	5
17		0.5	Osteo Media	0.27	4	20	10
18		0.5	Osteo Media	0.27	4	20	5
19		0.5	XPAN	0.27	4	20	5
20		0.5	XPAN	0.27	4	20	10
21		0.1	Osteo Media	2.7	4	20	5
22		0.5	Osteo Media	2.7	4	20	10
23		0.1	XPAN	2.7	4	20	10
24		0.5	XPAN	2.7	4	20	5
25		0.1	Osteo Media	0.27	8	20	5
26		0.5	Osteo Media	0.27	8	20	10
27		0.1	XPAN	0.27	8	20	10
28		0.5	XPAN	0.27	8	20	5
29		0.1	Osteo Media	2.7	8	20	10
30		0.5	Osteo Media	2.7	8	20	5
31		0.1	XPAN	2.7	8	20	5
32		0.5	XPAN	2.7	8	20	10
33		0.5	Osteo Media	0.27	4	5	5
34		0.5	Osteo Media	0.27	4	5	10
35		0.5	XPAN	0.27	4	5	10
36		0.5	XPAN	0.27	4	5	5
37		0.1	Osteo Media	2.7	4	5	10
38		0.5	Osteo Media	2.7	4	5	5

Sample		Cell Density (x10^6 / ml)	Media	nHA (mg/ml)	Collagen Concentration (mg/ml)	Oxygen Tesion (%)	Retinoic Acid (µM)
39		0.1	XPAN	2.7	4	5	5
40		0.5	XPAN	2.7	4	5	10
41		0.1	Osteo Media	0.27	8	5	10
42		0.5	Osteo Media	0.27	8	5	5
43		0.1	XPAN	0.27	8	5	5
44		0.5	XPAN	0.27	8	5	10
45		0.1	Osteo Media	2.7	8	5	5
46		0.5	Osteo Media	2.7	8	5	10
47		0.1	XPAN	2.7	8	5	10
48		0.5	XPAN	2.7	8	5	5
49		0.5	Osteo Media	0.27	4	20	10
50		0.5	Osteo Media	0.27	4	20	5
51		0.5	XPAN	0.27	4	20	5
52		0.5	XPAN	0.27	4	20	10
53		0.1	Osteo Media	2.7	4	20	5
54		0.5	Osteo Media	2.7	4	20	10
55		0.1	XPAN	2.7	4	20	10
56		0.5	XPAN	2.7	4	20	5
57		0.1	Osteo Media	0.27	8	20	5
58		0.5	Osteo Media	0.27	8	20	10
59		0.1	XPAN	0.27	8	20	10
60		0.5	XPAN	0.27	8	20	5
61		0.1	Osteo Media	2.7	8	20	10
62		0.5	Osteo Media	2.7	8	20	5
63		0.1	XPAN	2.7	8	20	5
64		0.5	XPAN	2.7	8	20	10
65		0.5	Osteo Media	0.27	4	5	5
66		0.5	Osteo Media	0.27	4	5	10
67		0.5	XPAN	0.27	4	5	10
68		0.5	XPAN	0.27	4	5	5
69		0.1	Osteo Media	2.7	4	5	10
70		0.5	Osteo Media	2.7	4	5	5
71		0.1	XPAN	2.7	4	5	5
72		0.5	XPAN	2.7	4	5	10
73		0.1	Osteo Media	0.27	8	5	10
74		0.5	Osteo Media	0.27	8	5	5
75		0.1	XPAN	0.27	8	5	5
76		0.5	XPAN	0.27	8	5	10
77		0.1	Osteo Media	2.7	8	5	5
78		0.5	Osteo Media	2.7	8	5	10
79		0.1	XPAN	2.7	8	5	10
80		0.5	XPAN	2.7	8	5	5

Sample		Cell Density (x10^6 / ml)	Media	nHA (mg/ml)	Collagen Concentration (mg/ml)	Oxygen Tesion (%)	Retinoic Acid (µM)
81		0.5	Osteo Media	0.27	4	20	10
82		0.5	Osteo Media	0.27	4	20	5
83		0.5	XPAN	0.27	4	20	5
84		0.5	XPAN	0.27	4	20	10
85		0.1	Osteo Media	2.7	4	20	5
86		0.5	Osteo Media	2.7	4	20	10
87		0.1	XPAN	2.7	4	20	10
88		0.5	XPAN	2.7	4	20	5
89		0.1	Osteo Media	0.27	8	20	5
90		0.5	Osteo Media	0.27	8	20	10
91		0.1	XPAN	0.27	8	20	10
92		0.5	XPAN	0.27	8	20	5
93		0.1	Osteo Media	2.7	8	20	10
94		0.5	Osteo Media	2.7	8	20	5
95		0.1	XPAN	2.7	8	20	5
96		0.5	XPAN	2.7	8	20	10

Appendix 4 Alternative cartilage vascularisation approach

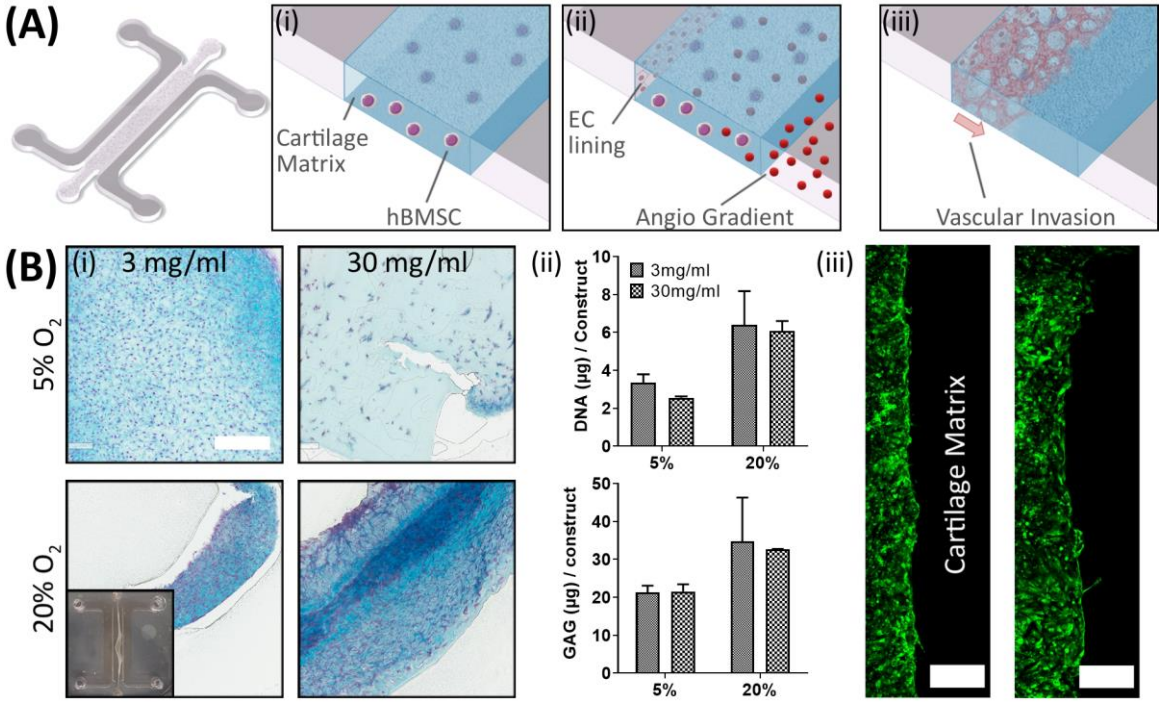

Figure Appendix 4: Alternative Cartilage Vascularisation approach. (A) Alternative approach to modelling EO where **(i)** hBMSCs were chondrogenically differentiated in a fibrin hydrogel. **(ii)** The hydrogel side was lined with endothelial cells and subjected to a gradient of basal EBM on the endothelial side, to fully supplemented EGM on the opposite side to **(iii)** induce vascular invasion into the cartilage matrix. **(B)(i)** Alcian blue staining for glycosaminoglycans (GAGs) indicate the optimal cartilage matrix was formed in in 3mg/ml fibrin hydrogel in 5% O2, as a uniform cartilage matrix was formed that did not contract. Scale bar = 500µm **(ii)** Biochemical analysis indicated increased proliferation and GAG deposition of hBMSC derived chondrocytes in 20% oxygen, however these matrices contracted over 3 weeks of culture, and were therefore unusable. **(iii)** Ultimately, in the optimal gel, EC did not exhibit angiogenic sprouting into the matrix with this vascularisation approach. Scale bar 200µm.

Appendix 5 Mechanisms involved in maintenance of cartilage avascularity

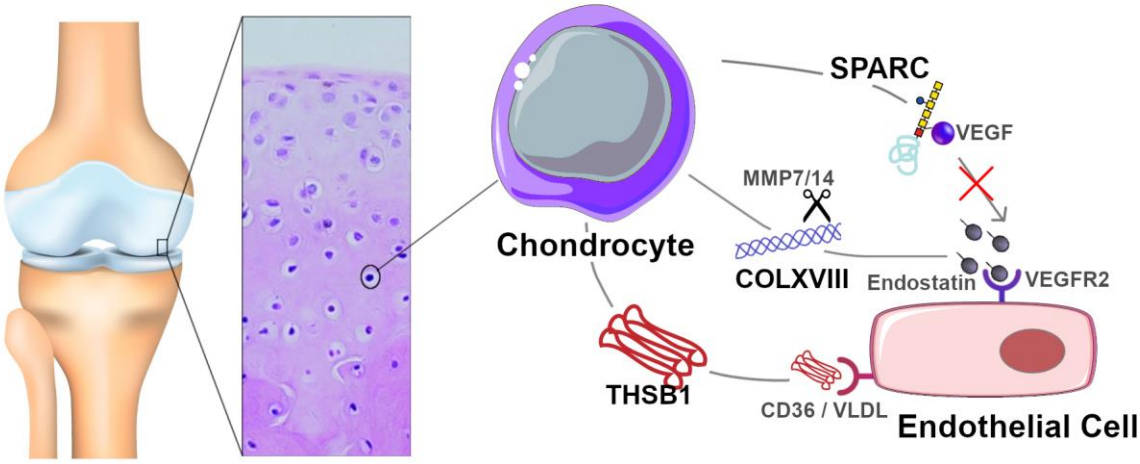

Figure Appendix 5: Mechanisms by which cartilage remains avascular. SPARC, COLXVIII and THBS1 are key secreted factors that maintain cartilage avascularity. SPARCs key mechanism in inhibiting vascularisation of cartilage is binding to and preventing VEGF from binding to VEGFR2 on endothelial cells. COLXVIII is a secreted component of the ECM, but becomes anti-angiogenic when cleaved by MMP7 or MMP14 to produce endostatin, which exhibits its antiangiogenic properties by binding to VEGFR2 and inhibit VEGF mediated angiogenesis. Finally, thrombospondin-1 (THBS1) exhibits its anti-angiogenic effects through ligation of CD36 on ECs to induce apoptosis or binding with the VLDL receptor to induce cell cycle arrest.

Appendix 6 $CaSO_4.2H_20$ was optimal for alginate crosslinking in the Collagen-nHA-Alg IPN

Table Appendix 5: Calcium source for Collagen-Alginate-nHA IPNs

Ca^{2+} source	Alginate (mg/ml)	Collagen (mg/ml)	nHA mg/ml	Concentration (Final)	GDL	Gel Quality
$CaCl_2$	8	8	0.027 – 0.27	20mM $CaCl_2$ (Bath)	0	Inhomogeneous gel: separation of alginate and collagen phases at the interface between gel and $CaCl_2$
$CaCO_3$	8	8	0.27	30-90mM	±120mM	Inhomogeneous gel: bulk gel is a collection of gelled discrete alginate agglomerates with a paste consistency. GDL improved gel strength, gel remained inhomogeneous
nACP	8	8	0.27	1,5,10 mg/ml	±120mM	Calcium release from nACP was too slow, resulting in settling of nanoparticles and inhomogeneous, weak gelation at all concentrations
$CaSO_4.2H_2O$	8	8	0.27	30,60,90 mM	0	Strong, uniform, homogeneous gel at 30mM. Gel inhomogeneity resulted from increasing concentrations of $CaSO_4$ (Figure 5.5)

Appendix 7 Increased collagen concentration beyond 8mg/ml does not further support osteogenesis

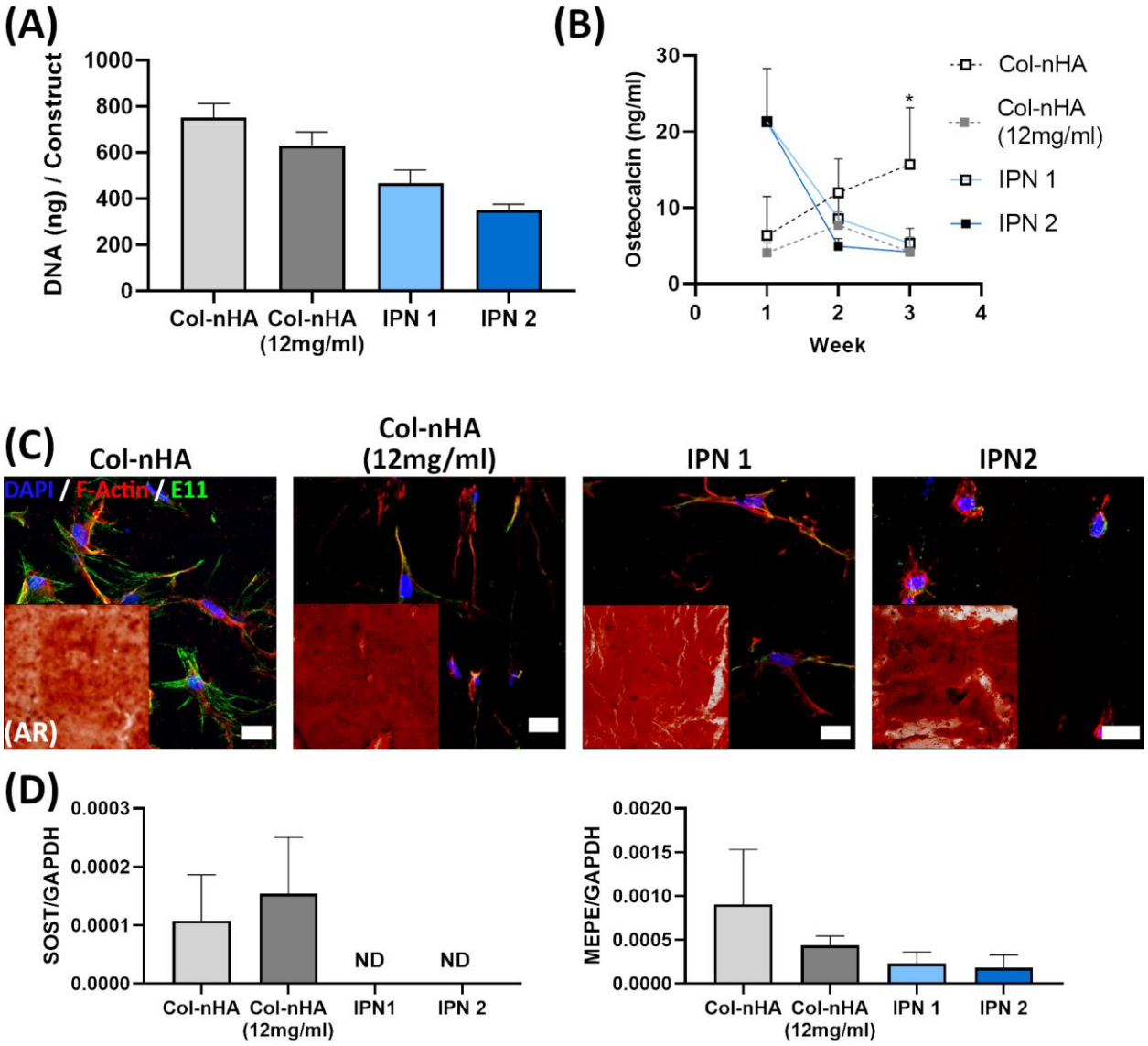

Figure Appendix 6: Increased collagen concentration beyond 8mg/ml does not further support osteogenesis. (A) dsDNA quantification indicates no improved cell viability in 12mg/ml collagen gels compared to 8mg/ml collagen-nHA hydrogels. **(B)** Of all tested hydrogels, only 8mg/ml collagen-nHA hydrogels secreted increasing amounts of OCN over the three week culture period. **(C)** 12mg/ml hydrogels produce hBMSCs with similar phenotype to 8mg/ml gels, and also produce a mineralised matrix. Scale bar = 20µm **(D)** 12mg/ml collagen-nHA hydrogels express osteocyte genes at similar levels to 8mg/ml collagen-nHA gels.

1. Mastrangeli, M., S. Millet, and J. van den Eijnden-van Raaij, *Organ-on-chip in development: towards a roadmap for organs-on-chip.* 2019.